

The Pennsylvania State University
The Graduate School

The Design and Development of an Automatic
Control System for the In-Duct Cancellation of
Spinning Modes of Sound

Engineering Report
in
Mechanical Engineering

by

Walter W. Harrington

Submitted in Partial Fulfillment
of the Requirements
for the Degree of

Master of Science

June 1973



NASA GRANT NGL-39-009-121

NASA-CR-132317) THE DESIGN AND DEVELOPMENT OF AN AUTOMATIC CONTROL SYSTEM FOR THE IN-DUCT CANCELLATION OF SPINNING MODES OF SOUND (Pennsylvania State Univ.) 249 p HC \$14.50 CSCL 20A N73-32540 Unclas 63/23 18692

The Pennsylvania State University

The Graduate School

The Design and Development of an Automatic
Control System for the In-Duct Cancellation of
Spinning Modes of Sound

Engineering Report
in
Mechanical Engineering

by

Walter W. Harrington

Submitted in Partial Fulfillment
of the Requirements
for the Degree of

Master of Science

June 1973

Date of Approval:

Dr. Gerhard Reethof, Alcoa Professor
of Mechanical Engineering,
Report Adviser

Dr. Donald R. Olson
Head of the Department of Mechanical
Engineering

ACKNOWLEDGEMENTS

The author wishes to thank Dr. Gerhard Reethof, Alcoa Professor of Mechanical Engineering, for his guidance and advice. Special acknowledgement is given to Michael Oslac, Research Assistant, for his dedicated guidance and assistance.

Acknowledgement is also given to Dr. Arthur Brickman, Mechanical Engineering, and to Dr. John Lewis, Electrical Engineering, for their advice and assistance in the development of an educational background necessary to this investigation.

Acknowledgement is given to Dr. J. L. Shearer for his thorough review of this Engineering Report.

TABLE OF CONTENTS

| | |
|---|------|
| Acknowledgements | ii |
| List of Tables | iv |
| List of Figures | v |
| Nomenclature | x |
| Abstract | xvii |
| | |
| I. Introduction | 1 |
| 1.1 Background to Problem | 1 |
| 1.2 Spinning Mode Synthesizer | 8 |
| 1.3 The Cancellation Concept | 18 |
| 1.4 Automatic Control of Cancellation | 20 |
| | |
| II. Experimental Verification of In-duct Sound Pressure Level Reduction by Cancellation | 21 |
| 2.1 Description of Apparatus | 21 |
| 2.2 Experimental Results | 30 |
| | |
| III. Automatic Control Problem | 108 |
| 3.1 Need for Automatic Control | 108 |
| 3.2 Statement of Control Problem | 110 |
| 3.3 Determination of System Model | 112 |
| 3.4 Synthesis of Adaptive Control Scheme | 144 |
| | |
| IV. Adaptive Optimization Procedures for Multidimensional, Unimodal, Noisy Systems | 149 |
| 4.1 Method of Steepest Descent | 149 |
| 4.2 Stochastic Approximation | 150 |
| 4.3 Adaptive Steps Size Random Search | 152 |
| 4.4 Matyas' Method | 152 |
| 4.5 Gradient Biased Random Search | 153 |
| | |
| V. Perturbation Type Adaptive Controller | 154 |
| 5.1 Perturbation Signals | 154 |
| 5.2 Perturbation Circle | 163 |
| 5.3 Analog Simulation of Control System | 174 |
| 5.4 Modified Circular Perturbation Controller | 189 |
| 5.5 Classical Perturbation Controller Features | 200 |
| | |
| VI. Discussion of Results | 205 |
| | |
| VII. Summary, Conclusion, and Recommendations | 218 |
| 7.1 Summary | 218 |
| 7.2 Conclusions | 219 |
| 7.3 Recommendations | 219 |
| | |
| Appendix 1 General Solution of the Wave Equation for a Semi-Infinite, Constant Radius, Rigid-Walled, Cylindrical Duct | 223 |

LIST OF TABLES

| Table | Page |
|-------|--|
| 1 | Roots of $J'_m(k_m b) = 0$ 13 |
| 2 | Cutoff Frequencies for One Foot Diameter Duct 15 |
| 3 | Optimal Solution for Plane Wave 32 |
| 4 | Variation of Transducer Response 45 |
| 5 | Symmetry of Free Field Radiation in Transducer Near Fields for Plane Wave 46 |
| 6 | Symmetry of Free Field Radiation in Transducer Near Fields for First Order Spinning Mode 47 |
| 7 | Symmetry of Free Field Radiation in Transducer Near Fields for a Cancelled First Order Spinning Mode 48 |
| 8 | m , μ , and f Range for Cancellation with $n = 4$ 136 |
| 9 | $\{ M(n) \}$ for $m_0 = 1$ 137 |
| 10 | $\{M(n)\}$ for $m_0 = 1$ 139 |
| 11 | $\{M(m_0)\}$ for the 4 Transducer Array Set for Cancellation. . 140, 207 |
| 12 | Steady State Error 177 |
| 13 | Sample Test Set 183 |
| 14 | Test Set for Modified Controller 194 |
| 15 | Frequency Range of Effective Cancellation 207 |
| 16 | Acoustic Phases for Optimal Cancellation of the $m_0 = 1$ Mode 208 |

LIST OF FIGURES

| Figure | | Page |
|--------|--|------|
| 1 | FAA Maximum Noise Limits for Certification | 1 |
| 2 | Takeoff Noise Levels - Present Aircraft | 3 |
| 3 | Approach Noise Levels - Present Aircraft | 5 |
| 4 | Current and Proposed Acoustical Treatment | 7 |
| 5 | Spinning Mode Synthesizer | 8 |
| 6 | Cylindrical Coordinate System | 10 |
| 7 | Circumferential Distribution of Sound Pressure | 12 |
| 8 | Radial Distributions of Sound Pressure | 16 |
| 9 | Radial Distributions of Sound Pressure Level | 17 |
| 10 | Transducer-Duct-Measurement System | 22 |
| 11 | Duct, SMS, and Probe Mechanism | 23 |
| 12 | Anechoic Termination | 24 |
| 13 | Spinning Mode Synthesizer | 24 |
| 14 | Amplitude and Phase Controller and Instrument Console. | 25 |
| 15 | Basic Duct Instrumentation | 27 |
| 16 | Probe Mechanism | 28 |
| 17 | Plate Microphone Mechanism | 29 |
| 18 | SPL versus Radial Distance at 6' from Plate for $m = 0$, $\mu = 1$ Mode at 1400 Hz | 34 |
| 19 | SPL versus Radial Distance at 6' from Plate for $m = 1$, $\mu = 0$ Mode at 690 Hz | 36 |
| 20 | SPL versus Radial Distance at 6' from Plate for $m = 1$, $\mu = 0$ Mode at 1240 Hz | 38 |

| Figure | Page |
|--------|---|
| 21 | SPL versus Radial Distance at 6' from Plate for $m = 1$, $\mu = 0$ Mode at 1560 Hz. 40 |
| 22 | SPL versus Radial Distance at 6' from Plate for $m = 1$, $\mu = 1$ Mode at 2180 Hz. 43 |
| 23 | Sound Pressure Level versus Frequency of Transducers in a Free Field at Constant Voltage at ($r = r_{oj}$, $\theta = \theta_{oj}$, $z = 0$) 51 |
| 24 | Phase Response versus Frequency of Transducers in a Free Field at Constant Voltage at ($r = r_{oj}$, $\theta = \theta_{oj}$, $z = 0$) 53 |
| 25 | Input Voltage versus SPL for a Single Transducer in a Free Field at ($r = r_{o1}$, $\theta = \theta_{o1}$, $z = 0$) 55 |
| 26 | SPL versus Frequency for a Transducer in a Free Field for Constant Voltages at ($r = r_{o1}$, $\theta = \theta_{o1}$, $z = 0$). . . 57 |
| 27 | $k_2(f)$ versus Frequency 60 |
| 28 | SPL and Phase Response versus Frequency at Constant Voltage (.9 volts) for Transducer 1 of the Ducted Array at ($r = r_{o1}$, $\theta = \theta_{o1}$, $z = 0$) 62 |
| 29 | SPL and Phase Response versus Frequency at Constant Voltage (.9 volts) for Transducer 2 of the Ducted Array at ($r = r_{o2}$, $\theta = \theta_{o2}$, $z = 0$). 64 |
| 30 | SPL and Phase Response versus Frequency at Constant Voltage (.9 volts) for Transducer 3 of the Ducted Array at ($r = r_{o3}$, $\theta = \theta_{o3}$, $z = 0$). 66 |
| 31 | SPL and Phase Response versus Frequency at Constant Voltage (.9 volts) for Transducer 4 of the Ducted Array at ($r = r_{o4}$, $\theta = \theta_{o4}$, $z = 0$). 68 |
| 32 | SPL and Phase Response versus Frequency at Constant Voltage (.9 volts) for Transducer 5 of the Ducted Array at ($r = r_{o5}$, $\theta = \theta_{o5}$, $z = 0$) 70 |
| 33 | SPL and Phase Response versus Frequency at Constant Voltage (.9 volts) for Transducer 6 of the Ducted Array at ($r = r_{o6}$, $\theta = \theta_{o6}$, $z = 0$). 72 |

| Figure | Page |
|--------|---|
| 34 | SPL and Phase Response versus Frequency at Constant Voltage (.9 volts) for Transducer 7 of the Ducted Array at $(r = r_{07}, \theta = \theta_{07}, z = 0)$ 74 |
| 35 | SPL and Phase Response versus Frequency at Constant Voltage (.9 volts) for Transducer 8 of the Ducted Array at $(r = r_{08}, \theta = \theta_{08}, z = 0)$ 76 |
| 36 | Angular Misalignment of Plate with Duct Centerline 77 |
| 37 | Displacement of Plate from Duct Centerline 78 |
| 38 | Plate Bolting Pattern 79 |
| 39 | SPL versus Radial Distance at 6' from Plate for $m = 1$, $\mu = 1$ Mode at 2000 Hz at a Circumferential Angle of 0 Radians with Respect to Transducer 1 of the Source Array 81 |
| 40 | Phase versus Radial Distance at 6' from Plate for $m = 1$, $\mu = 1$ Mode at 2000 Hz at a Circumferential Angle of 0 Radians with Respect to Transducer 1 of the Source Array 83 |
| 41 | SPL versus Radial Distance at 6' from Plate for $m = 1$, $\mu = 1$ Mode at 2000 Hz at a Circumferential Angle of $\frac{\pi}{4}$ Radians with Respect to Transducer 1 of the Source Array 85 |
| 42 | Phase versus Radial Distance at 6' from Plate for $m = 1$, $\mu = 1$ Mode at 2000 Hz at a Circumferential Angle of $\frac{\pi}{4}$ Radians with Respect to Transducer 1 of the Source Array 87 |
| 43 | Input Voltage versus SPL for a Single Transducer in the Ducted Array at $(r = r_{01}, \theta = \theta_{01}, z = 0)$ 90 |
| 44 | SPL versus Frequency for Transducer 1 of the Ducted Array at a Constant Voltage (.9 volts) at $(r = r_{01}, \theta = \theta_{01}, z = 0)$ 92 |
| 45 | SPL versus Frequency for Transducer 1 of the Ducted Array at a Constant Voltage (.9 volts) at $(r = r_{01}, \theta = \theta_{01}, z = 0)$ 94 |
| 46 | SPL versus Radial Distance at 2' from Plate for $m = 1$, $\mu = 0$ Mode at 750 Hz with Acoustic Parameters of each Transducer set by use of Plate Microphone 96 |

| Figure | Page |
|--------|--|
| 47 | Phase versus Radial Distance at 2' from Plate for m = 1, $\mu = 0$ Mode at 750 Hz with Acoustic Parameters of each Transducer set by use of Plate Microphone . . . 98 |
| 48 | SPL versus Radial Distance at 6' from Plate for m = 1, $\mu = 0$ Mode at 750 Hz with Acoustic Parameters of each Transducer set by use of Plate Microphone . . . 100 |
| 49 | Phase versus Radial Distance at 6' from Plate for m = 1, $\mu = 0$ Mode at 750 Hz with Acoustic Parameters of each Transducer set by use of Plate Microphone . . . 102 |
| 50 | SPL versus Radial Distance at 8' from Plate for m = 1, $\mu = 0$ Mode at 750 Hz with Acoustic Parameters of each Transducer set by use of Plate Microphone . . . 104 |
| 51 | Phase versus Radial Distance at 8' from Plate for m = 1, $\mu = 0$ Mode at 750 Hz with Acoustic Parameters of each Transducer set by use of Plate Microphone . . . 106 |
| 52 | Plant Schematic 111 |
| 53 | Cylindrical Coordinates of SMS 112 |
| 54 | Angle Between Cancelling Array and Source Array 114 |
| 55 | Acoustic Phases for m = 0, 1 and 2 for n = 4 120 |
| 56 | Generation of m = 4 Mode Above Cancelled m = 0 Mode . . . 130 |
| 57 | Generation of m = 3 Mode Over Cancelled m = 1 Mode. . . 132 |
| 58 | Generation of Cancelling Submodes 135 |
| 59 | Mathematical Plant Model 142 |
| 60 | A Hypothetical Realization of the Cost Function Surface 147 |
| 61 | One Dimensional Perturbation 155 |
| 62 | Realization of Cost Function in i th Dimension 158 |
| 63 | Two Dimensional, Single Frequency Perturbation 166 |
| 64 | Bias Voltage 175 |
| 65 | Steady State Error Due to Circular Perturbation 176 |

| Figure | | Page |
|--------|---|------|
| 66 | Schematic for Analog Simulation of Circular Perturbation System | 180 |
| 67 | Details of Special Elements | 182 |
| 68 | $\underline{x}(t)$ for $\underline{x}(0) = \begin{bmatrix} 8 \\ 8 \end{bmatrix}$ volts | 185 |
| 69 | $\underline{x}(t)$ for $\underline{x}(0) = \begin{bmatrix} -9 \\ 8 \end{bmatrix}$ volts | 185 |
| 70 | $J(t)$ for $\underline{x}(0) = \begin{bmatrix} 8 \\ 8 \end{bmatrix}$ volts | 187 |
| 71 | Modified Circular Perturbation Controller | 189 |
| 72 | Schematic of Modified Perturbation System | 193 |
| 73 | Optimal Convergence Response | 197 |
| 74 | Optimal Convergence Response | 197 |
| 75 | Optimal Load Change Response | 199 |
| 76 | Optimal Load Change Response | 199 |
| 77 | Single Dimensional Perturbation Adaptive Controller . . | 200 |
| 78 | Implementation of Narrowband Filter | 202 |
| 79 | Schematic for Analog Simulation of Modified Perturba- tion System with Bandpass Filter | 204 |
| 80 | SPL versus Radial Distance for $m = 0, \mu = 1$ Mode at 2000 Hz. | 211 |
| 81 | SPL versus Radial Distance for $m = 2, \mu = 0$ Mode at 1500 Hz. | 213 |
| 82 | Cylindrical Coordinate System | 223 |

NOMENCLATURE

| Symbol | Description | Units |
|-------------------|---|-------------------------|
| A | Perturbation amplitude | volts |
| A_y | Amplitude of sinusoidal information signal | volts |
| $A_{m\mu}$ | Amplitude coefficient in solution to wave equation | ft ² /sec |
| $A_{0\mu}$ | Amplitude coefficient in solution to wave equation for $m = 0$ | ft ² /sec |
| B | Number of fan or compressor blades | — |
| B | Controller bias voltage | volts |
| $B_{m\mu}$ | Amplitude coefficient in solution to wave equation | ft ² /sec |
| $B_{0\mu}$ | Amplitude coefficient in solution to wave equation for $m = 0$ | ft ² /sec |
| b | Duct radius | ft |
| $C_{m\mu}$ | Amplitude coefficient used in solution of wave equation | ft/sec |
| $C_{0\mu}$ | Amplitude coefficient used in solution of wave equation for $m = 0$ | ft/sec |
| c | Local speed of sound | ft/sec |
| $D_{m\mu}$ | Amplitude coefficient used in solution of wave equation | ft/sec |
| $D_{0\mu}$ | Amplitude coefficient used in solution of wave equation for $m = 0$ | ft/sec |
| d | End plate displacement | ft |
| dB | Decibel | dB |
| E | Expected value | — |
| $E_{m\mu}^\sigma$ | Amplitude coefficient in solution to wave equation | lbf-sec/ft ⁵ |
| $E_{m\mu}$ | Amplitude coefficient in solution to wave equation for $\sigma = 0$ | lbf-sec/ft ⁵ |

| Symbol | Description | Units |
|------------------------------|--|-----------------------------------|
| EPNdB | Effective perceived noise level in decibels "It embodies the results of extensive psychological measurements of the relative "noisiness" or "annoyance" of aircraft-flyover sounds." (13) It embodies correction for loudness level, duration, and puretone content. | dB |
| e | Error | volts |
| e _{ss} | Steady state error | volts |
| F _{mμ} | Amplitude coefficient used in the determination of the index of performance for the effectiveness of reduction of {Re[P]} ² | lbf-sec/ft ⁴ |
| f | Frequency | Hz |
| f(r,θ,0) | Amplitude of velocity at source | ft/sec |
| f _{mμ} | Cutoff frequency | Hz |
| G _{mμ} | Partial solution to wave equation | ft ³ /sec |
| g | Function relating pressure to e ^{±imθ} | lbf/ft ² |
| H _{mμ} | Partial solution to wave equation | ft ³ /sec |
| IP | Index of performance for the effectiveness the reduction of {Re [P]} ² | lbf ² /ft ⁴ |
| i | Complex number $\sqrt{-1}$ | — |
| J | Cost function relating SPL to the input parameters | volts |
| J _m | Bessel function of the first kind of order m | — |
| K _{mμ} | Part of solution to wave equation | ft ³ /sec |
| k(f) | Frequency dependent parameter in equation for transducer response | dB |
| k _{mμ} ^σ | Eigenvalue of order μ for the m th mode having a hub-tip ratio σ | 1/ft |

| Symbol | Description | Units |
|----------------------------------|--|----------------------|
| $k_{m\mu}$ | Eigenvalue of order μ for the m^{th} mode having a hub-tip ratio $\sigma = 0$ | 1/ft |
| $k_{o\mu}, k_{oq}$ | Eigenvalues of order μ and q with $m = 0$ and $\sigma = 0$ | 1/ft |
| $L_{m\mu}^{\sigma}$ | Amplitude coefficient in solution to wave equation | — |
| $L_{m\mu}$ | Amplitude coefficient in solution to wave equation for $\sigma = 0$ | — |
| ℓ | Integer numbers $0, \pm 1, \pm 2, \dots$ | — |
| {M} | Set of modes | — |
| $\{M_{m\mu}\}$ | Set of modes restricted to specified m and μ | — |
| m | Circumferential mode number | — |
| m_o | Desired circumferential mode | — |
| N | Angular speed of rotor shaft | cycles/sec |
| N_e | Signal processing error | — |
| $N(x)$ | Random process, function of representative variable x | — |
| n | Number of transducers | — |
| n' | Harmonic number | — |
| $P(r, \theta, z, t)$ | Pressure solution to wave equation | lbf/ft ² |
| $\bar{P}(i\omega, r, \theta, z)$ | Complex amplitude of pressure solution to wave equation | lbf/ft ² |
| $P_{m\mu}$ | Amplitude coefficient used in solution of wave equation | ft ² /sec |
| p | RMS sound pressure | lbf/ft ² |
| Q_{oj} | Source strength of j^{th} source array transducer | ft ³ /sec |
| q_{oj} | Source strength of j^{th} cancelling array transducer | ft ³ /sec |

| Symbol | Description | Units |
|-----------------|--|------------------------------------|
| $R(r)$ | Radial component of solution to wave equation | — |
| Re | Denotes the "real part of" | — |
| r | Radial cylindrical coordinate | ft. |
| r_0 | Radius of circular transducer array | ft. |
| S | Slope | depends on application |
| SPL | Sound Pressure Level in decibels | dB |
| s | Laplace transform variable | — |
| $T(t)$ | Time component of solution to wave equation | — |
| t | Time | sec |
| $U(t)$ | Information signal for adaptive controller | volts |
| V_{oj} | Electrical voltage to j^{th} source transducer | volts |
| v | Amplitude input parameter to plant | volts |
| v | Number of fan or compressor vanes | — |
| \underline{v} | Particle velocity | ft/sec |
| v_s | Particle velocity a source | ft/sec |
| v_{oj} | Electrical voltage to j^{th} cancelling transducer | volts |
| x_i | System state variable | units of i^{th} dimension |
| x_{io} | Operating position of system in i^{th} system dimension | units of i^{th} dimension |
| x_m | Distance from x_{iopt} to x_{io} | units of i^{th} dimension |

| Symbol | Description | Units |
|------------------------|---|------------------------------------|
| $x_{i\text{opt}}$ | Position of minimum in i^{th} system dimension | units of i^{th} dimension |
| $Y(t)$ | Filtered output of simulated system | volts |
| Y_m | Bessel function of the second kind of order m | — |
| $Z(z)$ | Axial component of solution to wave equation | — |
| z | Axial cylindrical coordinate | feet |
| α | Phase angle parameter of controller | radians |
| α_{oj} | Acoustic phase of the j^{th} cancelling array transducer | radians |
| β | Weighting factor | — |
| β_1, β_2 | Phase lags | radians |
| γ^* | Angle of the negative gradient direction of J on the (X_1, X_2) plane | radians |
| γ^1 | Aberrant value of γ^* | radians |
| $\gamma_{m\mu}^\sigma$ | Wave number in the axial direction | 1/ft. |
| $\gamma_{m\mu}$ | Wave number in the axial direction for $\sigma = 0$ | 1/ft |
| $\gamma_{0\mu}$ | Wave number in the axial direction for $m = 0$ and $\sigma = 0$ | 1/ft |
| Δ | Angle between adjacent transducers on plate | radians |
| ϵ_m | Discrete weighting functions | — |
| $\Theta(\theta)$ | Circumferential component of solution to wave equation | — |
| θ_{oj} | Electrical phase to j^{th} source transducer | radians |
| θ | Angular cylindrical coordinate | radians |

| Symbol | Description | Units |
|----------------------------------|---|---|
| μ | Radial mode number | — |
| Π | Denotes Product | — |
| ρ | Density | Slugs/ft ³ or lbf-sec ² /ft ⁴ |
| Σ | Denotes Summation | — |
| σ | Hub-tip ratio (ratio of the radius of the duct center section to the duct radius b) | — |
| σ_N | Standard deviation of random process N | — |
| $\Phi(r,\theta,z,t)$ | Velocity potential | ft ² /sec. |
| $\bar{\Phi}(i\omega,r,\theta,z)$ | Complex amplitude of velocity potential | ft ² /sec. |
| ϕ_{oj} | Acoustic phase of j th source array transducer | radians |
| ω | Acoustic frequency | radians/sec. |
| ω_1 | Perturbation frequency | radians/sec. |
| $ \quad $ | Denotes "norm" | — |
| ∇^2 | Laplacian operator | — |
| L | Laplacian operator | — |

Subscripts

| | |
|-------|-----------------------------|
| m | Circumferential mode number |
| μ | Radial mode number |
| j | Summing index |
| k | Summing index |
| ref | Reference |
| - | Vector notation |
| q | Summing index |

Superscripts

| | |
|-------|---|
| ' | Differential with respect to argument |
| * | Optimal |
| ~ | Value determined by Stochastic analysis |
| <hr/> | Average |
| T | Transpose |

ABSTRACT

The reduction of the discrete tones generated by jet engines is essential for jet aircraft to meet present and proposed noise standards. Present reduction methods based on acoustic duct treatment are plagued by high cost, as well as severe weight, efficiency, and maintenance penalties. The discrete tones generated by the blades and vanes propagate in the inlet and exhaust duct in the form of spiraling acoustic waves, or spinning modes. The reduction of these spinning modes by the cancellation effect of the combination of two acoustic fields is the thrust of this research.

The Spinning Mode Synthesizer has provided the means for effective study of this noise reduction scheme. Two sets of electrical-acoustical transducers located in an equally-spaced circular array simultaneously generate a specified spinning mode and the cancelling mode. Analysis of the wave equation for the synthesizer has established the optimum cancelling array acoustic parameters for maximum sound pressure level reduction. The parameter dependence of the frequency ranges of propagation of single, specified circumferential modes generated by a single array, and of effective cancellation of the modes generated by two arrays, has been determined. Substantial sound pressure level reduction has been obtained for modes within these limits.

Analysis of the system has shown that adaptive control is necessary for the closed-loop maximization of cancellation. A two-dimensional, perturbation type, gradient-adaptive controller has been developed. Analog simulation has yielded favorable convergence and load change response. This research has established a firm basis for the development of the cancellation system for fan-duct sources.

I. Introduction

1.1 Background to Problem

The aviation industry is currently facing technologically demanding and financially burdensome noise restrictions. The Federal Aviation Administration has been empowered by Public Law 90 - 411, "Control and Abatement of Aircraft Noise and Sonic Boom", to establish rules and regulations for the control of aircraft noise. Certification noise limits for new aircraft have since been established and are shown in Figure 1. These limits are for a three point certification test.

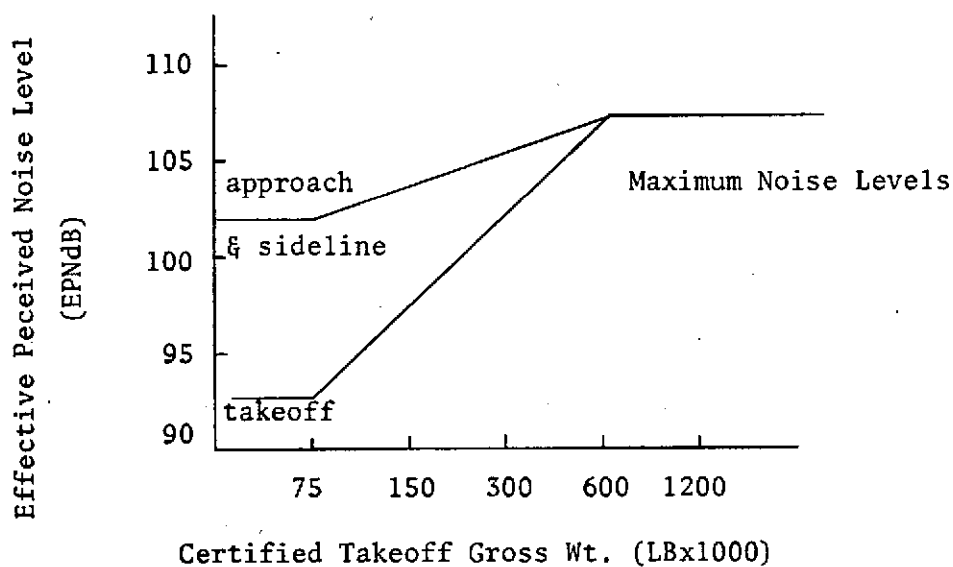


FIGURE 1 (Reference 1)

FAA Maximum Noise Limits for Certification

As shown in Figures 2 and 3, current aircraft, with few exceptions, do not meet the certification requirements. Future reduction of certification noise limits can be expected.

FIGURE 2

(Reference 1)

Takeoff Noise Levels - Present Aircraft

(3.5 N. miles @ 1000 ft.)

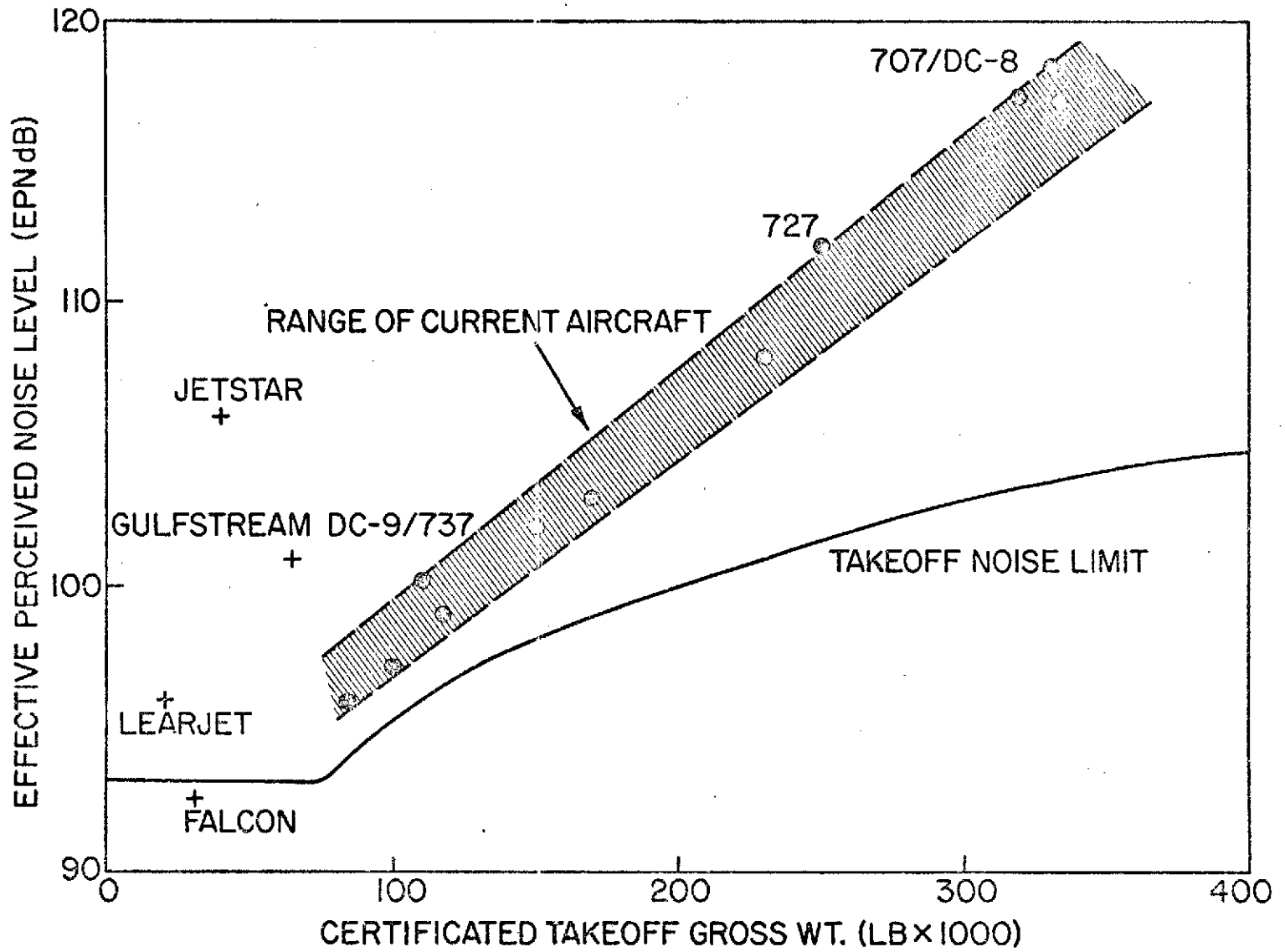
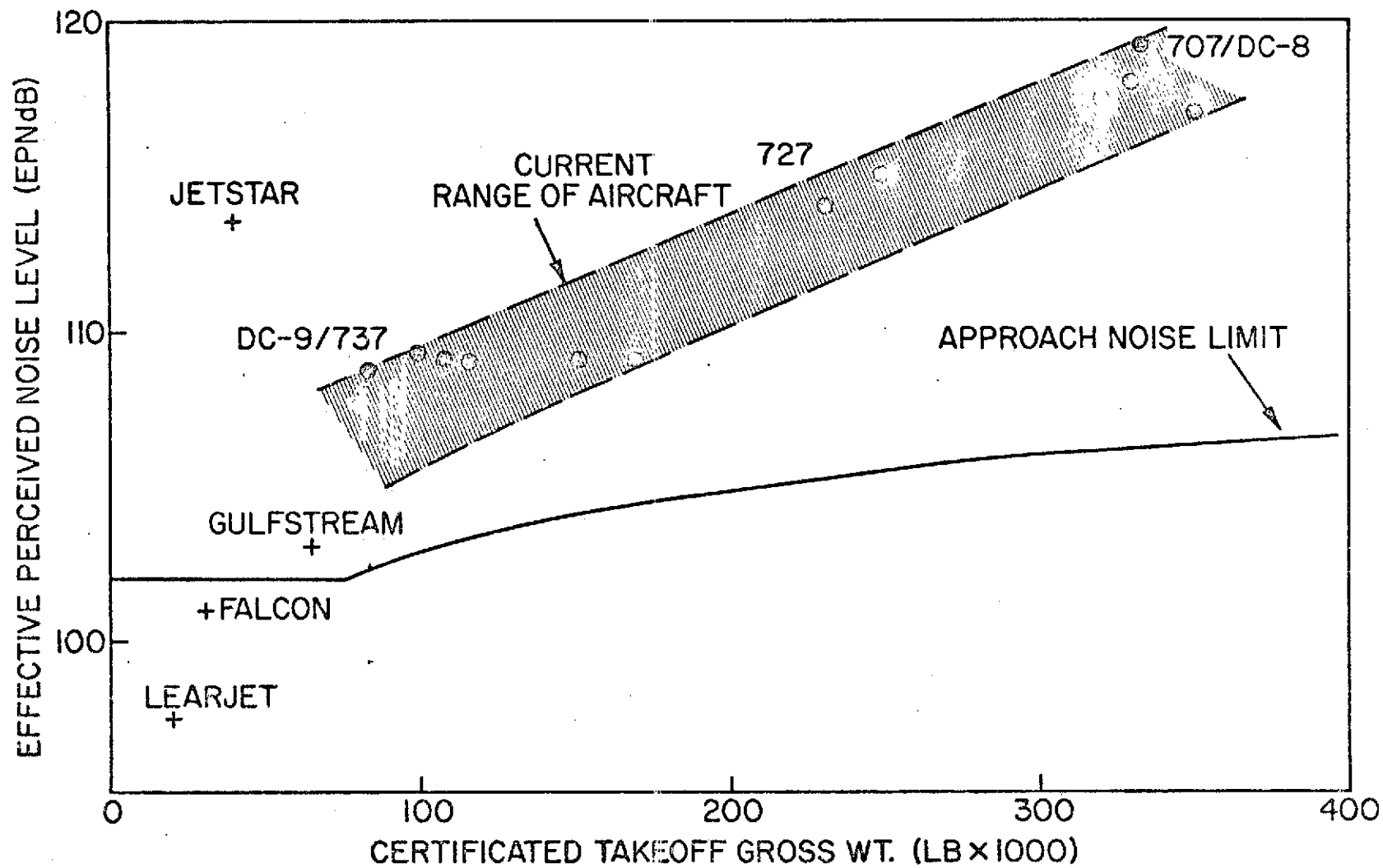


FIGURE 3

(Reference 1)
Approach Noise Levels - Present Aircraft

(1.0 N. miles on 3° Glide Slope)



The early pure jet engines such as the Pratt & Whitney JT3C (for the Boeing 707's) or the General Electric CJ 805-3 produced broad band noise at high sound pressure levels. These unacceptably high broad band noises were reduced a few dB's by recourse to multiple tube jet nozzles. After much research, it was established that such pure jets were inherently noisy with little chance to substantially reduce noise without unacceptable thrust losses.

Since this jet noise is proportional to anywhere from the 6th to the 8th power of the jet velocity the next generation of engines utilised medium bypass ratio fans. This resulted in much higher airflows and reduced jet velocities thereby reducing the jet noise problem. The early fan engines such as Pratt & Whitney JT3D and JT4D (for Boeing's 707 and 720, and Douglas' DC8's) produced high levels of noise resulting from the high speed fans. This fan noise is characterized by pure tones at the blade passage frequency and harmonics giving the typical "whine" of these aircraft.

Extensive research has been conducted on noise reduction schemes for these engines. Substantial noise reductions have been obtained by proper selection of the primary cycle variables. The design of the bypass ratio and the fan pressure ratio consistent with mission and noise considerations has later resulted in quieter engines due to reduced flow noise.

Jet noise and pure tones from the fan, compressor, and turbine are of concern. The reduction of the dominant pure tone noises for these later engines is especially important for the EPNdB rating where pure tones are penalized. The installation of acoustical treatment in the

engine ducts and acoustically treated splitters has been shown to provide effective pure tone reduction, but with high cost, as well as weight, efficiency, and maintenance penalties. Current and proposed acoustical treatment is illustrated in Figure 4.

To reduce these adverse effects the possibility of acoustically cancelling the pure tones appeared very attractive, provided this feat could be accomplished economically. The cancellation device would only operate on take-off and landing and thus not effect mission performance except for

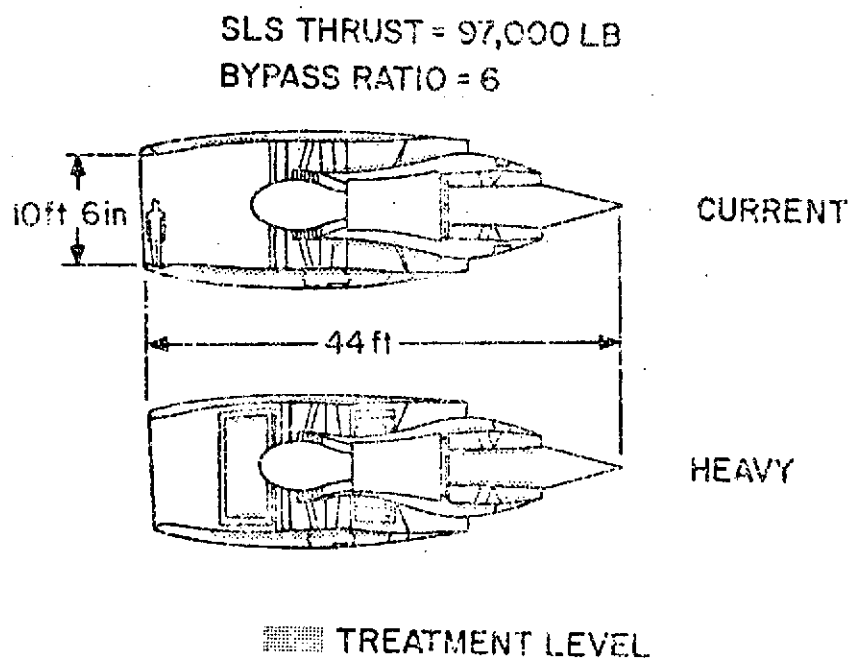


FIGURE 4 (Ref. 3)

Current and Proposed Acoustical Treatment

the additional weight which would conceivably be less than the added weight of the acoustically treated ducts.

1.2 Spinning Mode Synthesizer

Pure tone noise reduction schemes have been tested on fan-duct systems. Broad band noise and the wide spectrum of modes of sound generated in a fan-duct system have made meaningful parameter variation studies difficult. The synthesis of these pure tones, or spinning modes of sound, would allow the isolation of specific modes. Effective analysis of noise reduction schemes could then be conducted.

In order to accomplish this isolation of individual duct modes, the Spinning Mode Synthesizer (SMS) was developed at the Noise Control Laboratory of The Pennsylvania State University to generate spinning modes of sound of controlled complexity without the generation of broad band noise (8, 14). The SMS consists of a circular array of electrical-acoustical transducers (commercial loudspeakers) mounted on a flat plate, as shown in Figure 5.

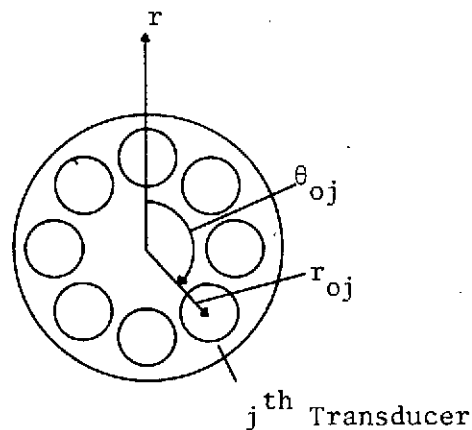


FIGURE 5

Spinning Mode Synthesizer

The transducer locations can be specified by:

$$z_0 = \text{axial position of array}$$

$$= 0$$

$$r_{0j} = \text{radial distance of } j^{\text{th}} \text{ transducer at } z = 0$$

$$= r_0, j = 1, 2, \dots, n, \text{ where } n \text{ is the number of transducers}$$

$$\theta_{0j} = \text{angular position of } j^{\text{th}} \text{ transducer at } z = 0$$

$$= \frac{2\pi}{n} (j - 1) \text{ radians, } j = 1, 2, \dots, n$$

The sound field within the ducts of a jet engine can be described by the wave equation for ducts of arbitrary shape. A logical basis for the study of the modes of sound associated with such a system would be provided by a semi-infinite, constant-radius, rigid-walled duct. This acoustic environment has been approximated by placing the Spinning Mode Synthesizer at the source end of a terra cotta duct having an anechoic termination. This acoustic system, together with the analytical background provided by Tyler and Sofrin (4), Lawson (5), and others (6,7), provides a basis for meaningful studies of spinning modes of sound.

A general analytical model has been established for a ducted acoustic system by the solution of the wave equation for a semi-infinite duct (See Appendix 1). For the system shown in Figure 6,

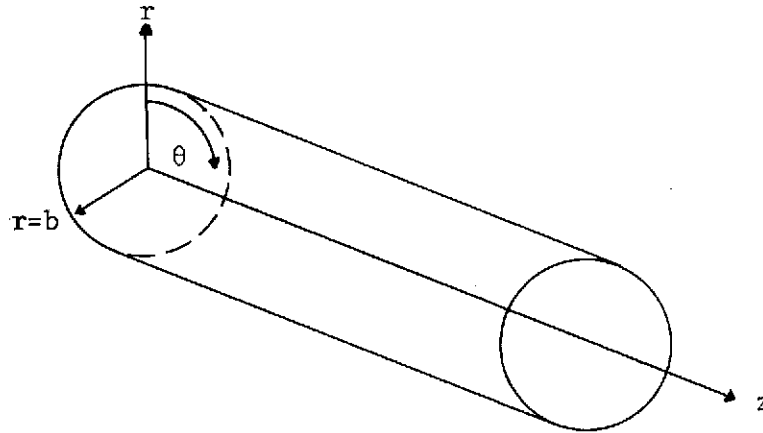


FIGURE 6
Cylindrical Coordinate System

we have

$$\nabla^2 \Phi (r, \theta, z, t) = \frac{1}{c^2} \frac{\partial^2 \Phi (r, \theta, z, t)}{\partial t^2}$$

where Φ is the acoustic velocity potential (Reference 15) and the ∇^2 operator for the cylindrical coordinate system is given by:

$$\nabla^2 = \frac{1}{r} \left[\frac{\partial}{\partial r} \left(r \frac{\partial}{\partial r} \right) \right] + \frac{1}{r^2} \frac{\partial^2}{\partial \theta^2} + \frac{\partial^2}{\partial z^2}$$

An assumed solution of the form

$$\Phi = R (r) \Theta (\theta) Z(z) T(t)$$

with an assumed sinusoidal input, the homogeneous boundary conditions

$$1) \quad \Theta (\theta) = \Theta (\theta + 2\pi)$$

$$2) \frac{\partial \theta(\theta)}{\partial \theta} = \frac{\partial \theta(\theta) + 2\pi}{\partial \theta}$$

$$3) \left. \frac{\partial R(r)}{\partial r} \right|_{r=b} = 0,$$

the inhomogeneous boundary condition

$$\left. \frac{v_z}{z} \right|_{z=0} = f(r, \theta, 0) e^{-i\omega t},$$

and the boundedness condition

$$1) R(0) = \text{finite}$$

yields an acoustic pressure field

$$P(r, \theta, z, t) = i \omega P \Phi$$

$$P = \sum_{m=0}^{\infty} \sum_{\mu=0}^{\infty} E_{m\mu} [G_{m\mu} e^{im\theta} + H_{m\mu} e^{-im\theta}] \cdot J_m(k_{m\mu} r) e^{i(\gamma_{m\mu} z - \omega t)}$$

The amplitude coefficients $E_{m\mu}$, $G_{m\mu}$, and $H_{m\mu}$ are given in Appendix 1. See nomenclature or Appendix 1 for parameter definitions.

The circumferential mode number m and the radial mode number μ are two basic descriptive parameters. The concepts associated with these parameters can be best explained by an examination of the appropriate components of the pressure solution.

The circumferential dependence of pressure can be shown by

$$P = g_+ e^{im\theta} + g_- e^{-im\theta}$$

where m is a non-negative integer. This reduces to

$$\text{Re. [P]} \rightarrow |g| \cos m \theta$$

Therefore, the circumferential distribution consists of m cycles of a cosine wave, as illustrated by Figure 7.

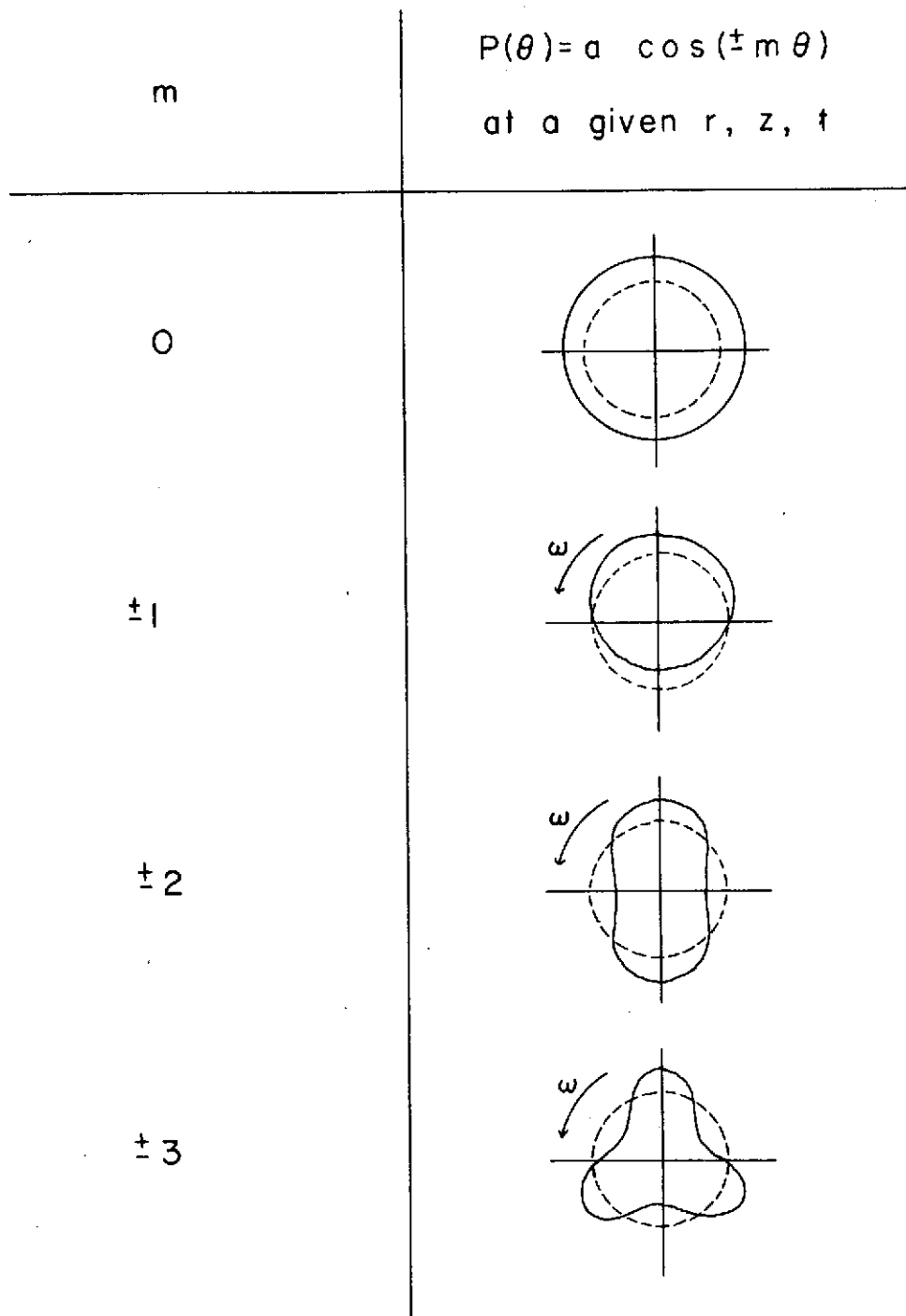


FIGURE 7

Circumferential Distribution of Sound Pressure

The radial distribution is governed by the boundary condition:

$$\left. \frac{\partial R}{\partial r} \right|_{r=b} = 0$$

where R = radial component of solution to wave equation

r = radial parameter

b = duct radius

From the solution of the wave equation for the system, we have

$$\left. \frac{\partial}{\partial r} [J_m(k_{m\mu} r)] \right|_{r=b} = 0$$

or

$$J'_m(k_{m\mu} b) = 0$$

where J_m = Bessel function of the first kind of order m

$k_{m\mu}$ = eigenvalue of order μ for the m^{th} mode having a hub-tip ratio

$$\sigma = 0$$

The values of $k_{m\mu} b$, for m and μ , that satisfy the equation are given in Table 1.

TABLE 1

Roots of $J'_m(k_{m\mu} b) = 0$

| $k_{m\mu} b$ | $\mu = 0$ | $\mu = 1$ | $\mu = 2$ | $\mu = 3$ | $\mu = 4$ |
|--------------|-----------|-----------|-----------|-----------|-----------|
| m = 0 | 0 | 3.830 | 7.012 | 10.168 | 13.317 |
| m = 1 | 1.840 | 5.328 | 8.522 | 11.700 | 14.856 |
| m = 2 | 3.053 | 6.703 | 9.964 | 13.164 | 16.339 |
| m = 3 | 4.199 | 8.011 | 11.340 | 14.578 | 17.780 |
| m = 4 | 5.315 | 9.278 | 12.675 | 15.955 | 19.186 |

The nature of propagation is determined from the term $e^{i\gamma_{m\mu}z}$ in the solution to the wave equation (see Appendix 1). The wave number, $\gamma_{m\mu}$, in the axial direction, is given by

$$\gamma_{m\mu} = \sqrt{\frac{\omega^2}{c^2} - k_{m\mu}^2}.$$

For $\gamma_{m\mu}$ to be real,

$$\frac{\omega}{c} > k_{m\mu}$$

or

$$f > \frac{k_{m\mu} c}{2\pi}$$

The frequency at which $\gamma_{m\mu} = 0$ is defined as the "cutoff" frequency,

$f_{m\mu}$:

$$f_{m\mu} = \frac{(k_{m\mu} b) c}{2\pi b}$$

where $b = .5$ ft. and $k_{m\mu}$ is given in Table 1. The "cutoff" frequencies for m and μ are given in Table 2.

TABLE 2
Cutoff Frequencies for One Foot Diameter Duct

| $f_{m\mu}$ | $\mu = 0$ | $\mu = 1$ | $\mu = 2$ | $\mu = 3$ | $\mu = 4$ |
|------------|-----------|-----------|-----------|-----------|-----------|
| $m = 0$ | 0 | 1378 | 2524 | 3660 | 4794 |
| $m = 1$ | 662 | 1918 | 3067 | 4212 | 5348 |
| $m = 2$ | 1099 | 2413 | 3587 | 4739 | 5882 |
| $m = 3$ | 1511 | 2883 | 4082 | 5248 | 6400 |
| $m = 4$ | 1913 | 3340 | 4563 | 5744 | 6906 |

Duct resonance occurs at $\gamma_{m\mu} = 0$ or $f = f_{m\mu}$. For $\gamma_{m\mu}$ real, or $f > f_{m\mu}$, the exponential term is complex and the mode propagates. For $\gamma_{m\mu}$ complex, or $f < f_{m\mu}$, the mode decays exponentially with axial distance since the exponential term is real and negative. The decay rate decreases as frequency increases and approaches zero as the frequency approaches the cutoff frequency.

The radial distribution of the pressure field inside a duct with no center section is given by $J_m(k_{m\mu} r)$ where m and μ are specified for a particular mode. The distributions for low order m and μ are shown in Figure 8. The radial mode number μ thus corresponds to the number of times $\frac{P}{P_{\max}}$ crosses the r - axis in Figure 8.

High intensity spinning modes with circumferential distribution m and radial distribution μ are generated by assigning all transducers equal source strength Q , by operating above the cutoff frequency for

the specified mode, and by assigning the j^{th} transducer the acoustic phase

$$\phi_{oj} = \frac{2\pi m}{n} (j - 1) \text{ radians, } j = 1, 2, \dots, n$$

where n is the number of transducers.

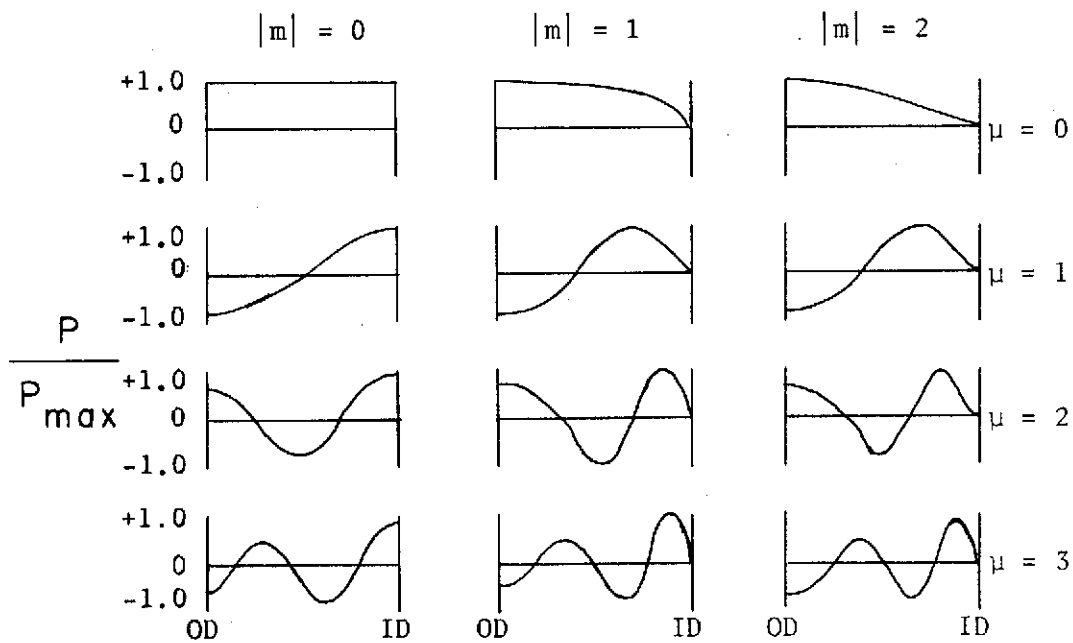


FIGURE 8

Radial Distributions of Sound Pressure

A set of modes $\{M\}$ is defined to contain the modes which can be excited by a given source amplitude and phase configuration. Although m must be positive for the wave equation analysis, both positive and negative m will be allowed in this set. The negative sign will designate spin in the opposite direction of the synthesized shaft rotation.

Amplitude measurements were made in terms of sound pressure level, which is given by

$$\text{SPL} = 20 \log_{10} \frac{p}{p_{\text{ref}}}$$

where p = rms sound pressure

$$p_{\text{ref}} = .0002 \text{ dynes/cm}^2.$$

The radial distribution of sound pressure level for low order m and μ are shown in Figure 9.

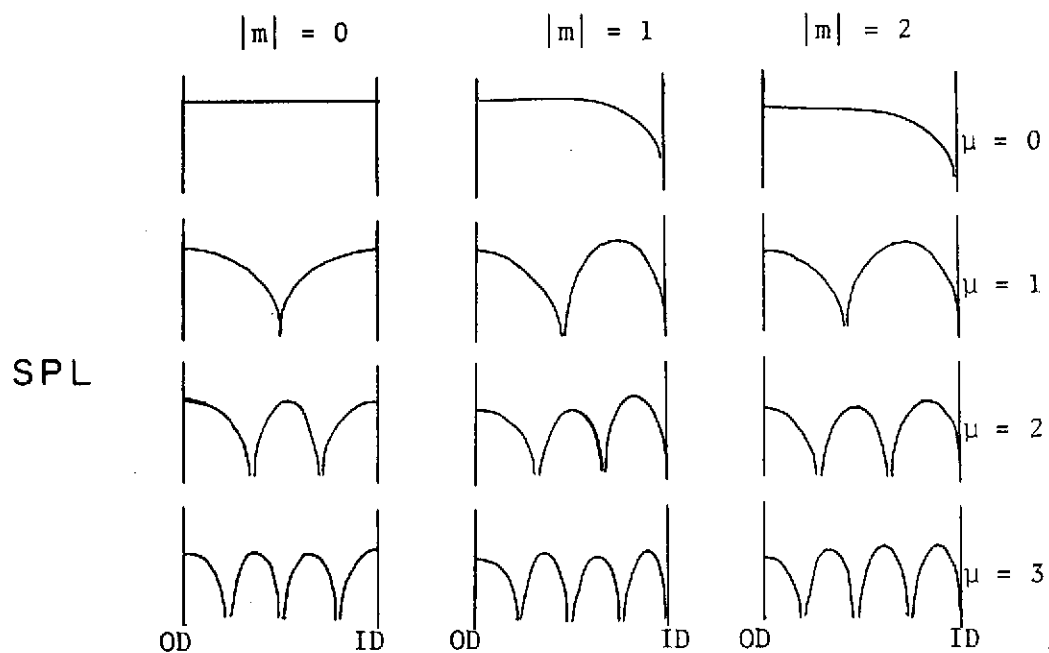


FIGURE 9

Radial Distributions of Sound Pressure Level

1.3 The Cancellation Concept

The high intensity discrete tones generated by rotor-stator interaction propagate in the ducts of jet engines in the form of complex spinning waves. But, only a few modes associated with any given interaction propagate unattenuated. The reduction of these modes could therefore provide a substantial reduction of the pure tone noise.

A method for the reduction of these spinning modes is the subject of this research project at The Pennsylvania State University. It has been proposed to reduce the sound pressure level of the unattenuated spinning modes of sound generated by a jet engine by the cancellation effect of the combination of two acoustic fields having equal amplitudes but opposite phase. Cancellation would be maximized by the optimization of an amplitude parameter and a phase parameter of another spinning mode source.

The Spinning Mode Synthesizer provides the means for effective study of this noise reduction scheme. In addition, a modified SMS can be used as the source for the cancelling acoustic field in actual application. The cancellation of simulated pure tone fan noise forms the basis for this investigation.

The noise source and cancelling source can be simulated simultaneously by the SMS by assigning half its transducers to each source. To obtain the necessary symmetry for proper mode excitation, every other transducer is assigned to the source array with the interstitial transducers being assigned to the cancelling array. The letter "n" shall designate the number of transducers in each array (4 for the case of an 8-transducer SMS) and the subscript j shall represent the j^{th}

transducer of the array in question. The acoustic phase formula presented in Section 1.2 applies to the source array. The optimal parameter solution for the cancelling array is to be determined.

By simple waveform analysis, the optimal solution for the minimization of the spinning mode for a field generated by a circular transducer array source given by

$$\begin{aligned} r_{oj} &= \text{radial distance of } j^{\text{th}} \text{ transducer} & (1.3-1) \\ &= r_o, \quad j = 1, 2, \dots, n \end{aligned}$$

$$\begin{aligned} \theta_{oj} &= \text{angular position of } j^{\text{th}} \text{ transducer} & (1.3-2) \\ &= \frac{2\pi}{n} (j - 1), \quad j = 1, 2, \dots, n \end{aligned}$$

having

$$\begin{aligned} Q_{oj} &= \text{source strength of } j^{\text{th}} \text{ transducer} & (1.3-3) \\ &= Q_o, \quad j = 1, 2, \dots, n \end{aligned}$$

$$\begin{aligned} \phi_{oj} &= \text{acoustic phase of } j^{\text{th}} \text{ transducer} & (1.3-4) \\ &= \frac{2\pi m}{n} (j - 1), \quad j = 1, 2, \dots, n \end{aligned}$$

by a circular cancelling transducer array positioned at

$$r_{oj} = r_o, \quad j = 1, 2, \dots, n \quad (1.3-5)$$

$$\theta_{oj} = \frac{2\pi}{n} (2j - 1) + \frac{\pi}{n}, \quad j = 1, 2, \dots, n \quad (1.3-6)$$

is expected to be

$$\begin{aligned} q_{oj} &= \text{source strength of } j^{\text{th}} \text{ transducer} & (1.3-7) \\ &= Q_o, \quad j = 1, 2, \dots, n \end{aligned}$$

$$\alpha_{oj} = \text{acoustic phase of } j^{\text{th}} \text{ transducer} \quad (1.3-8)$$

$$= \frac{m\pi}{n} (2j - 1) + \pi, \quad j = 1, 2, \dots, n.$$

It is assumed that both arrays are driven at the same frequency. Successful test cases utilizing the principles of the above solution were obtained previous to this author's investigation.

1.4 Automatic Control of Cancellation

The radial and circumferential distribution of spinning waves generated by a jet engine depend upon engine parameters and operating conditions. The numbers of blades and vanes in a rotor-stator set and the engine rpm are related directly to the blade passage frequency,

$$f = n' B N$$

where

f = blade passage frequency

n' = harmonic number

B = number of blades

N = angular speed of shaft in cps

which determines the modes generated by rotor-stator interaction. The rotor speed alone determines the modes generated by the rotor only. Throttle setting and air speed are major factors in variation of blade loading, and thus the pressure fields which generate spinning modes. The magnitude of the pressure fields along with duct geometry determine the amplitudes of the spinning modes generated.

Engine RPM, throttle setting, and air speed are time variables. In control systems context, these parameters are slowly time varying. Thus there will be time variation of the dominant modal distributions and wave parameters. The reduction of the sound pressure level of the dominant modes by a cancellation technique will therefore require automatic control.

The development of automatic control for the Spinning Mode Synthesizer used in this research will provide the background necessary for the application of these approaches to full scale. The automatic control design objective will provide an organized approach to the investigation of the system. The implementation of automatic control would enable efficient parameter variation, and thus rigorous evaluation of the synthesizer and of the cancellation concept. The design and development of an automatic controller is thus the intended scope of this research.

II. Experimental Verification of In-Duct Sound Pressure Level Reduction by Cancellation

2.1 Description of Apparatus

The Spinning Mode Synthesizer was operational at the start of this research. The transducer-duct-measurement system is shown schematically in Figure 10.

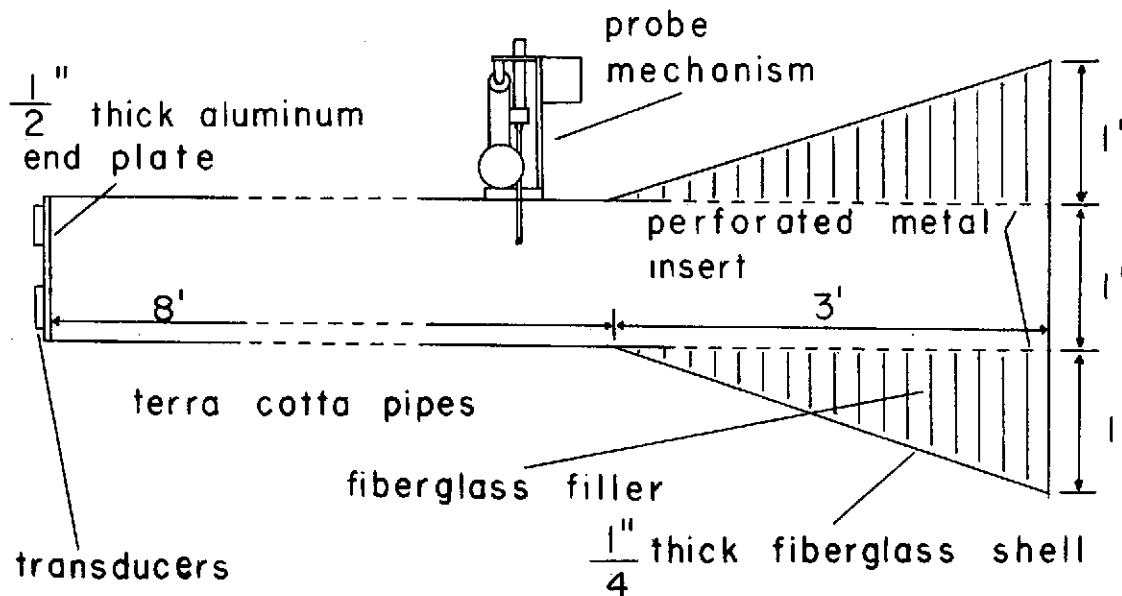


FIGURE 10

Transducer-Duct-Measurement System

The duct consists of four terra cotta pipe sections (Figure 11), which provided an inexpensive, acoustically rigid duct. The anechoic termination (Figure 12) reduces acoustic boundary effects and provides an approximation to an infinite duct with all waves travelling in the positive axial direction. The duct diameter is 12 inches.

The Spinning Mode Synthesizer as developed by John M. Seiner (8) consists of the end plate, transducers, and control electronics. Figure 13 shows the end plate and transducers. The transducer amplitude and phase controller is shown in Figure 14.

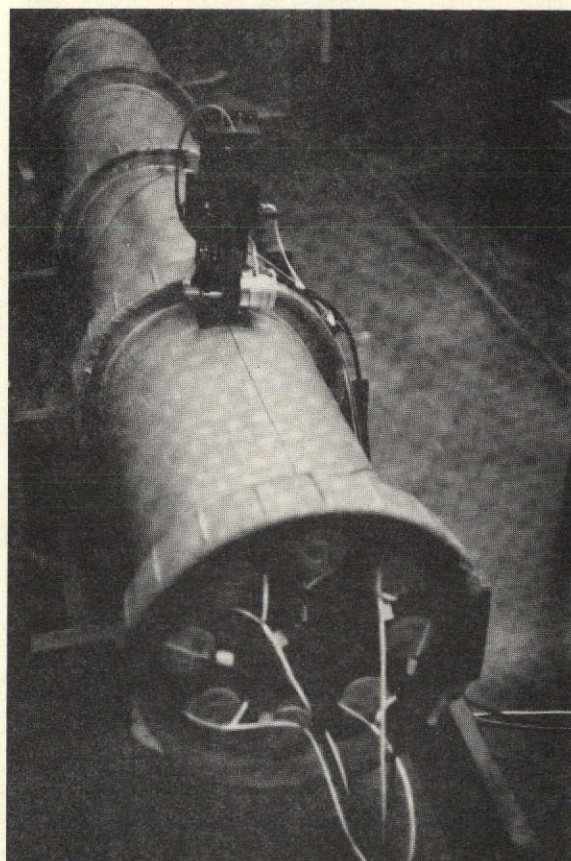


Figure 11

Duct, SMS, and Probe Mechanism



Figure 12
Anechoic Termination

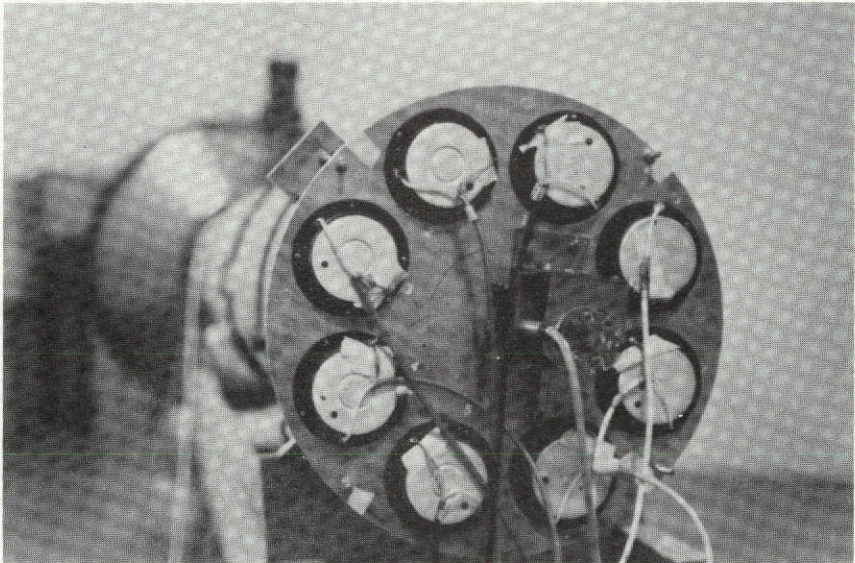


Figure 13
Spinning Mode Synthesizer

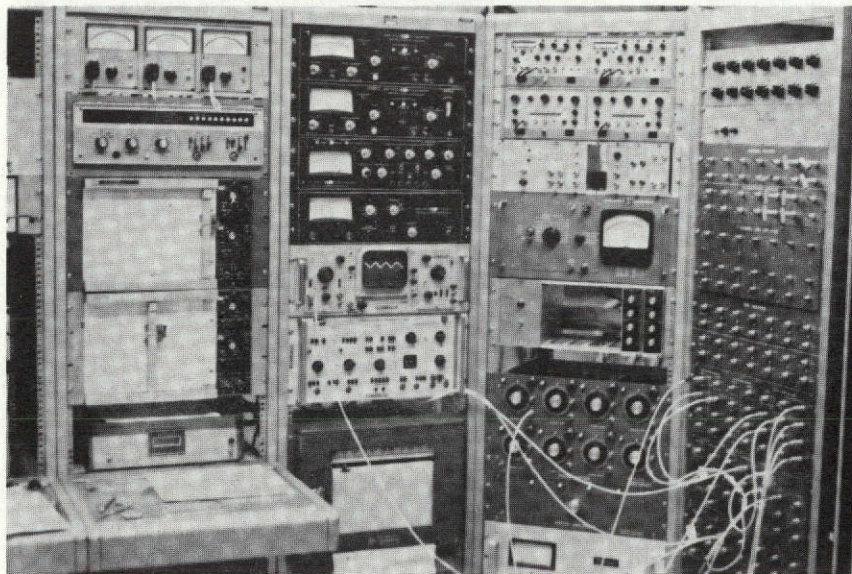
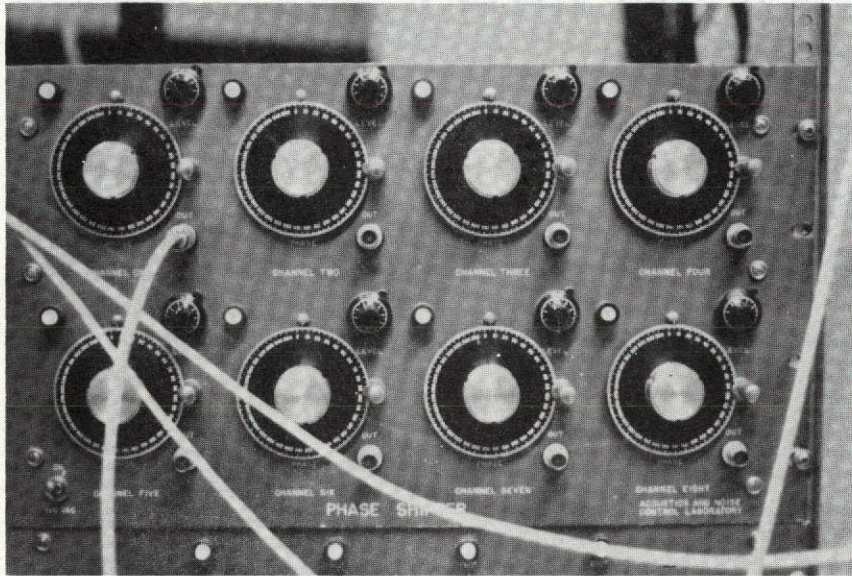


Figure 14

Amplitude and Phase Controller and Instrument Console

The basic duct instrumentation is shown in Figure 15. A well equipped console was available (Figure 14) so other instrumentation schemes were utilized when needed.

In-duct measurements were made by several systems. The probe mechanism (Figure 16) is a microphone probe capable of continuously traversing the duct radially from the center to the wall of the duct at selected circumferential and axial positions. The abscissa for radial X-Y recorder plot distributions was obtained by generating an electrical signal proportional to radial distance by a potentiometer circuit (Figure 15). Two probe mechanisms and two recorders were used to accelerate testing.

Measurements near the transducers were obtained by a plate-supported microphone mechanism (Figure 17). The microphone was positioned manually to a point centered on the transducer and flush with the protective screen, as illustrated in Figure 17. This results in approximately a quarter inch distance from the transducer membrane to the microphone diaphragm. For the frequency range under consideration, 500 Hz. to 6000 Hz., the wavelengths exceed the 1/2 inch transducer radius, so such a close measurement position is allowed. To position the microphone circumferentially the transducer under concern was operated at low voltage. The microphone was then positioned by maximizing the amplitude of the measurement signal, which was observed on an oscilloscope. It is important to note at this time that all sound pressure level measurements were made with respect to 1 volt.

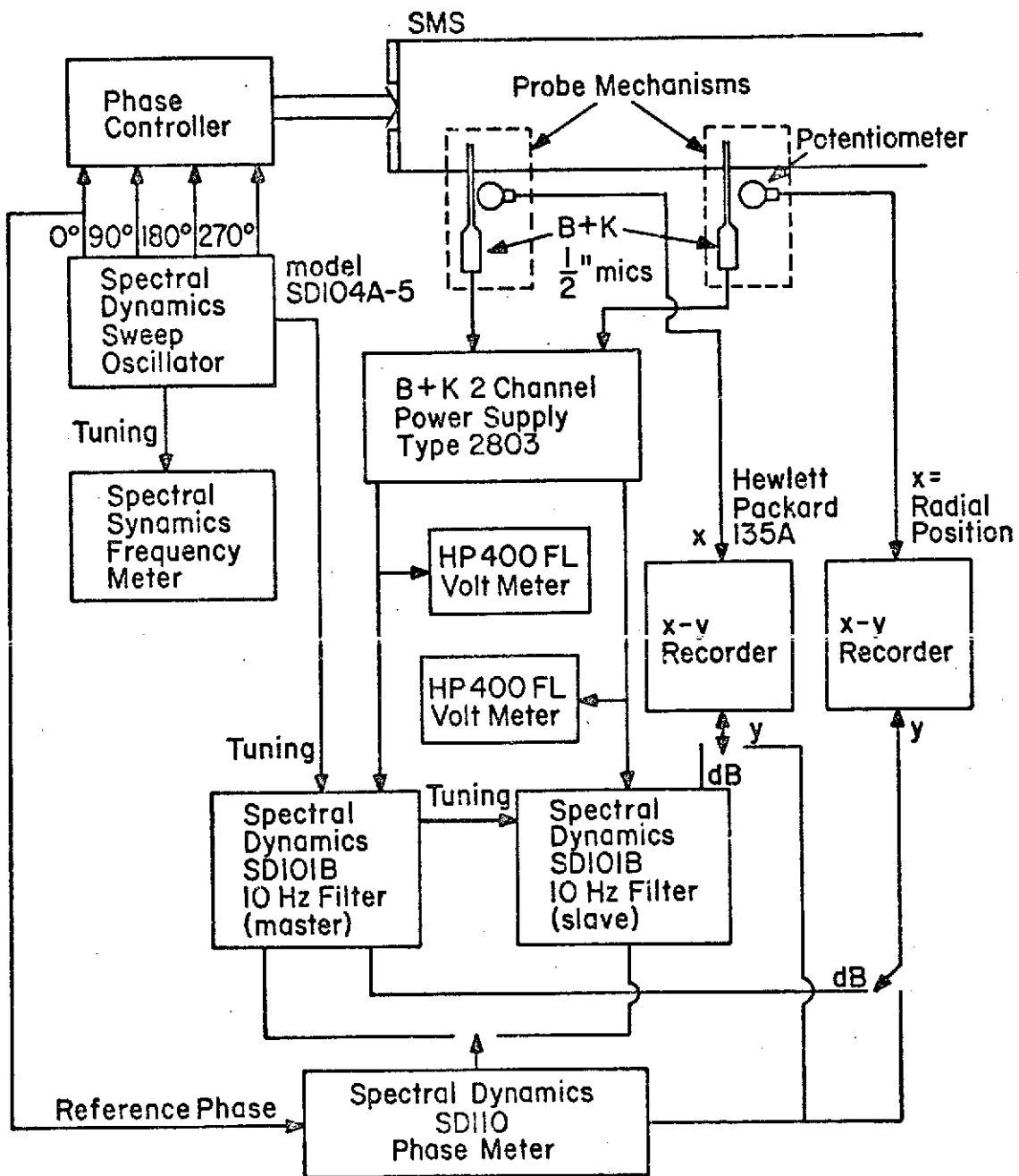


Figure 15

Basic Duct Instrumentation

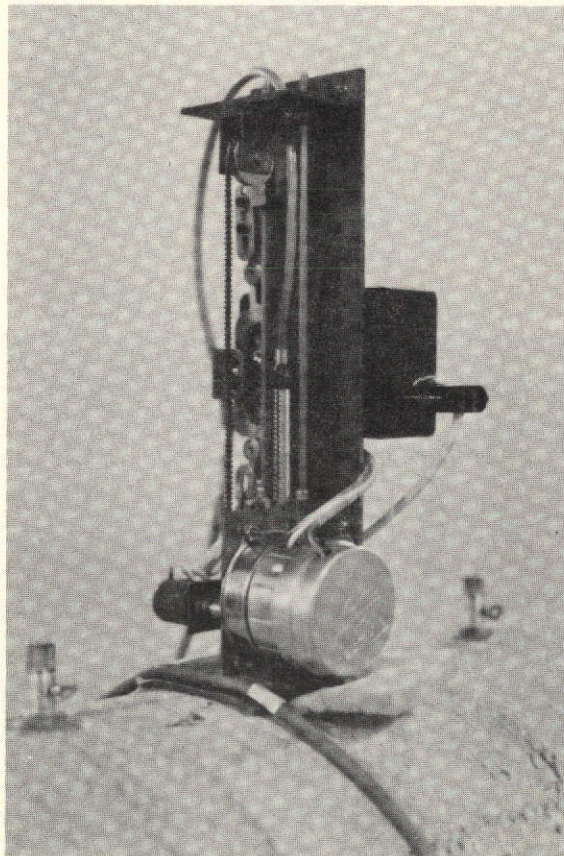


Figure 16
Probe Mechanism

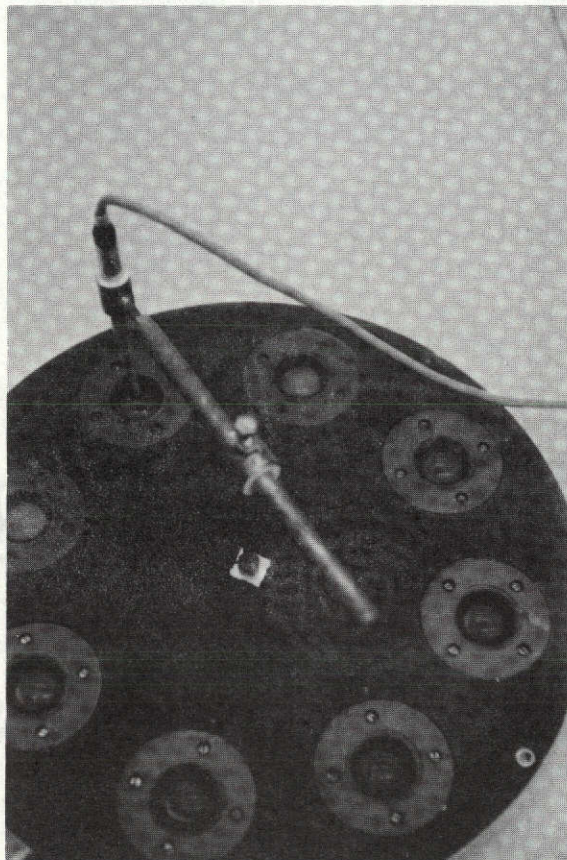


Figure 17

Plate Microphone Mechanism

2.2 Experimental Results

Preliminary experimentation was of an exploratory nature. Successful cancellation test cases had been obtained previous to this author's investigation. The experimental determination of the set of modes $\{M_{m\mu}\}$, $m = 0, \pm 1, \pm 2, \dots$, $\mu = 0, 1, 2, \dots$, which could be generated and cancelled by a 4-transducer array was considered basic to this initial investigation. It was also desired to establish the best open loop cancellation procedure.

The assumption of an ideal electrical-acoustical system provides a logical basis for initial investigation. This encompasses the following specific assumptions:

- 1) perfectly round, rigid-walled duct
- 2) an ideal anechoic termination so that traveling waves propagate only in the positive axial direction
- 3) symmetric transducer location on the end plate
- 4) identical transducers

These assumptions enable application of equations 1.3-3 through 1.3-8, governing the acoustic strength and phase of transducers for generation and cancellation of spinning modes, to the electrical inputs to the transducers. The appropriate form is:

$$V_{oj} = \text{input voltage to } j^{\text{th}} \text{ source transducer} \quad (1.3-3a)$$

$$= V, \quad j = 1, 2, \dots, n$$

$$\theta_{oj} = \text{electrical phase to } j^{\text{th}} \text{ source transducer} \quad (1.3-4a)$$

$$= \frac{2\pi m}{n} (j - 1), \quad j = 1, 2, \dots, n$$

$$v_{oj} = \text{input voltage to } j^{\text{th}} \text{ cancelling transducer} \quad (1.3-7a)$$

$$= V, j = 1, 2, \dots, n$$

$$\theta_{oj} = \text{electrical phase to } j^{\text{th}} \text{ cancelling transducer} \quad (1.3-8a)$$

$$= \frac{m\pi}{n} (2j - 1) + \pi, j = 1, 2, \dots, n$$

To verify the predicted optimal solution for the cancelling array, the cancelling array can be controlled as a two-dimensional open loop system of the form:

$$v_{oj} = v, \text{ the first variable, } j = 1, 2, \dots, n \quad (1.3-7b)$$

$$\theta_{oj} = \frac{m\pi}{n} (2j - 1) + \alpha, j = 1, 2, \dots, n \quad (1.3-8b)$$

where α is the second variable

The parameters v and α are then to be controlled to optimize system performance. Further adjustment can be obtained by control of the cancelling array as an eight dimensional system, with a voltage and phase for each transducer.

Previous to the investigation of spinning modes, plane wave test cases were run. Significant sound pressure level (SPL) reduction was obtained utilizing the predicted solution:

TABLE 3

Optimal Solution for Plane Wave

| n | Source ∇ | Array θ | Cancelling v | Array θ |
|---|--------------------|-------------------|-----------------|-------------------|
| 1 | 1.0 volt | 0 rad | 1.0 volts | π rad |
| 2 | 1.0 | 0 | 1.0 | π |
| 3 | 1.0 | 0 | 1.0 | π |
| 4 | 1.0 | 0 | 1.0 | π |

A test case with frequency of 1400 Hz is shown in Figure 18.

The fundamental circumferential spinning mode, $M_{1\mu}$ $\mu = 0, 1, 2, \dots$, was investigated next. The source transducers were assigned the relative electrical phases of $0, \frac{\pi}{2}, \pi$, and $\frac{3\pi}{2}$ radians for the respective transducers according to equation 1.3-4a. The cancelling transducers were set respectively to $\frac{\pi}{4} + \alpha, \frac{3\pi}{4} + \alpha, \frac{5\pi}{4} + \alpha$, and $\frac{7\pi}{4} + \alpha$ radians, where $0 \leq \alpha \leq 2\pi$. From the idealized far field analysis, the cancellation concept, α_{opt} is expected to be π radians (equation 1.3-8a). All transducer voltages were made equal according to equations 1.3-3a and 1.3-7a.

The M_{11} spinning mode ($m = 1, \mu = 1, 662 \text{ Hz} \leq f < 1918 \text{ Hz}$) was thoroughly investigated. The desired SPL reduction was obtained for frequencies below 1400 Hz. The manipulation of the cancelling array as an 8-dimensional system after 2-dimensional cancellation had been optimized resulted in almost complete cancellation (Figures 19 and 20). Above 1400 Hz, the system behavior departed significantly from ideal. As illustrated by Figure 21, $\alpha = \pi$ radians did not provide maximum cancellation. Acceptable SPL reduction could not be obtained with any α . Investigation of the M_{12} mode ($m = 1, \mu = 2, 1918 \text{ Hz} \leq f < 3067 \text{ Hz}$)

FIGURE 18

SPL versus Radial Distance at 6' from Plate

for $m = 0$, $\mu = 1$ Mode at 1400 Hz

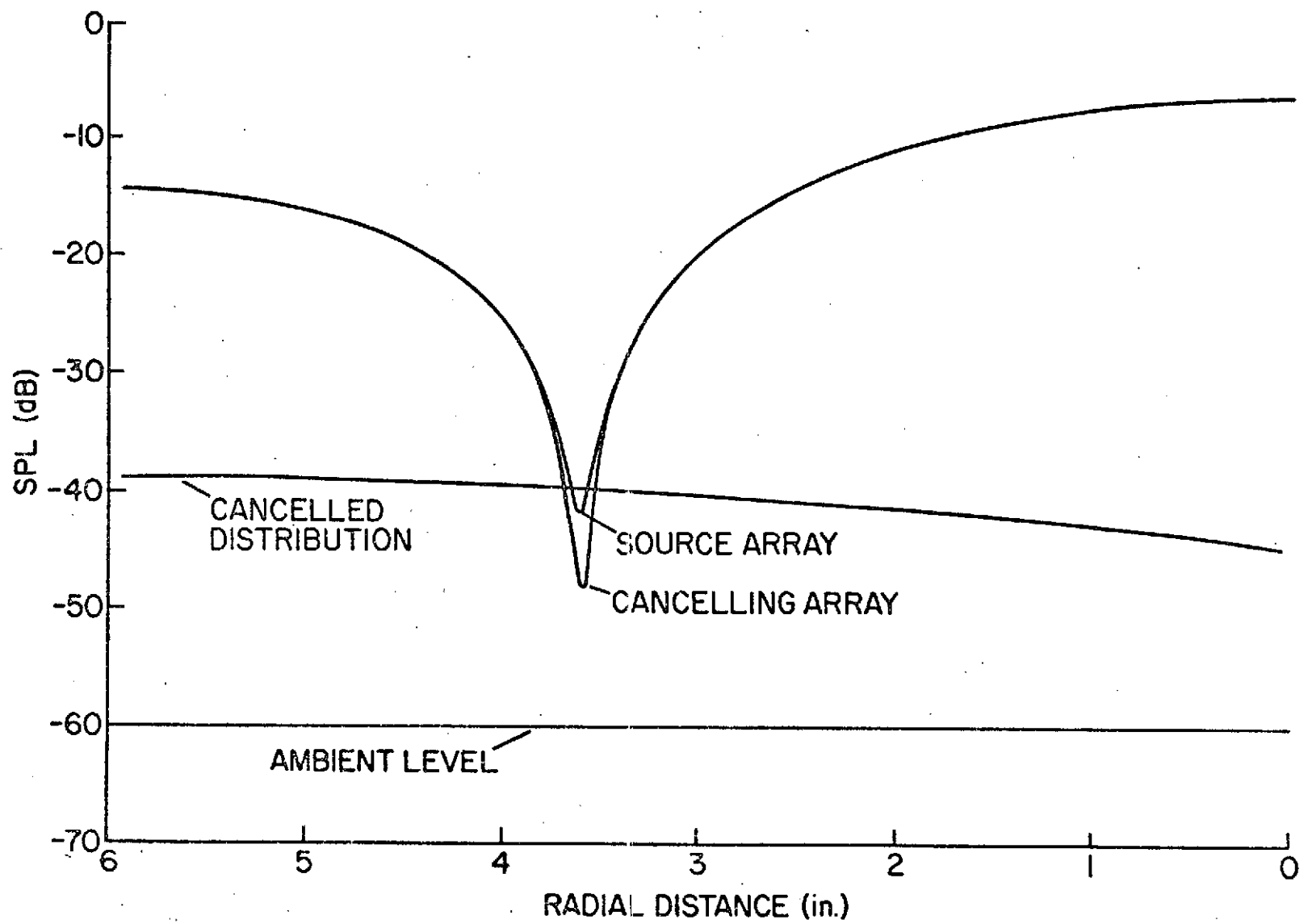


FIGURE 19

SPL versus Radial Distance at 6' from Plate

for $m = 1$, $\mu = 0$ Mode at 690 Hz

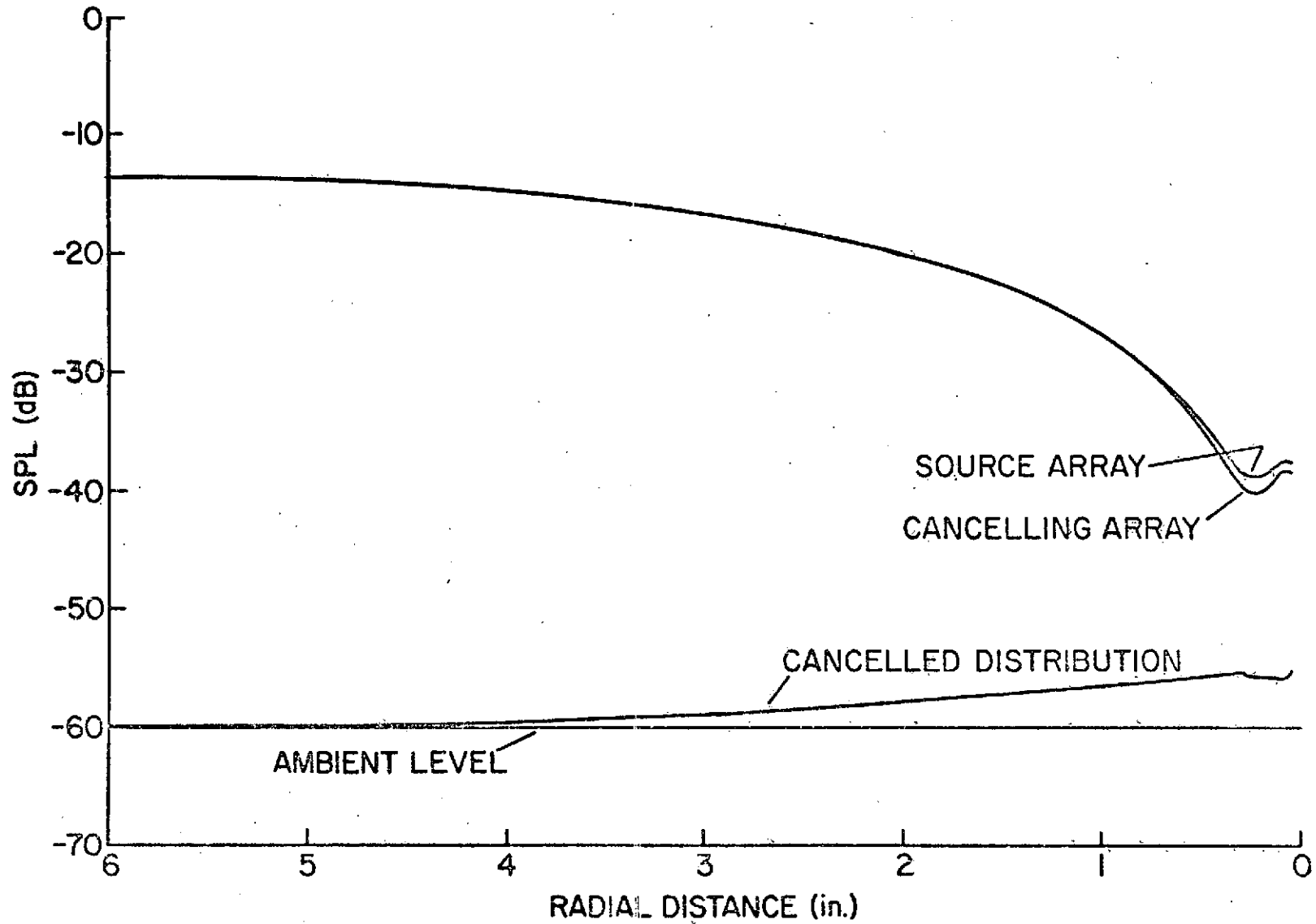


FIGURE 20

SPL versus Radial Distance at 6' from Plate

for $m = 1$, $\mu = 0$ Mode at 1240 Hz

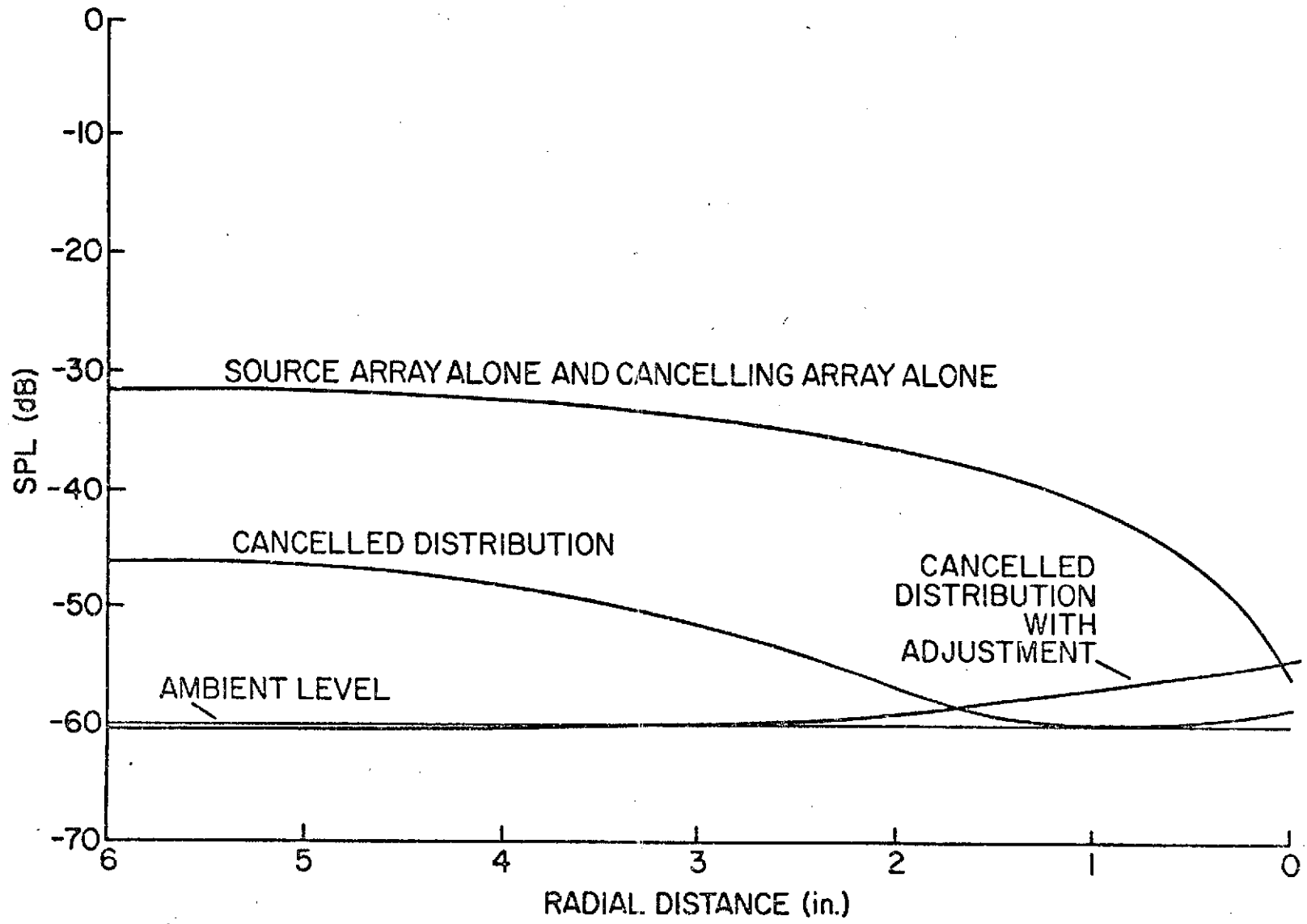
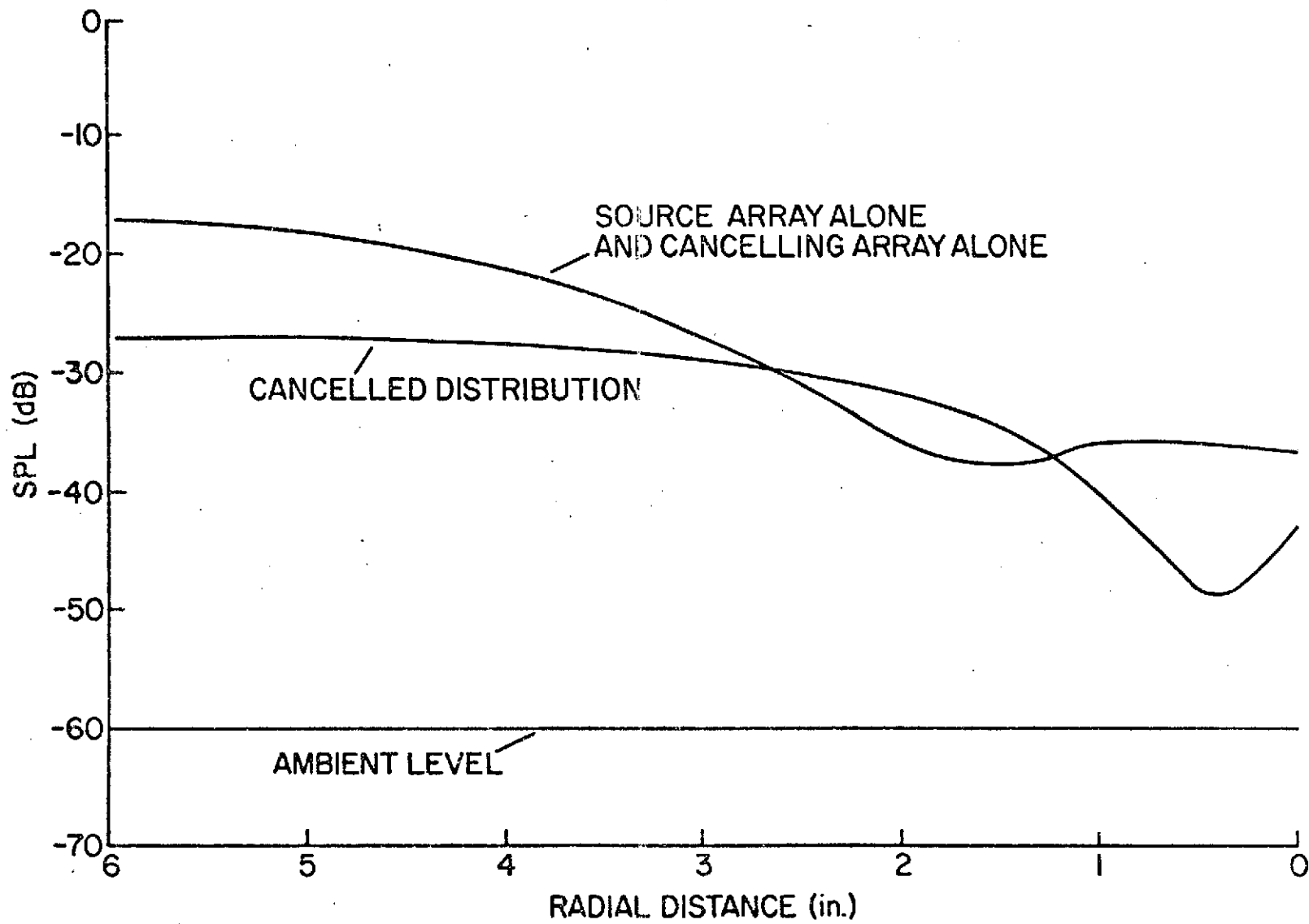


FIGURE 21

SPL versus Radial Distance at 6' from Plate

for $m = 1$, $\mu = 0$ Mode at 1560 Hz



did not clarify the undesirable high frequency cancellation performance of the system because of the complexity and variation of the results (Figure 22). Investigation of higher order radial distributions (larger μ) resulted in similar unpredictable response. Further testing did not contribute to interpretation of the results.

Manipulation of the cancelling array as an 8-dimensional system to improve system performance resulted in an additional complication of a "point cancellation" effect. The sound pressure level could be reduced to the ambient level at any single point in the duct. But, this often resulted in degradation of the overall system performance. Thus, the SPL at a single point could not be used as a system sound pressure level index of performance. By a trial and error technique, the SPL at single points was manipulated until an overall improvement in the radial distribution of the SPL was obtained. The testing process would have been greatly accelerated by a measurement system yielding a signal proportional to overall cancellation performance.

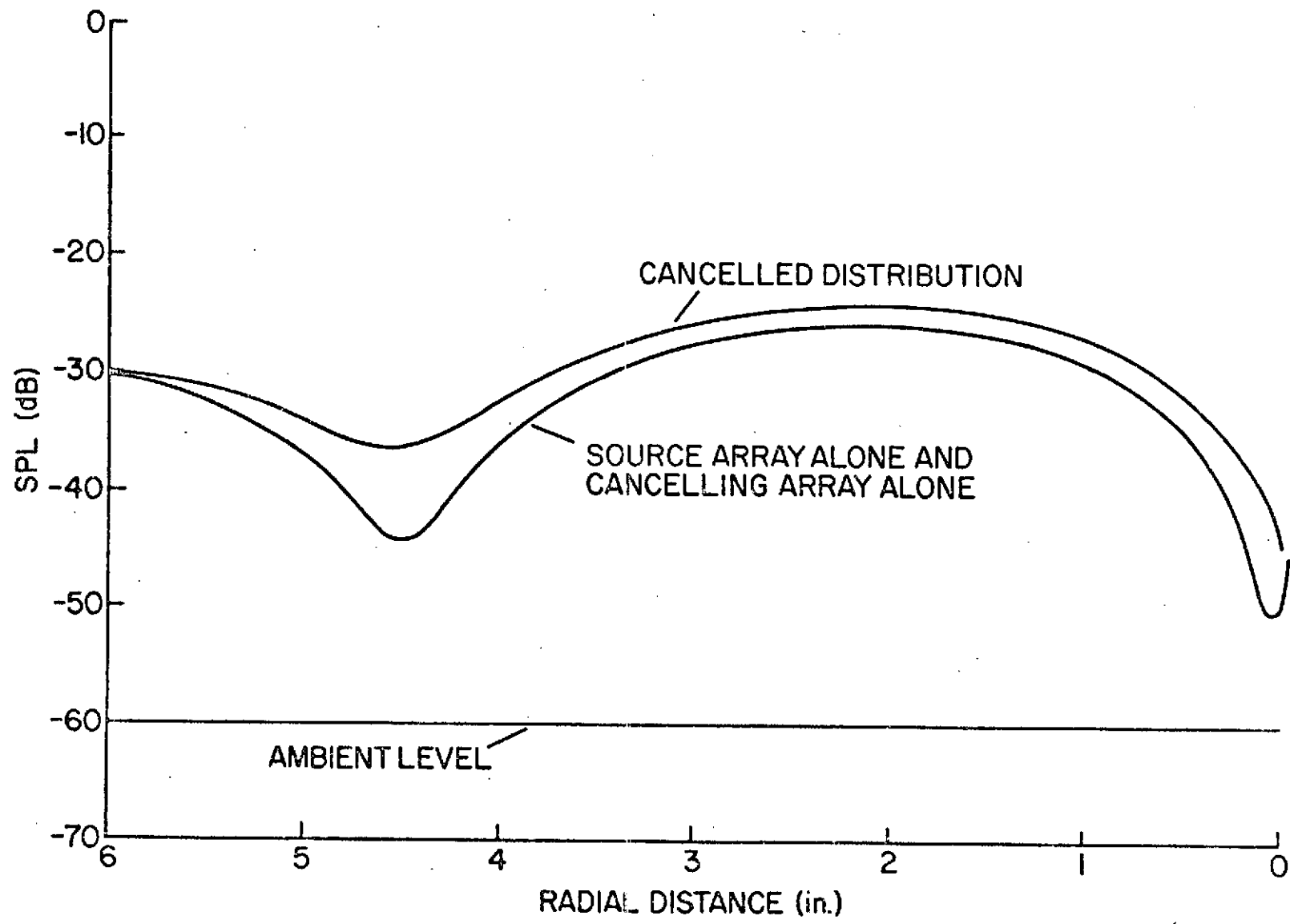
The limited frequency range of acceptable sound pressure level reductions was not considered adequate cancellation performance. An extensive investigation of the system was begun to uncover the source of this behavior and to expand the knowledge of the system.

The mass loading by the air of an individual transducer would be effected by the acoustic outputs of the other transducers as well as the duct. In the ideal system, such loading should be equal on all transducers. An unsymmetric duct or variation in the transducer responses could alter the acoustic field. This would result in performance degradation.

FIGURE 22

SPL versus Radial Distance at 6' from Plate

for $m = 1$, $\mu = 1$ mode at 2180 Hz



The symmetry of both duct loading and variation of transducer response were investigated. The plate probe described in Section 2.1 was used to set all transducers individually to 0 rad phase and -38 dB relative at 1500 Hz. A wide range of electrical voltages and phases were required to produce the same acoustic output at the given probe position (see Table 4). This could have been caused by significant transducer response variation or unsymmetric duct loading.

The results of this test indicated a need for an in-depth study. Such a study could facilitate system performance improvement, the determination of an appropriate cancellation procedure, and the definition of the plant for synthesis of an automatic controller. Testing would involve the individual isolation and investigation of system parameters. Then progressively elements of the system would be combined to study the effects of each addition until the complete system has been re-established.

The study of the plate-transducer system in the free field provided by a large anechoic chamber enabled sufficient isolation of system components for the basic investigation. Tests were repeated with the ducted system to evaluate the duct. Acoustic measurements were made in the anechoic chamber with an available microphone system. All measurements were made near the transducers as described for the plate microphone in Section 2.1, so effects due to radiation from the back side of the plate were negligible.

Variation of transducer response was investigated by comparing the electrical inputs necessary to produce a 0 rad phase, -34 dB acoustic output. The range of electrical phases was 15° (Table 5). The range of variation of electrical voltage inputs was .1 volts or 10% of the total voltage range of 1.0 volts (Table 5). Therefore,

variation of transducer response is significant and contributes to performance degradation.

TABLE 4
Variation of Transducer Response

| Transducer | Acoustic Parameters | | Electrical Parameters | |
|------------|---------------------|--------|-----------------------|----------|
| | SPL _o | ϕ | V | θ |
| 1 | -38dB | 0 rad. | 1.125 volts | 36 rad. |
| 2 | -38 | 0 | .98 | 29 |
| 3 | -38 | 0 | 1.11 | 33 |
| 4 | -38 | 0 | 1.10 | 33 |
| 5 | -38 | 0 | 1.10 | 49 |
| 6 | -38 | 0 | 1.11 | 53 |
| 7 | -38 | 0 | 1.09 | 27 |
| 8 | -38 | 0 | 1.10 | 41 |

Transducers were operated individually at 1500 Hz.

The symmetry of free field radiation was investigated by the generation of low order modes by the source array alone, by the cancelling array alone, and by the combined arrays. Near perfect symmetry was observed for a plane wave for the M_{10} spinning wave, and for both arrays set for a cancelled M_{10} spinning wave (Tables 5, 6, and 7). Therefore, as expected, free field radiation and thus transducer interaction is symmetric.

TABLE 5

Symmetry of Free Field Radiation in
Transducer Near Fields for Plane Wave

| Transducer | Electrical Parameters | | Plane Wave | | | | | |
|------------|-----------------------|----------|-------------|--------|--------------|--------|------------------|--------|
| | | | Total Array | | Source Array | | Cancelling Array | |
| | V | θ | dB | ϕ | dB | ϕ | dB | ϕ |
| 1 | .628 volts | -170° | -34.15 | 3.0° | -33.7 | -3.0° | | |
| 2 | .660 | -175 | -34.2 | 4.0 | | | -33.68 | -4.0° |
| 3 | .690 | -171 | -33.96 | 4.5 | -33.62 | -2.5 | | |
| 4 | .562 | -165 | -34.18 | 3.0 | | | -33.78 | -3.5 |
| 5 | .582 | -170 | -34.22 | 4.5 | -33.72 | -4.0 | | |
| 6 | .590 | -161 | -34.1 | 3.5 | | | -33.68 | -2.5 |
| 7 | .605 | -172 | -34.1 | 4.0 | -33.68 | -4.0 | | |
| 8 | .613 | -170 | -34.2 | 4.0 | | | -33.80 | -4.0 |

Transducers were set individually to -34dB and 0° phase at 1500 Hz. Measurements were then taken in the transducer near fields while plane waves were generated.

TABLE 6

Symmetry of Free Field Radiation in Transducer Near Fields
for First Order Spinning Mode

| Transducer | | Electrical Parameters | | Spinning Modes | | | | | |
|------------|--------|-----------------------|----------|----------------|--------------|--------------|--------------|------------------|--------------|
| | | | | Total Array | | Source Array | | Cancelling Array | |
| n | ϕ | V | θ | Δ dB | $\Delta\phi$ | Δ dB | $\Delta\phi$ | Δ dB | $\Delta\phi$ |
| 1 | 0° | .650 volts | -175° | -1.3 | 2.0° | 0.0 | -.5 | | |
| 2 | 45 | .685 | -130 | -1.53 | 1.5 | | | -.1 | -.5 |
| 3 | 90 | .720 | -80 | -1.4 | 2.0 | -.02 | -.5 | | |
| 4 | 135 | .570 | -30 | -1.3 | 2.5 | | | 0.0 | -.5 |
| 5 | 180 | .590 | 14 | -1.58 | 2.0 | -.11 | -1.0 | | |
| 6= | 225 | .610 | 65 | -1.15 | .5 | | | .07 | -1.5 |
| 7 | 270 | .640 | 97 | -1.2 | 1.0 | 0.0 | -2.0 | | |
| 8 | 315 | .640 | 144 | -1.3 | 1.0 | | | -.1 | -1.5 |

Transducers were set individually to -34 dB and the appropriate acoustic phase for an $m = 1$ spinning mode at 1500 Hz. Measurements were then taken in the transducer near fields while spinning modes were generated.

TABLE 7

Symmetry of Free Field Radiation in Transducer
Near Fields for a Cancelled First Order Spinning Mode

| Transducer | ϕ_0 | Cancelled Spinning Mode | |
|------------|----------|-------------------------|--------------|
| | | ΔdB | $\Delta\phi$ |
| 1 | 0 | 1.15 | -4.0° |
| 2 | 225 | 1.05 | -4.0 |
| 3 | 90 | 1.1 | -4.0 |
| 4 | 315 | 1.1 | -4.5 |
| 5 | 180 | 1.1 | -4.0 |
| 6 | 45 | 1.1 | -4.0 |
| 7 | 270 | 1.1 | -5.0 |
| 8 | 135 | .95 | -4.5 |

Transducers were set individually to -34 dB and the appropriate acoustic phase for a cancelled $m = 1$ spinning mode at 1500 Hz. Measurements were then taken in the transducer near fields while the cancelled mode was generated.

The frequency dependence of the variation of transducer response was investigated next. Each transducer was individually set to -36 dB at 1000 Hz. The frequency was then swept from 500 Hz. to 6000 Hz. The input voltage and phase were governed by a compressor circuit, a special purpose voltage regulator, greatly simplifying testing and still enabling meaningful conclusions. There was appreciable variation between transducers over the frequency range for both SPL (Figure 23) and phase (Figure 24). Thus the variation of transducer response from unit to unit is also frequency dependent.

The duct loading on the transducers can be evaluated by a comparison of the free field frequency response with the ducted frequency response. The magnitude of duct interaction is expected to greatly exceed transducer variation. So, only a single transducer need be studied in the free field.

Figure 25 shows SPL versus voltage for a variety of frequencies. An empirical relation can be established from this figure:

$$\text{SPL}(v, f) = k_1(f) + k_2(f) \left[20 \log \frac{v}{v_{\text{ref}}} \right] \quad (2.2-1)$$

where $k_1(f)$ and $k_2(f)$ are frequency dependent parameters. $k_1(f)$ is the SPL as a function of frequency for the reference voltage.

Figure 26 shows $k_1(f)$ for three references candidates. The functional complexity of $k_1(f)$ can be an important factor in the synthesis of an automatic controller. The parameter $k_2(f)$ is the slope of the lines for SPL versus input voltage (Figure 25). k_2 is a constant for any

FIGURE 23

Sound Pressure Level Versus Frequency of
Transducers in a Free Field at Constant Voltage

at $(r = r_{0j}, \theta = \theta_{0j}, z = 0)$

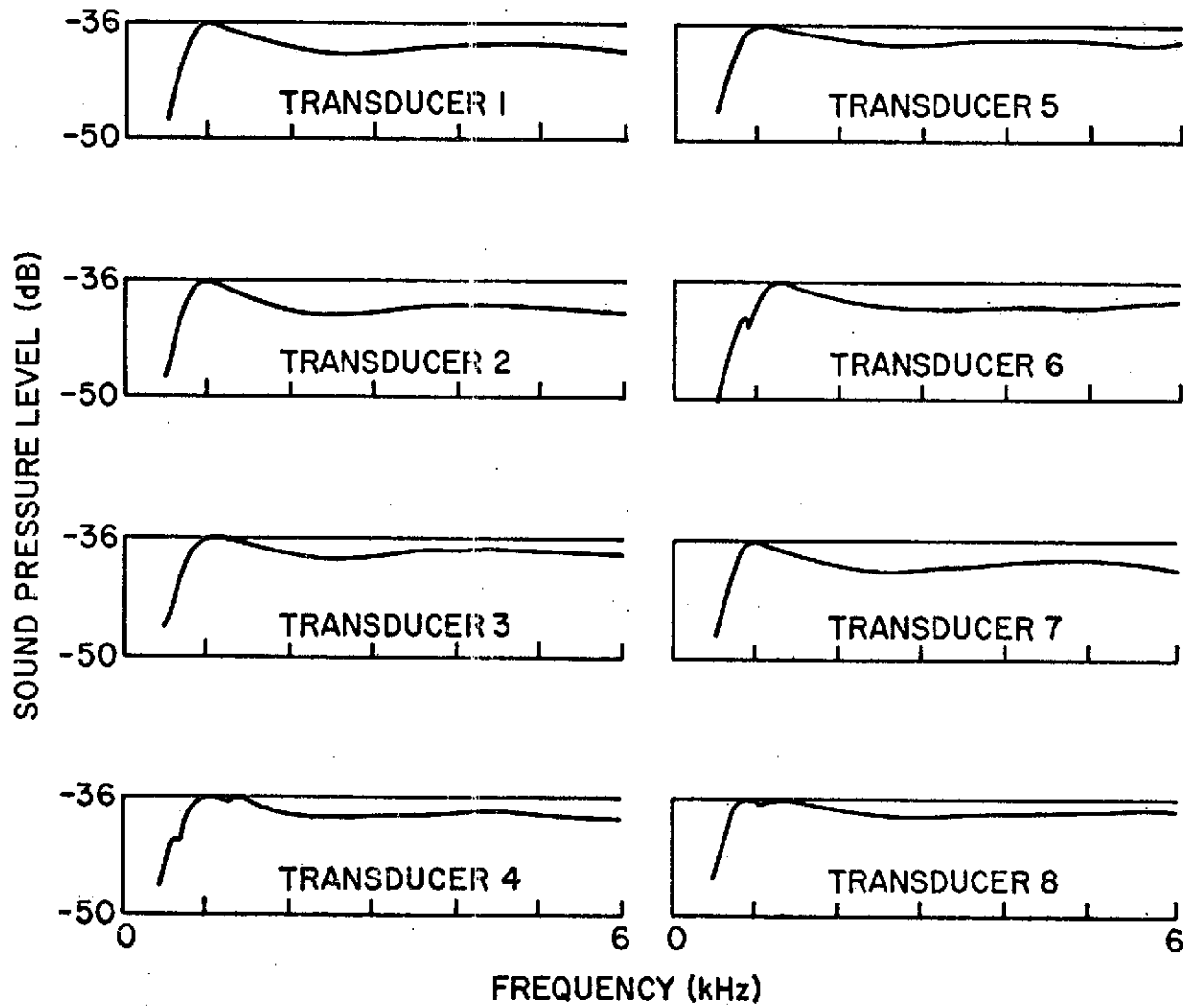


FIGURE 24

Phase Response versus Frequency of
Transducers in a Free Field at Constant Voltage
at $(\theta = \theta_{0j}, r = r_{0j}, z = 0)$

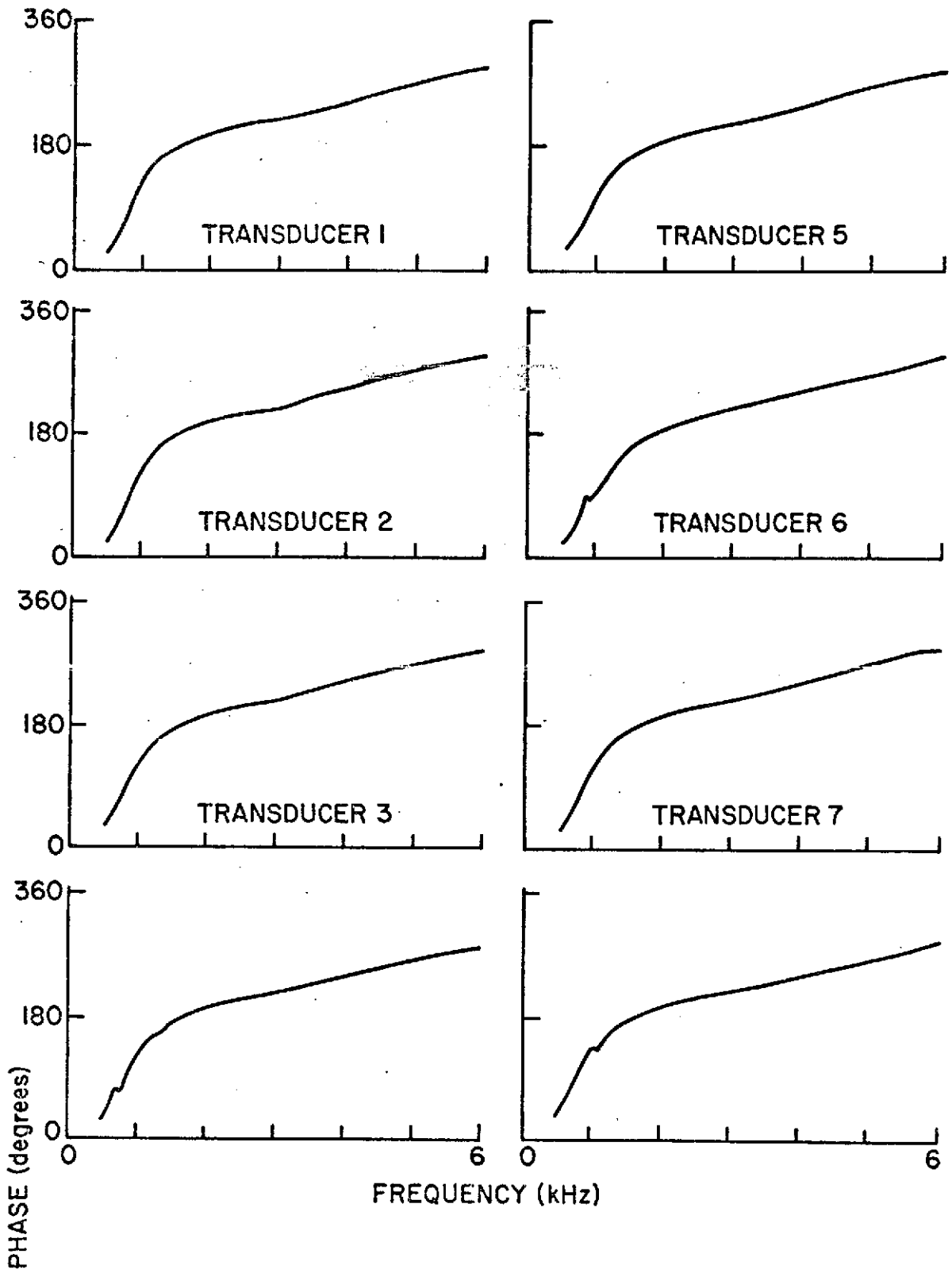


FIGURE 25

Input Voltage versus SPL for a
Single Transducer in a Free Field
at ($r = r_{01}$, $\theta = \theta_{01}$, $z = 0$)

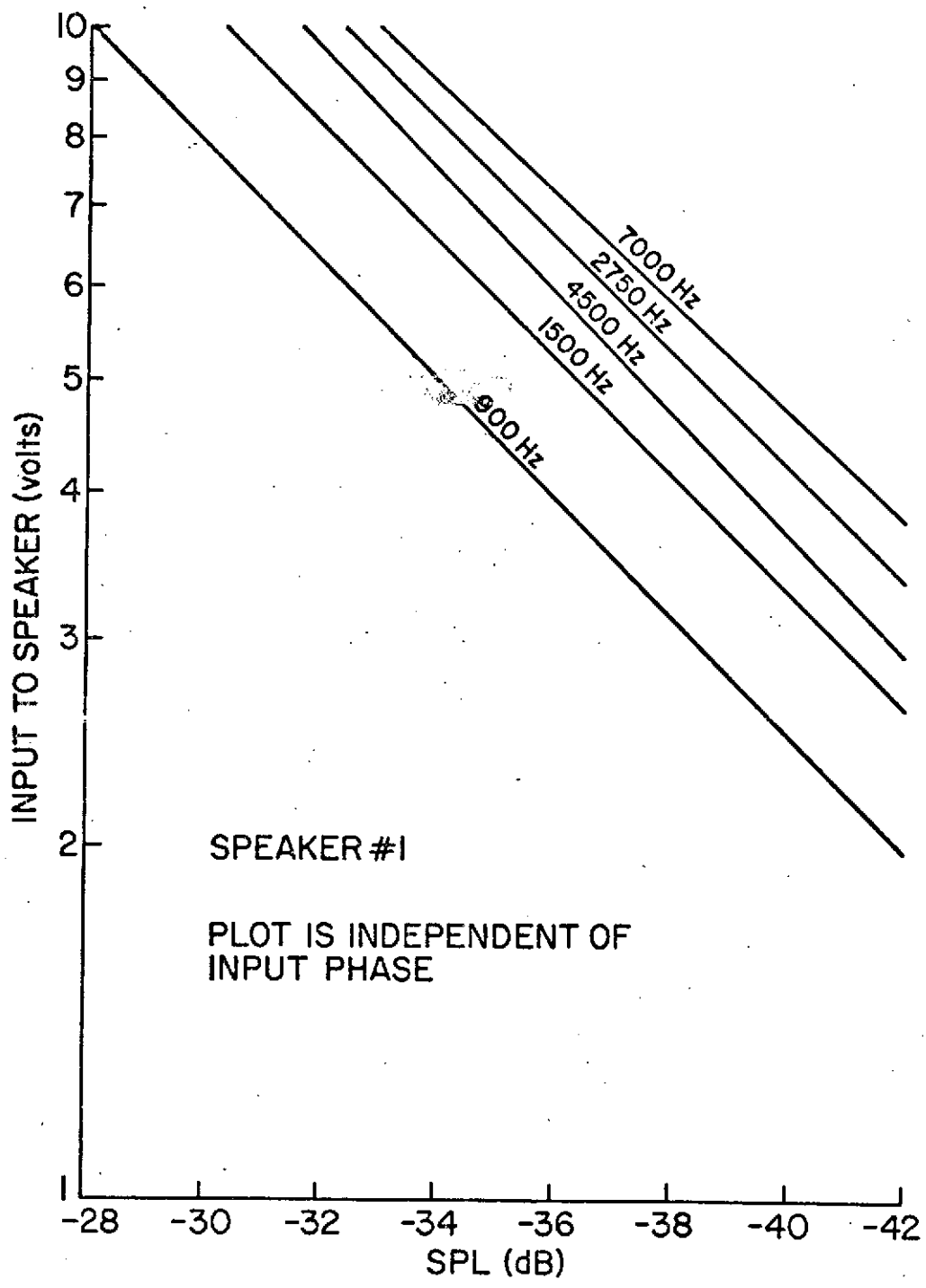
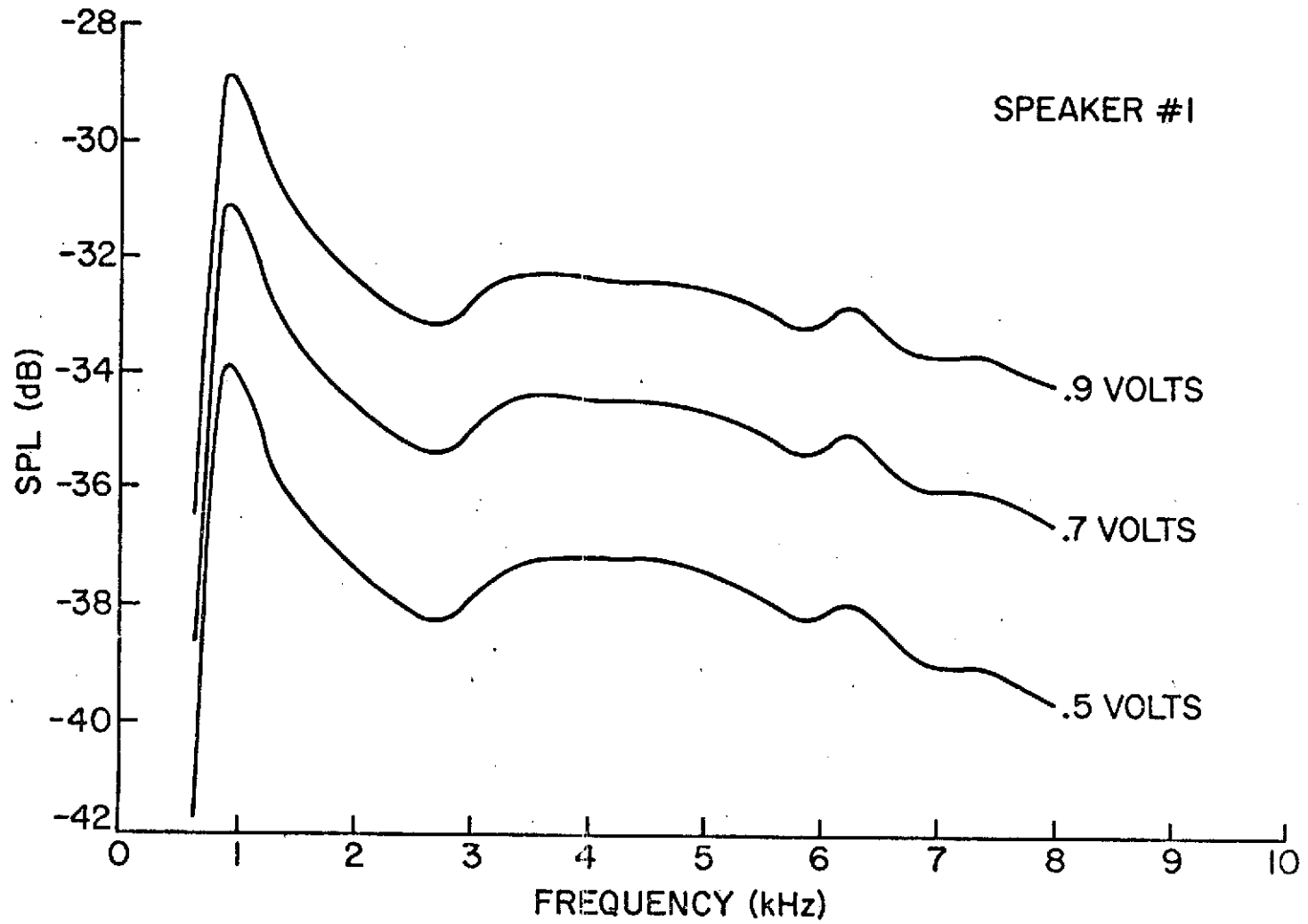


FIGURE 26

SPL versus Frequency for a Transducer in
a Free Field for Constant Voltages

at $(r = r_{01}, \theta = \theta_{01}, z = 0)$



given frequency so it can be determined from Figure 26 by calculating the rate of change of SPL between any two constant voltage curves. The results are given in Figure 27.

The plate was remounted to the duct and the same tests as those conducted in the large anechoic chamber were repeated. Figures 28 through 35 show SPL and phase response, measured near the transducers by the plate microphone mechanism, versus frequency at constant voltage from 500 Hz to 1000 Hz for all eight transducers. A wide variation of frequency response of opposing transducers (1 and 5, 2 and 6, 3 and 7, 4 and 8) was nearly identical. Re-examination of the free field results (Figures 23 and 24) yielded few indications of this behavior. So, the duct was decidedly responsible.

It is important to note the lack of permanent phase change as the frequency is swept through the $m = 1, \mu = 0$ resonance at 670 Hz. There is a clear 90° phase shift as resonance is reached, but the phase returns to its previous value after resonance is passed. Examination of the SPL response clarifies this apparent dilemma. The SPL and phase at the microphone are the result of the transducer parameters and the combination of all circumferential and radial modes which can be excited in a semi-infinite duct. Decaying modes, as well as propagating modes, contribute to the SPL and phase because the measurement point is near $z = 0$, so axial decay is small. The SPL rapidly drops off after the $m = 1, \mu = 0$ resonance, indicating a rapid increase in damping of this mode. The corresponding rapid decay of

FIGURE 27

$k_2(f)$ versus Frequency

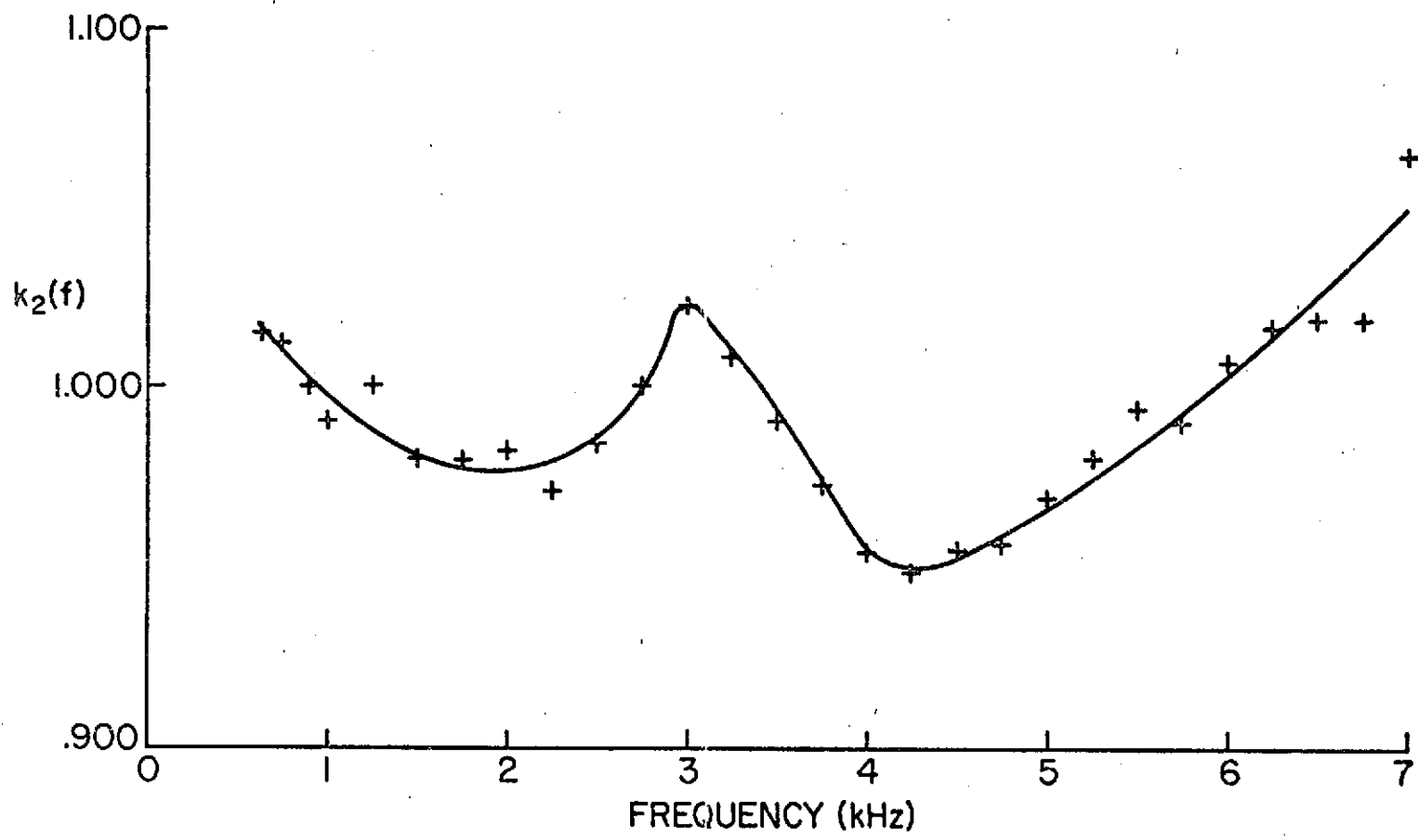


FIGURE 28

SPL and Phase Response versus Frequency at
Constant Voltage (.9 volts)
for Transducer 1 of the Ducted Array
at $(r = r_{01}, \theta = \theta_{01}, z = 0)$

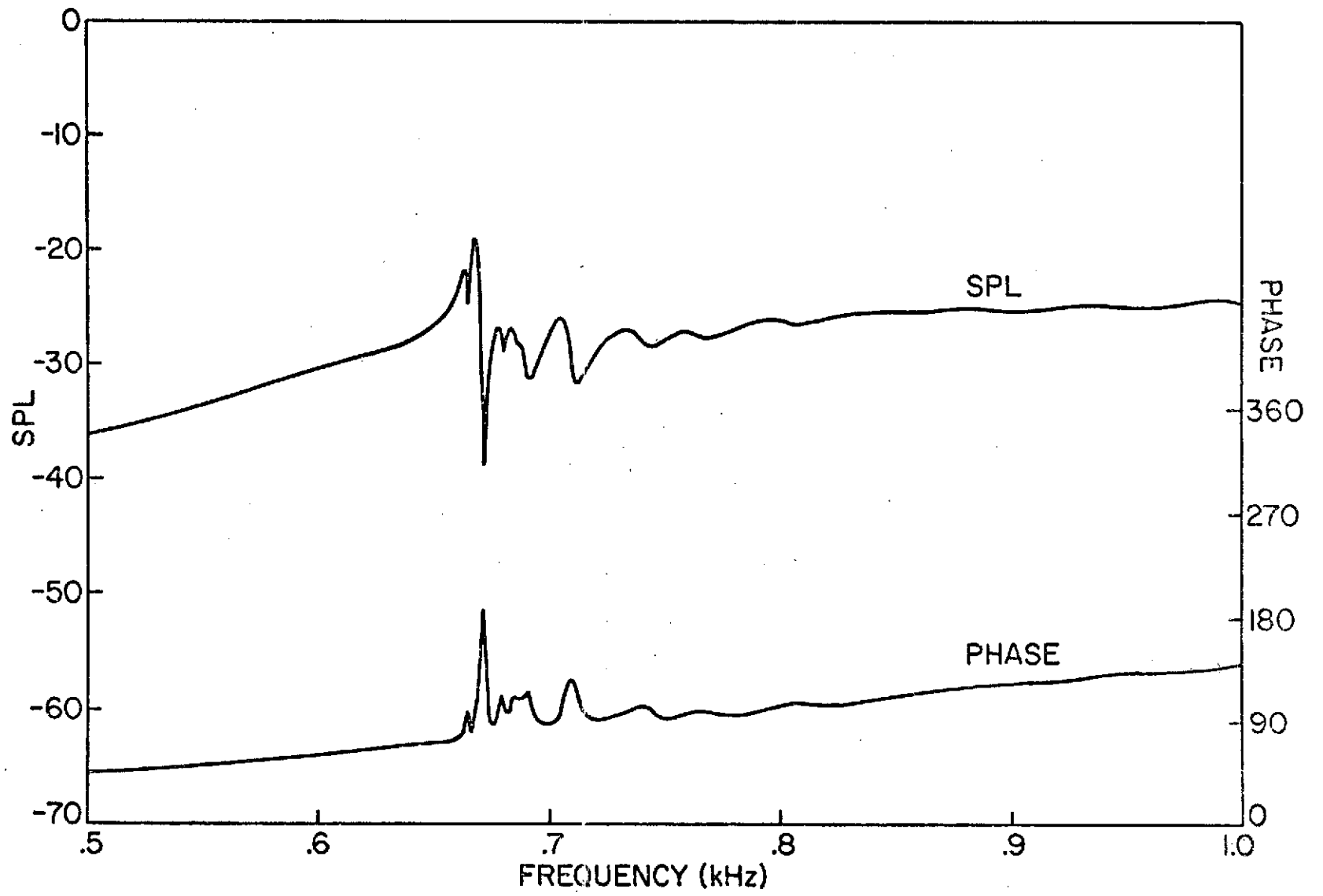


FIGURE 29

SPL and Phase Response versus Frequency
at Constant Voltage (.9 volts) for
Transducer 2 of the Ducted Array
at ($r = r_{02}$, $\theta = \theta_{02}$, $z = 0$)

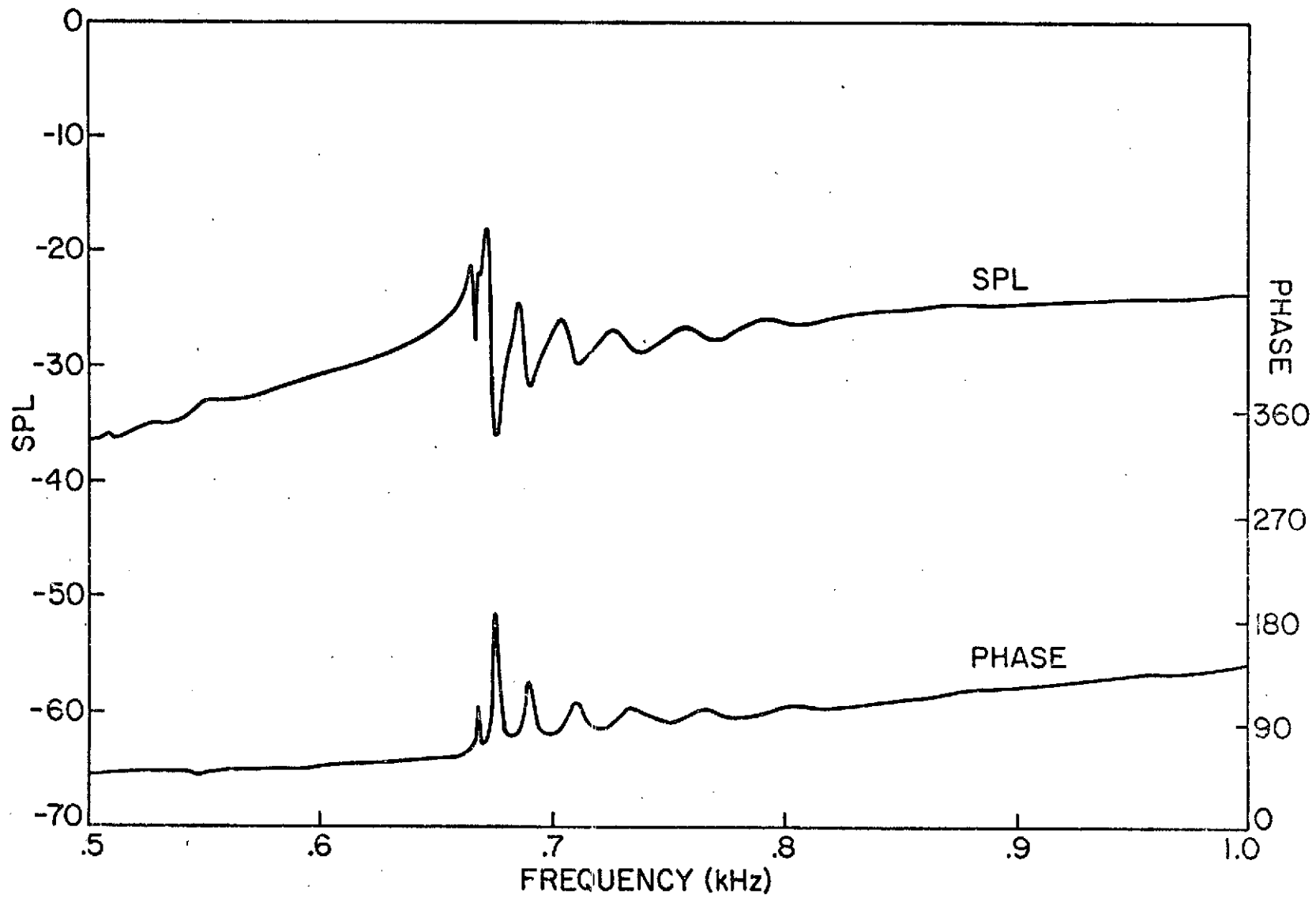


FIGURE 30

SPL and Phase Response versus Frequency

at Constant Voltage (.9 volts) for

Transducer 3 of the Ducted Array

at $(r = r_{03}, \theta = \theta_{03}, z = 0)$

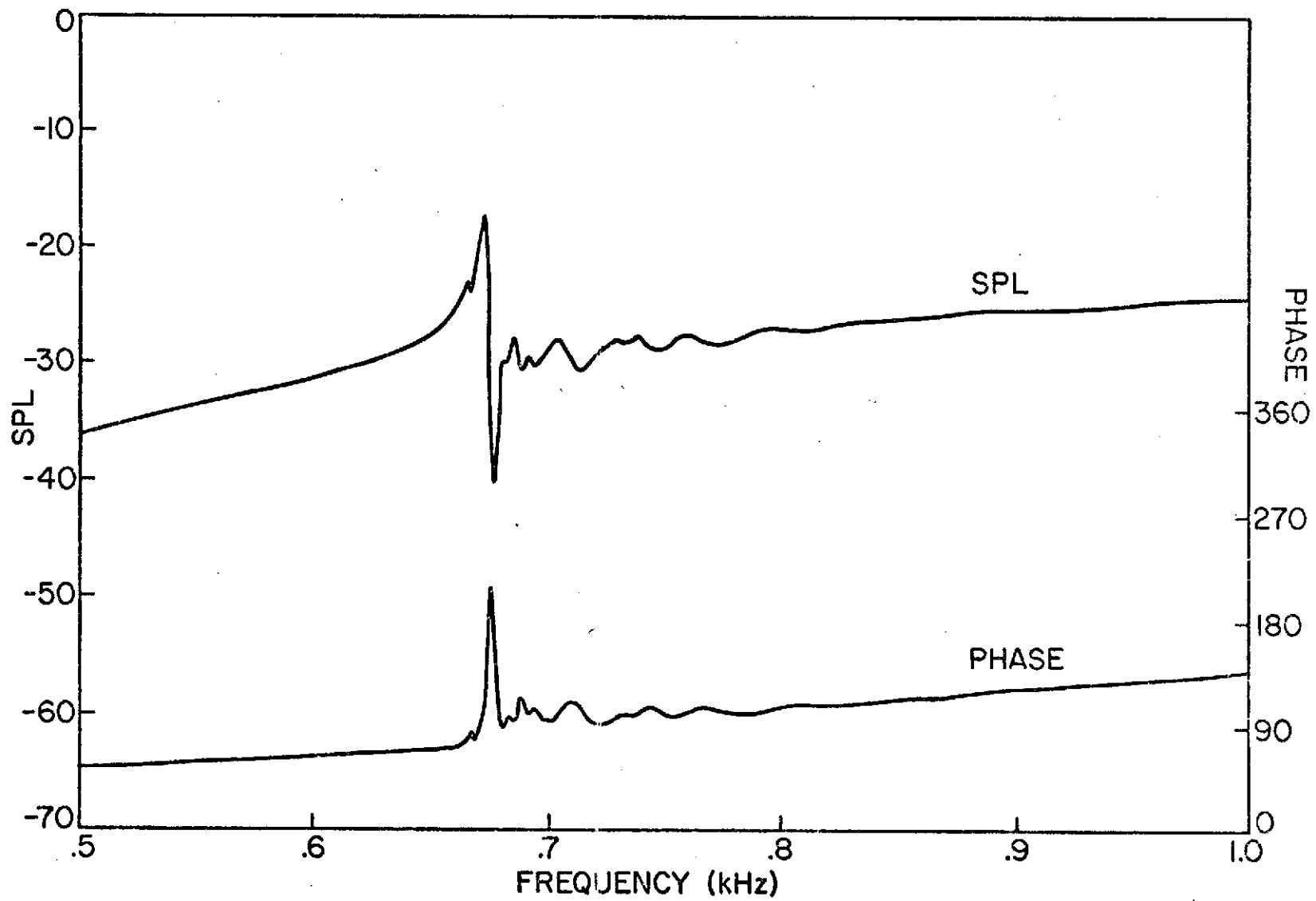


FIGURE 31

SPL and Phase Response versus Frequency at
Constant Voltage (.9 volts) for
Transducer 4 of the Ducted Array
at $(r = r_{04}, \theta = \theta_{04}, z = 0)$

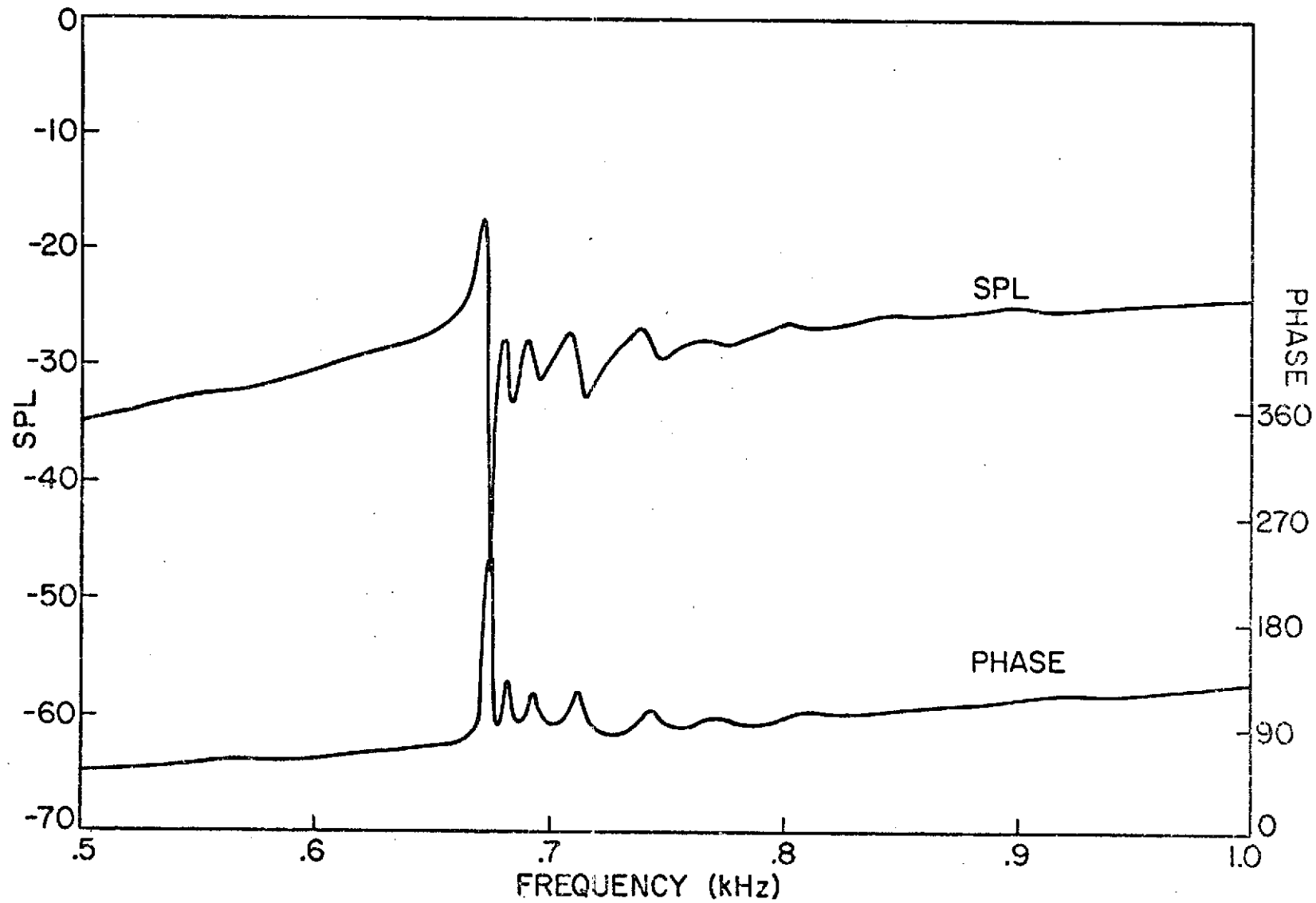


FIGURE 32

SPL and Phase Response versus Frequency

at Constant Voltage (.9 volts) for

Transducer 5 of the Ducted Array

at $(r = r_{05}, \theta = \theta_{05}, z = 0)$

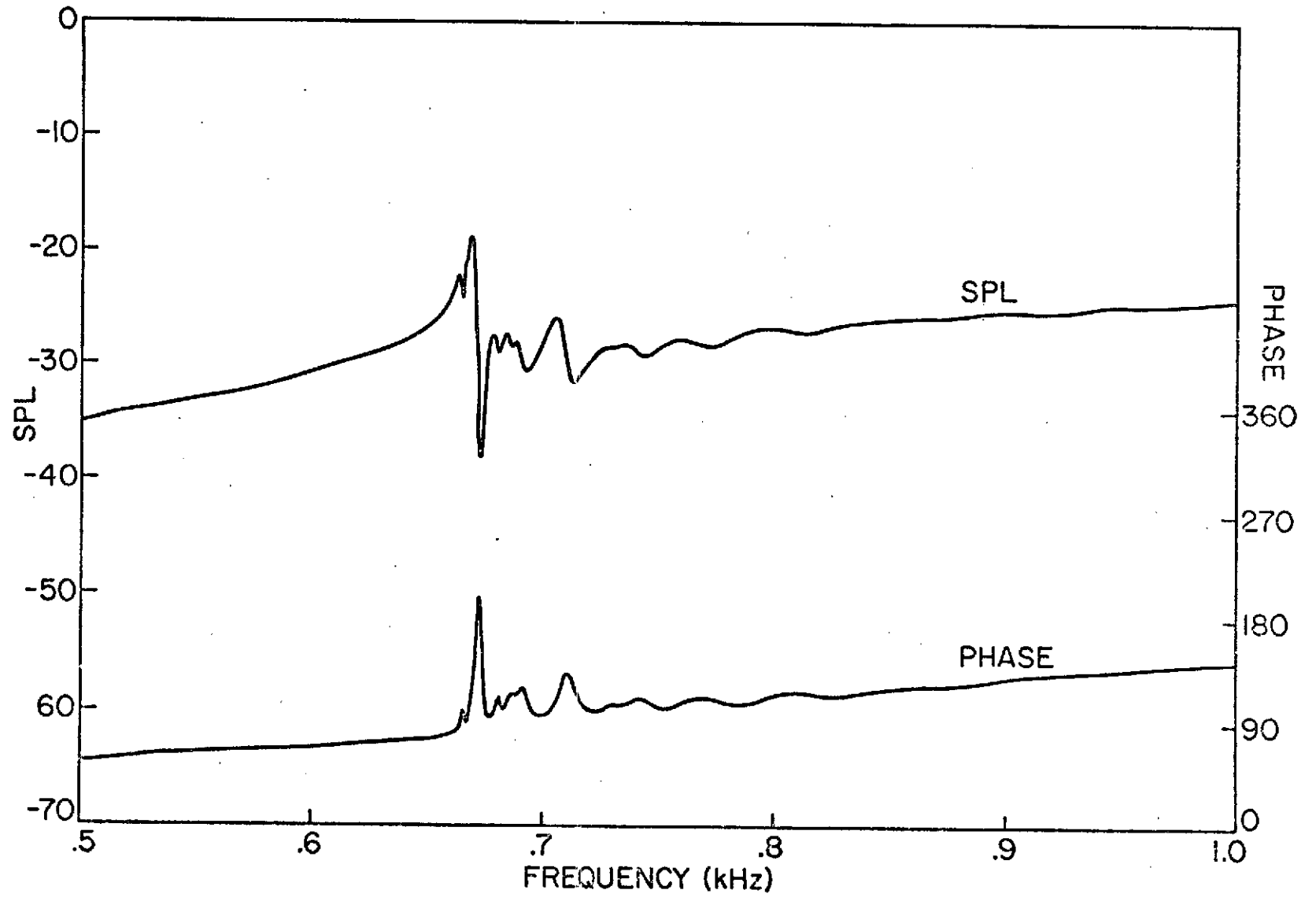


FIGURE 33

SPL and Phase Response versus Frequency at
Constant Voltage (.9 volts) for
Transducer 6 of the Ducted Array
at $(r = r_{06}, \theta = \theta_{06}, z = 0)$

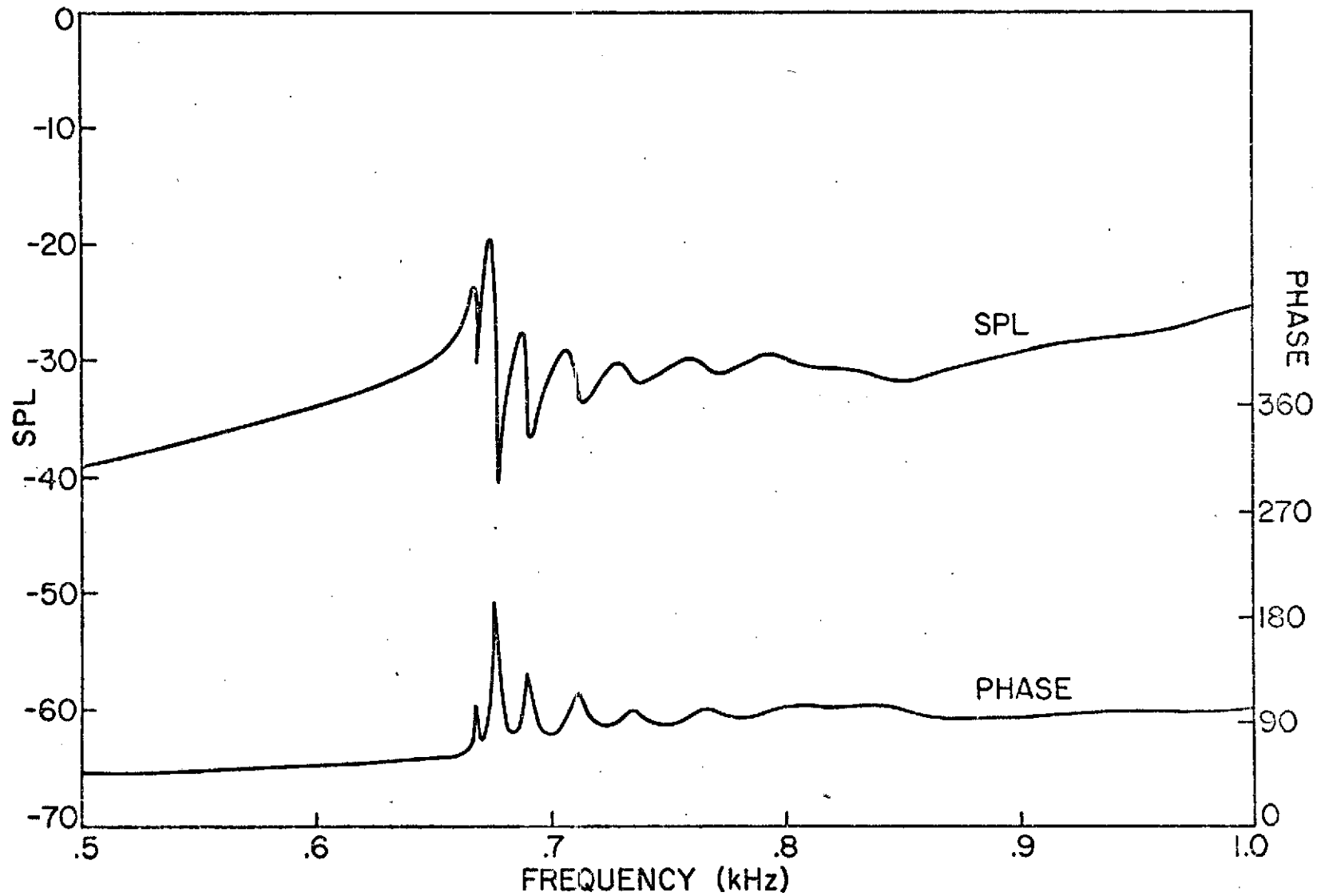


FIGURE 34

SPL and Phase Response versus Frequency

at Constant Voltage (.9 volts) for

Transducer 7 of the Ducted Array

at $(r = r_{07}, \theta = \theta_{07}, z = 0)$

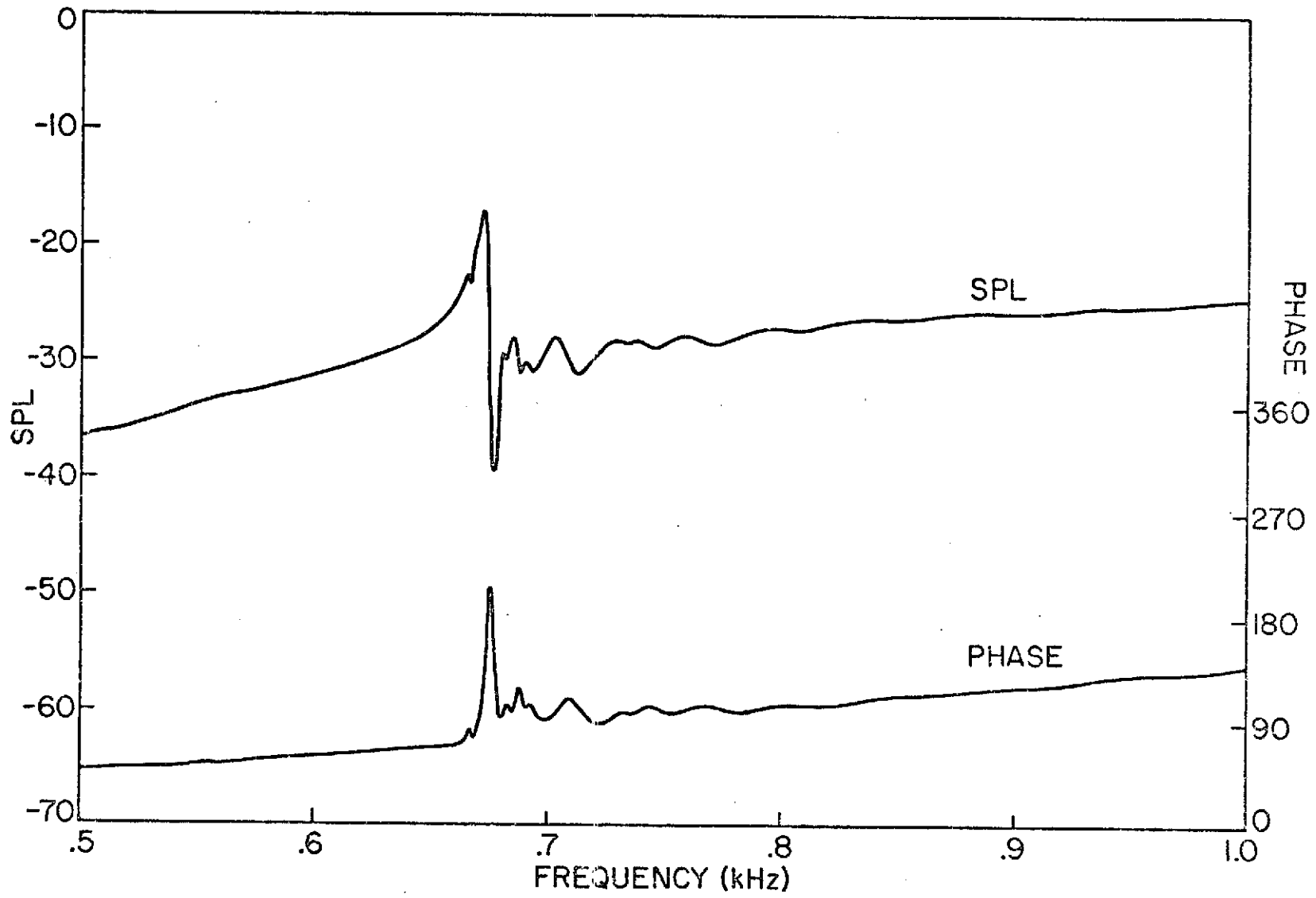


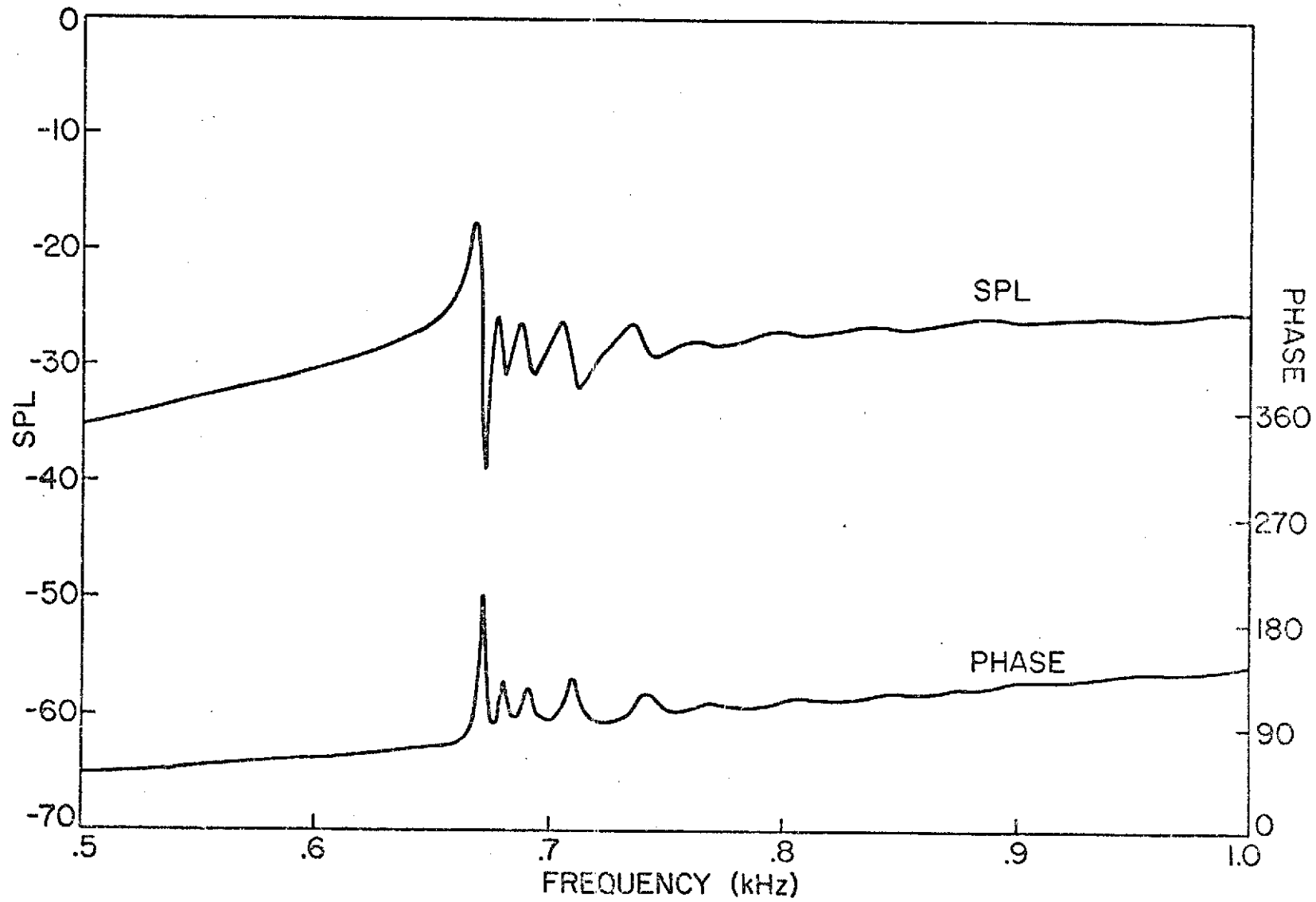
FIGURE 35

SPL and Phase Response versus Frequency

at Constant Voltage (.9 volts) for

Transducer 8 of the Ducted Array

at $(r = r_{08}, \theta = \theta_{08}, z = 0)$



the amplitude coefficient of this mode results in negligible contribution to the overall SPL and phase at the measurement point. Thus the phase shift still exists; it merely cannot be detected.

The parameters of duct geometry were investigated to uncover the source of this undesirable response. The transducers were mounted on the plate within machining tolerances, so the problem was elsewhere. There are four possible dimensions of misalignment of the plate with respect to the duct centerline. Angular displacements, illustrated in Figure 36,

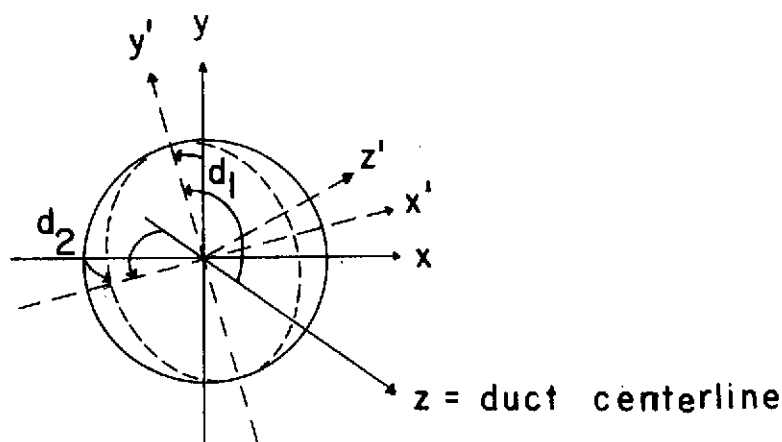


FIGURE 36

Angular Misalignment of Plate with Duct Centerline

were found to be within a half a degree. This alone could not cause the observed behavior. The center of the plate could be displaced from the duct centerline as illustrated in Figure 37. But d_3 and d_4 were found to be negligible.

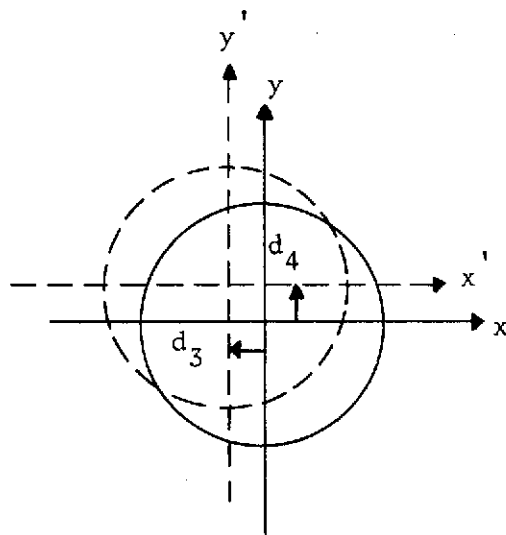


FIGURE 37

Displacement of Plate from Duct Centerline

The terra cotta pipes which form the duct do not have high dimensional tolerances. An out-of-round duct section could easily be present and provide the observed unsymmetric acoustic loading. It was found that the third duct section from the plate was oval with major and minor axis differing by a half inch. This was a likely candidate for the observed behavior.

Excitation of plate vibrational modes by the transducers could also contribute to the observed behavior. The plate is bolted at three points as shown in Figure 38. This bolting pattern would allow vibration in the basic plate modes. A test was conducted to determine the effect and magnitude of such vibration on the acoustic field. Figures 39 through 42 show radial distributions of SPL and phase for

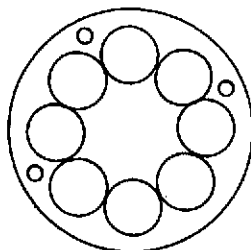


FIGURE 38

Plate Bolting Pattern

an M_{11} spinning wave of 2000 Hz. Note that at only one position was a desired radial distribution observed (Figure 41). Automotive undercoat was then applied to the plate to reduce radiation from the plate. Radial distributions at the same probe positions were again recorded (Figures 39 through 42). A slightly greater symmetry of the distributions at both probe positions was observed, an improvement obtained at the expense of the well defined radial distribution mentioned above. Though a performance improvement was not achieved, the test served to show the sensitivity of the system to slight parameter variation.

It was shown that several possible causes for unsymmetric transducer loading exist. The magnitude of the contribution of each was not investigated in this analysis.

FIGURE 39

SPL versus Radial Distance at 6' from Plate
for $m = 1$, $\mu = 1$, Mode at 2000 Hz at a Circumferential
Angle of 0 radians with Respect to Transducer 1
of the Source Array

C2

C2⁰⁸

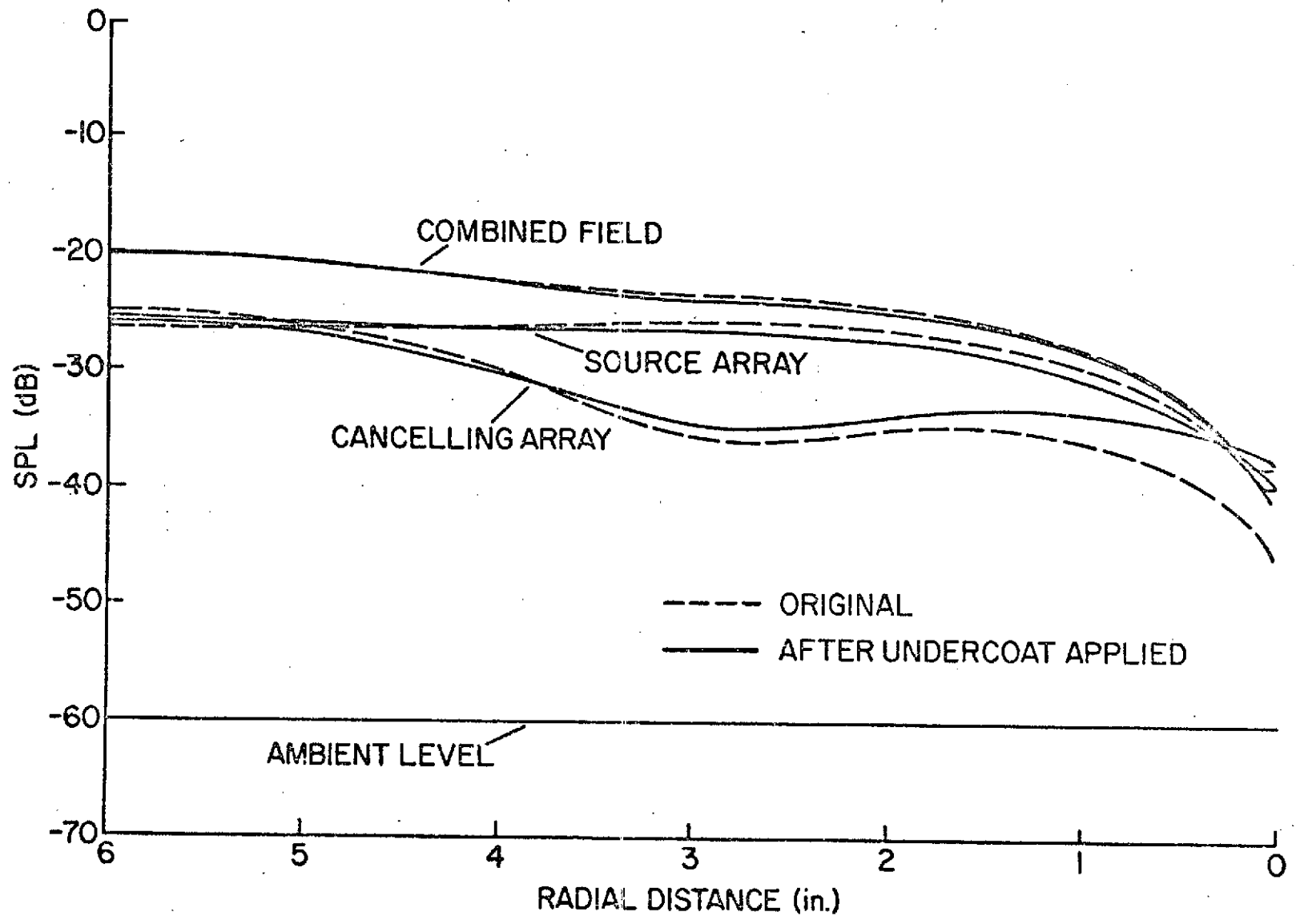


FIGURE 40

Phase versus Radial Distance at 6' from Plate
for $m = 1$, $\mu = 1$, Mode at 2000 Hz at a Circumferential Angle
of 0 radians with Respect to Transducer 1 of the Source Array

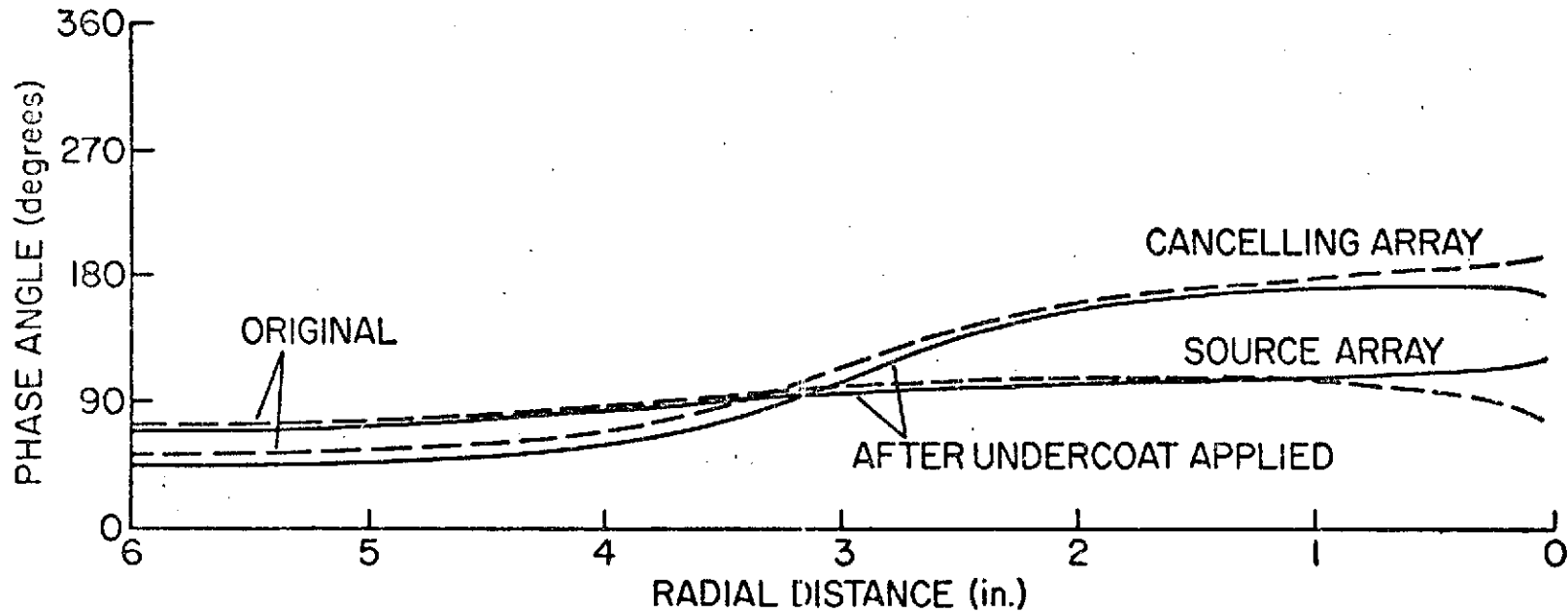


FIGURE 41

SPL versus Radial Distance at 6' from Plate
for $m = 1$, $\mu = 1$, Mode at 2000 Hz at a Circumferential Angle
of $\frac{\pi}{4}$ radians with Respect to Transducer 1 of the Source Array

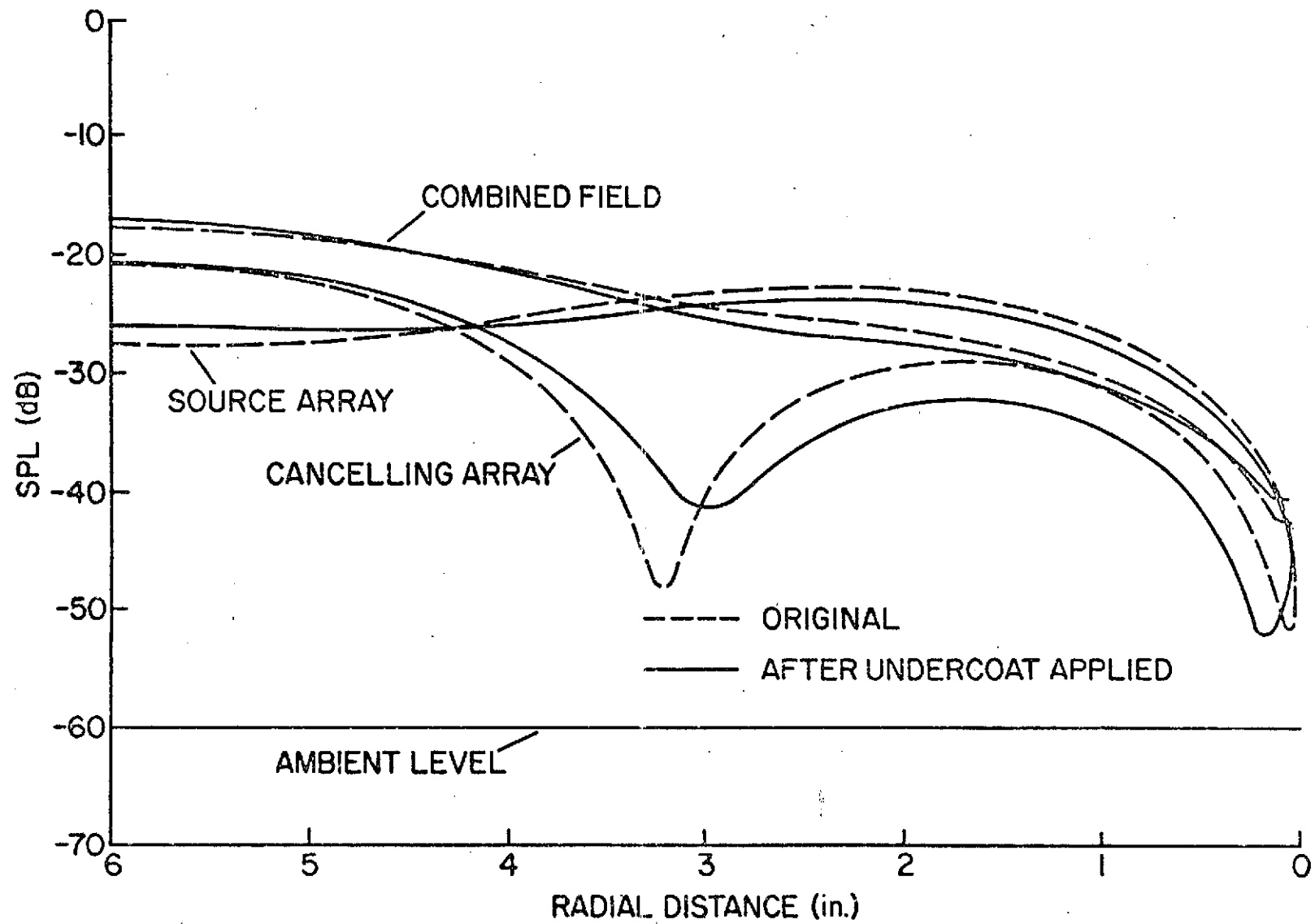
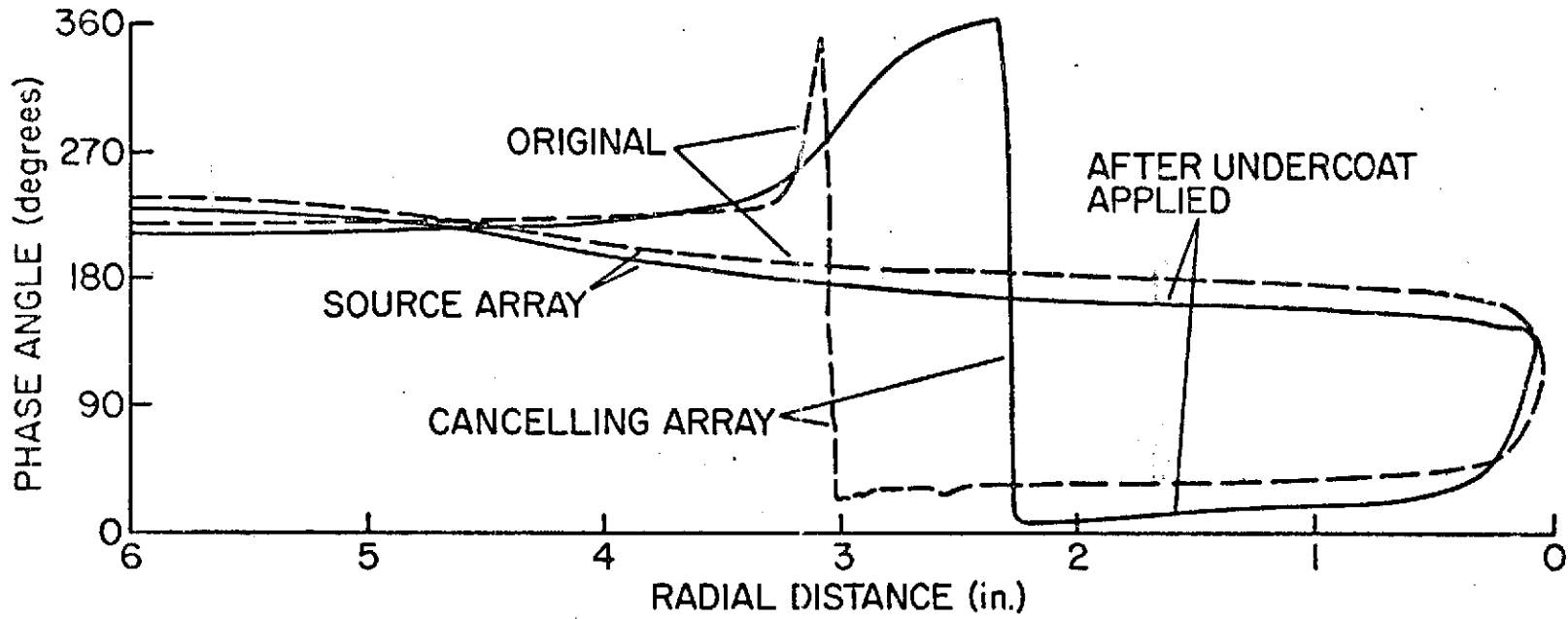


FIGURE 42

Phase versus Radial Distance at 6' from Plate
for $m = 1$, $\mu = 1$, Mode at 2000 Hz at a Circumferential Angle
of $\frac{\pi}{4}$ radians with Respect to Transducer 1 of the Source Array



The evaluation of duct loading on the transducers was completed by the determination of the ducted transducer frequency response. Figure 43 shows that the empirical equation developed for the free field frequency response is appropriate:

$$\text{SPL}(v, f) = k_1(f) + k_2(f) \left[20 \log \frac{v}{v_{\text{ref}}} \right] \quad (2.2-1)$$

Some of the curves are nonlinear, making $k_2(f)$ a multi-valued function of voltage at some frequencies. But the magnitude of variations is small so an approximate value would be adequate. The parameter $k_1(f)$, the SPL for v_{ref} , is shown for a single transducer with $v_{\text{ref}} = .9$ volts at frequencies from 500 Hz. to 4000 Hz in Figures 28, 44, and 45. Peaks can be observed at the duct cutoff frequencies. So, the frequency response for the ducted transducer is of the same form for a transducer in a free field, but reflects the frequency dependent behavior of the duct. The complexity of $k_1(f)$ along with transducer variation can clearly contribute to cancellation difficulties.

A new cancellation procedure was devised to account for unsymmetric transducer loading and the complexity of the transducer frequency response. Transducers were individually set by the plate probe microphone to the appropriate acoustic phases and equal SPL output. The procedure was tested with an M_{10} spinning wave of 750 Hz. Results are given in Figure 46 through 51. Reduction of over 20 dB was obtained at all probe positions for the cancelling condition. The field produced by the cancelling array is 5 to 7 degrees from the desired 180° phase displacement from the source array field. Compensation by the adjustment of the acoustic phases of the cancelling

FIGURE 43

Input Voltage versus SPL for a
Single Transducer in the Ducted Array
at $(r = r_{01}, \theta = \theta_{01}, z = 0)$

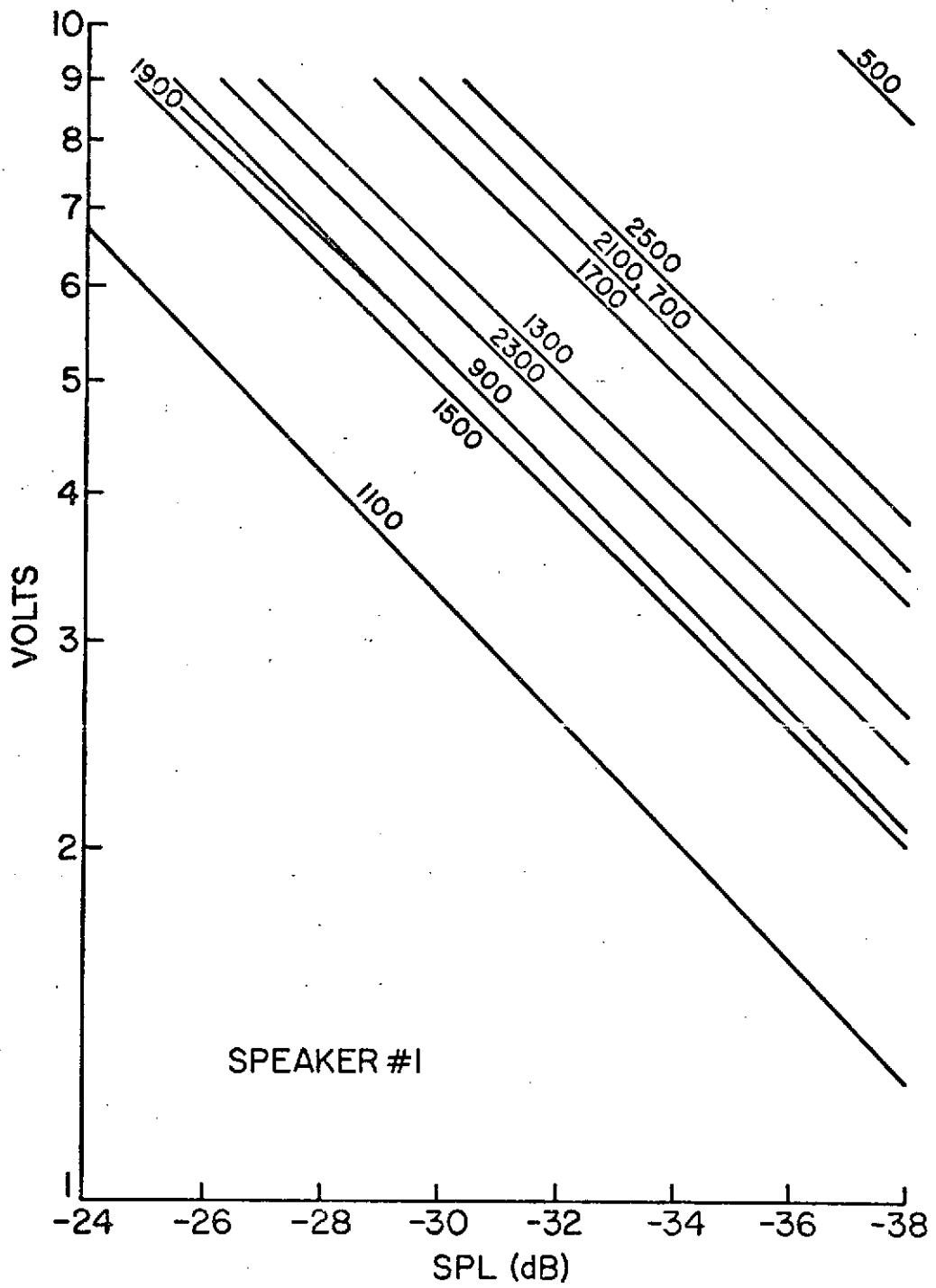


FIGURE 44

SPL versus Frequency for Transducer 1
of the Ducted Array at a Constant Voltage (.9 volts)
at $(r = r_{01}, \theta = \theta_{01}, z = 0)$

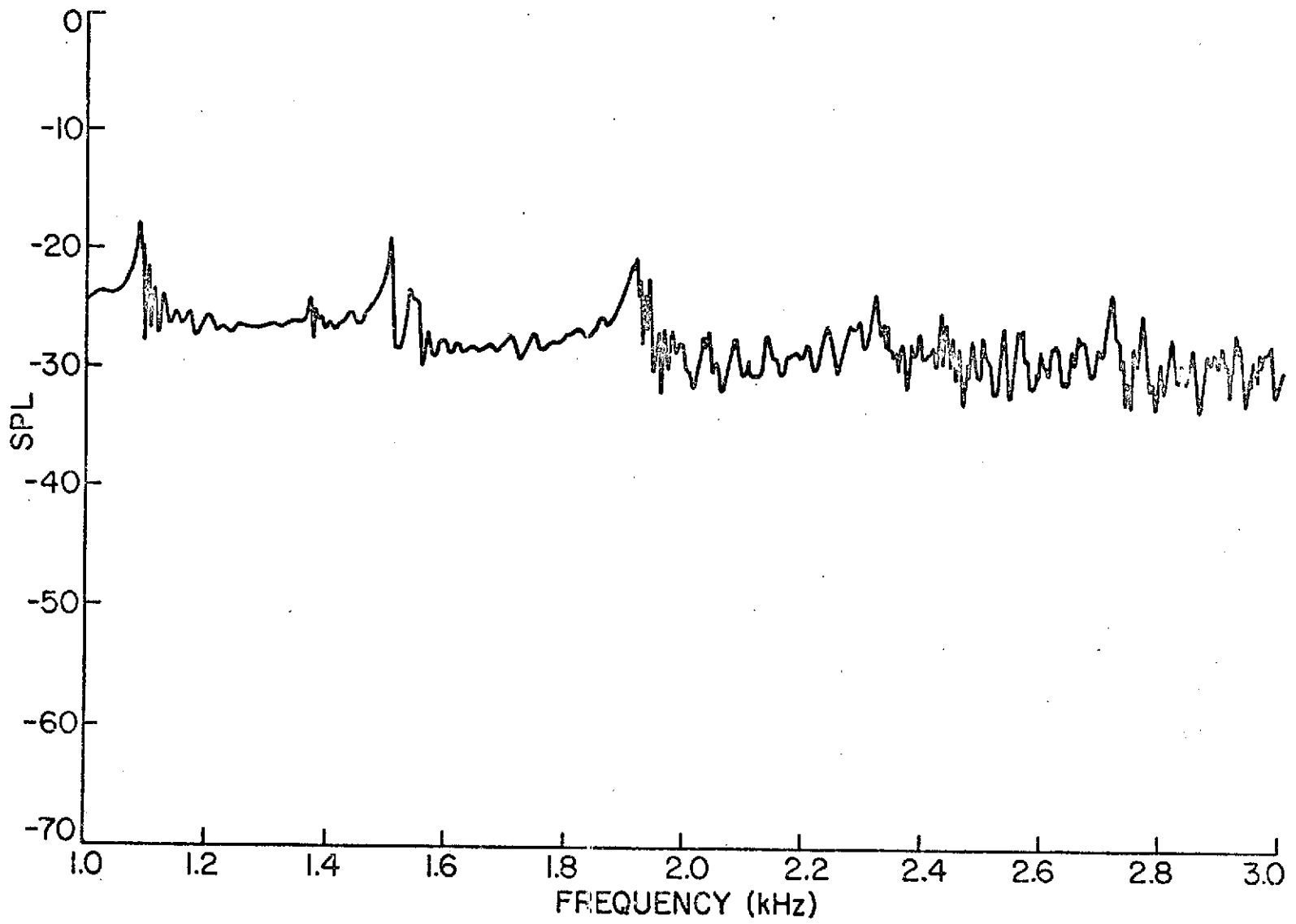


FIGURE 45

SPL versus Frequency for Transducer 1
of the Ducted Array at a Constant Voltage (.9 volts)
at $(r = r_{01}, \theta = \theta_{01}, z = 0)$

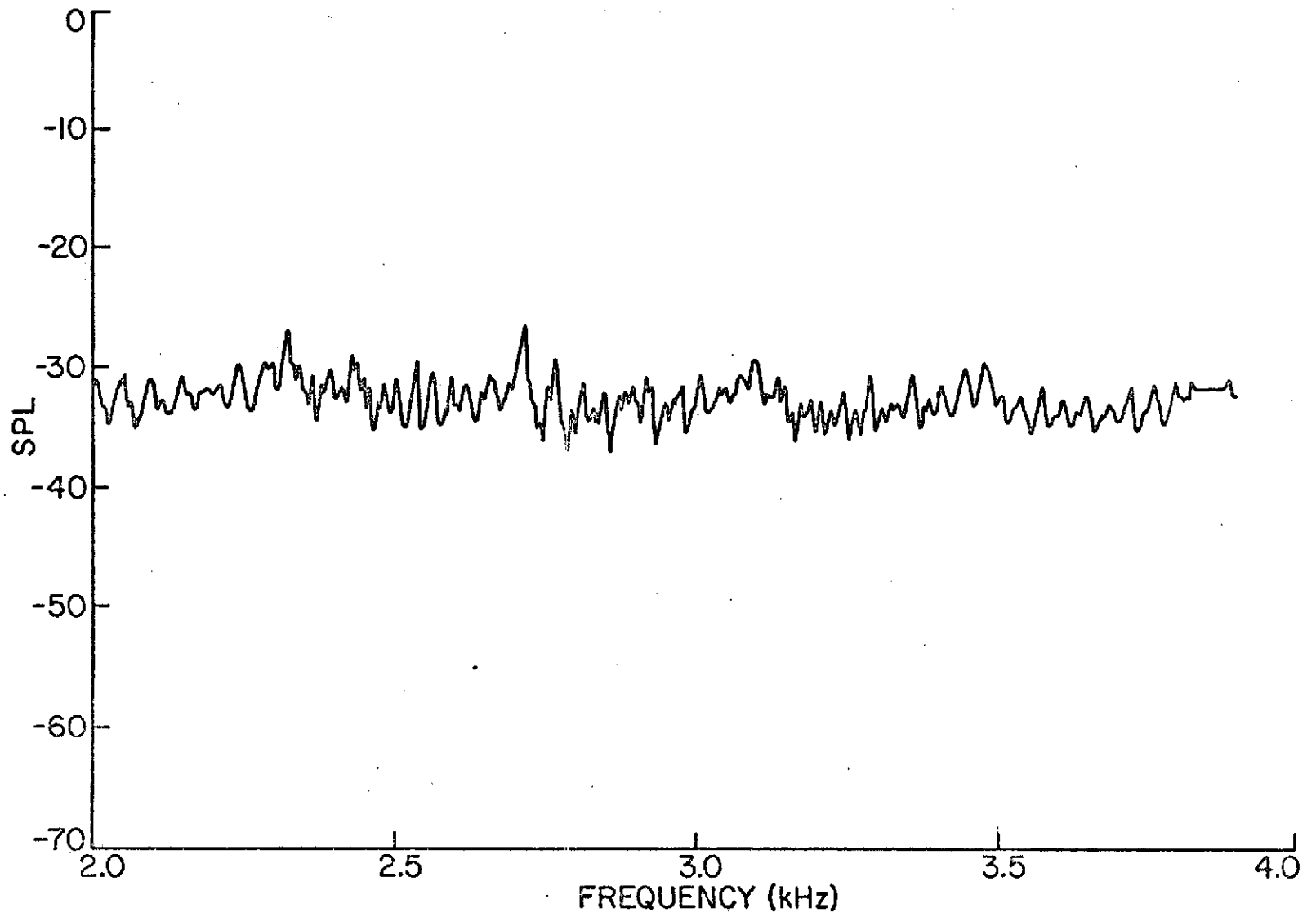


FIGURE 46

SPL versus Radial Distance at 2' from Plate for $m = 1$, $\mu = 1$,
Mode at 750 Hz with Acoustic Parameters of
each Transducer set by use of
Plate Microphone

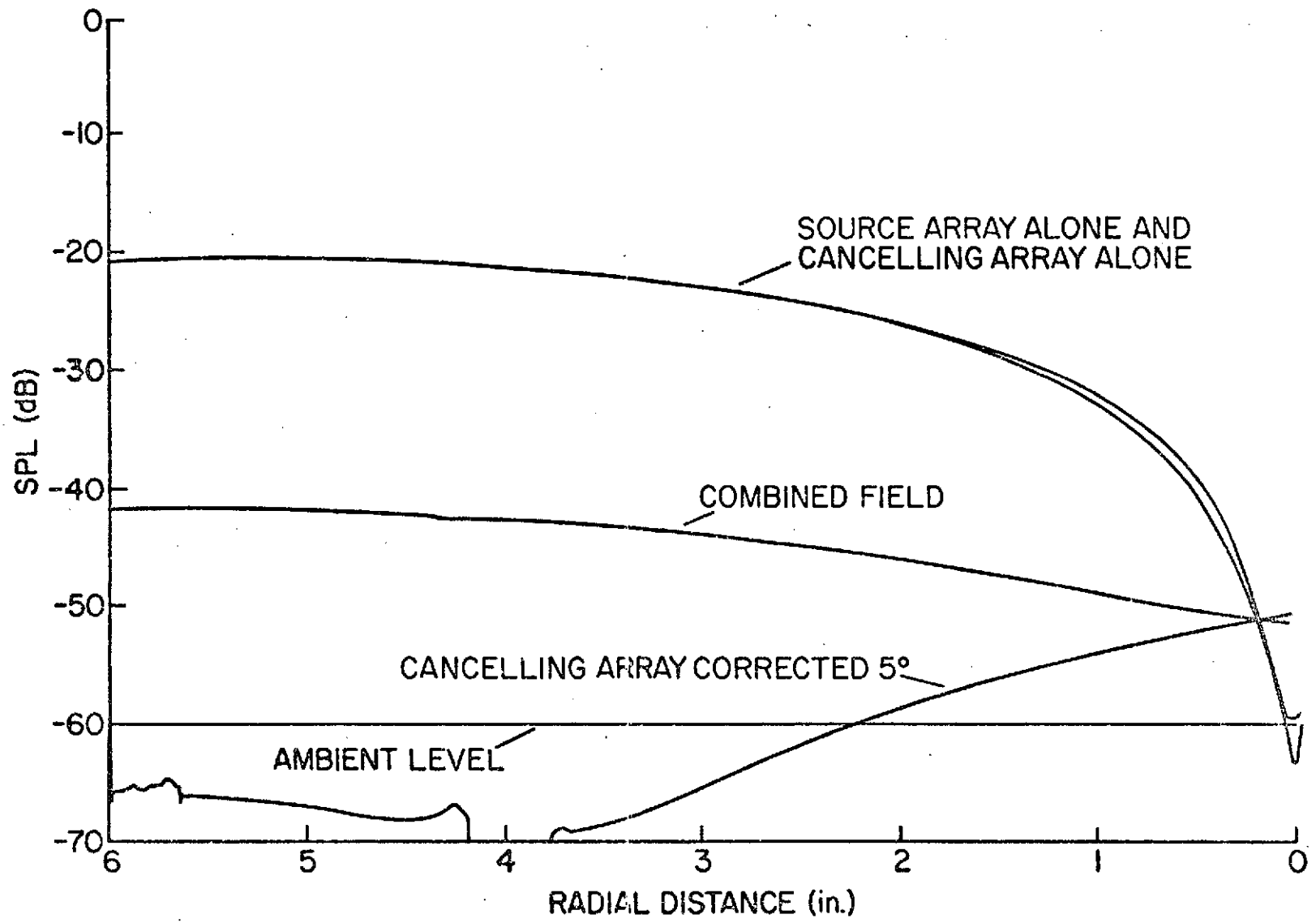


FIGURE 47

Phase versus Radial Distance at 2' from Plate for
 $m = 1, \mu = 0$ Mode at 750 Hz with Acoustic Parameters of each Transducer
set by use of Plate Microphone

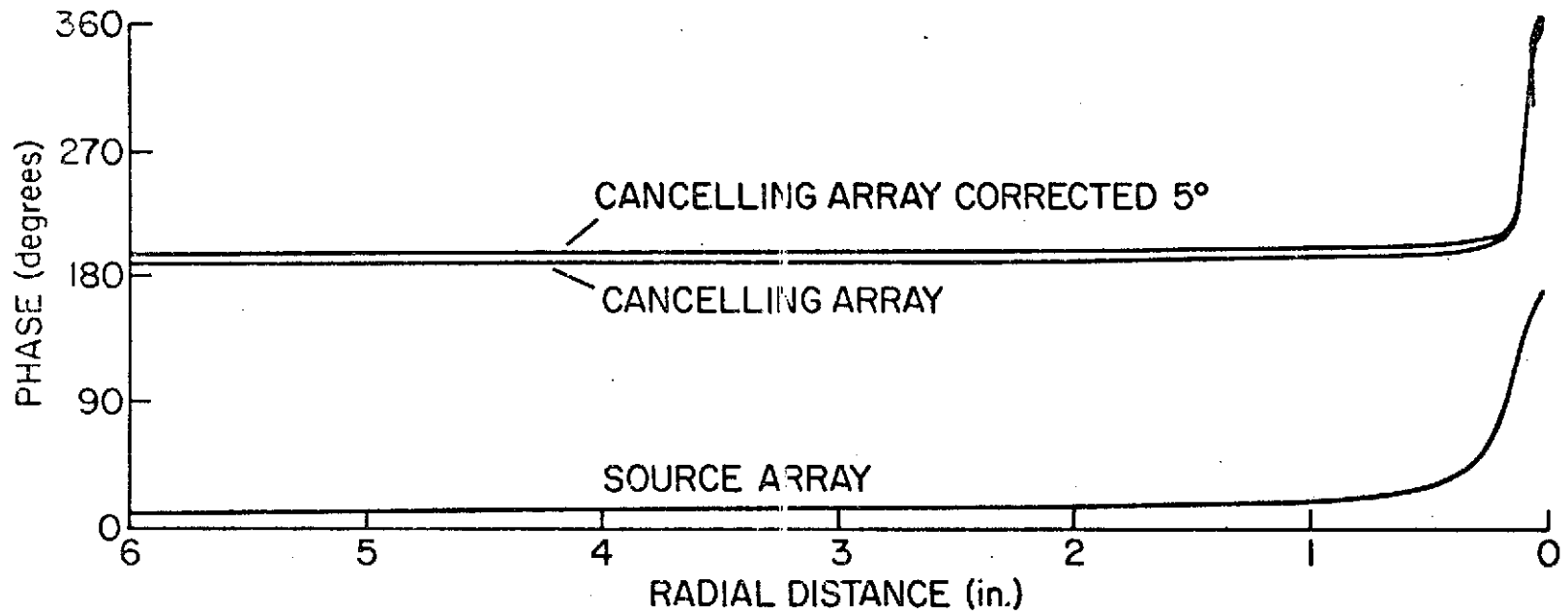


FIGURE 48

Phase versus Radial Distance at 6' from Plate

for $\mu = 0$ Mode at 750 Hz with Acoustic Parameters of each Transducer
set by use of Plate Microphone

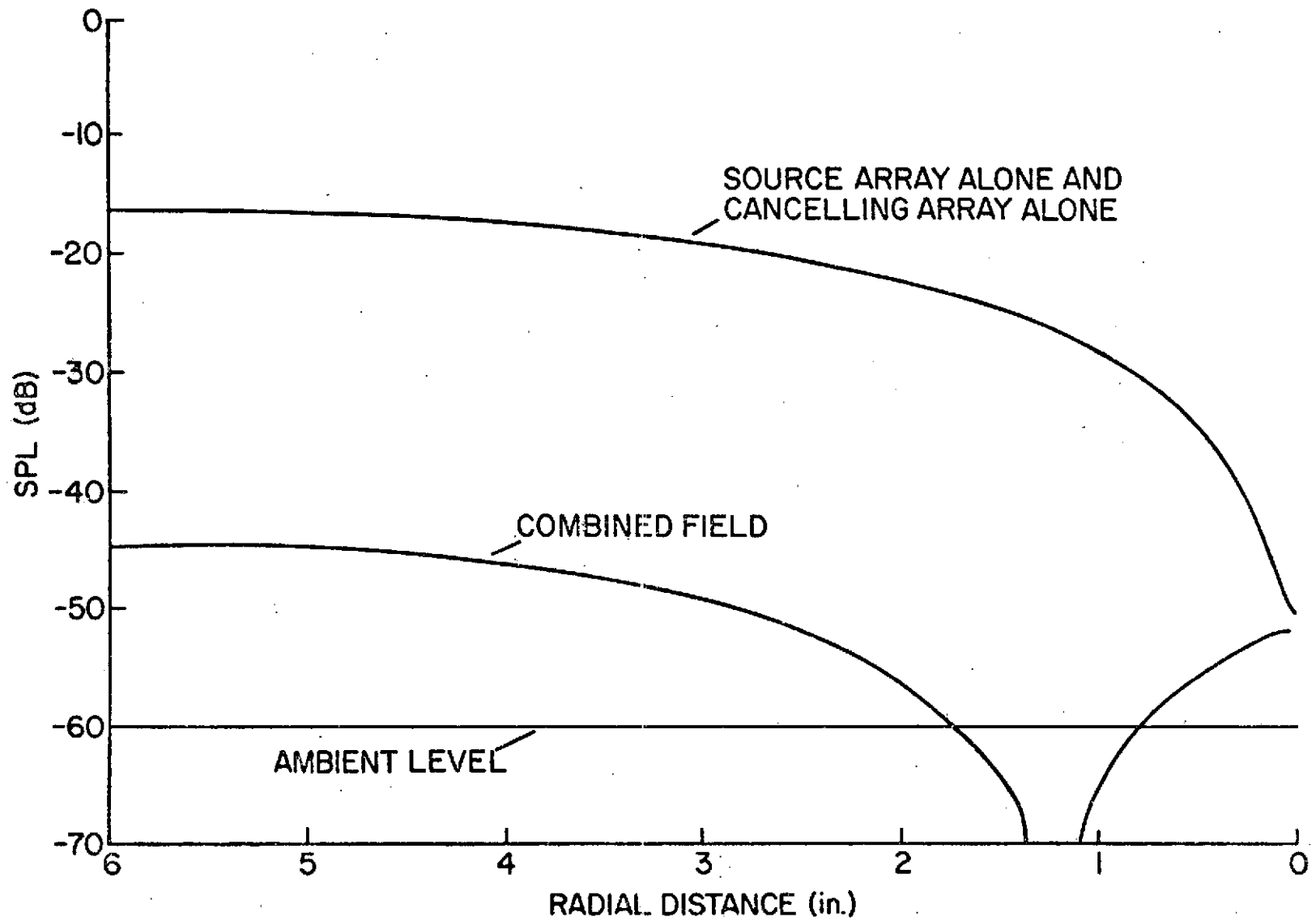


FIGURE 49

Phase versus Radial Distance at 6' from Plate for $m = 1$,
 $\mu = 0$ Mode at 750 Hz with Acoustic Parameters of each Transducer
set by use of Plate Microphone

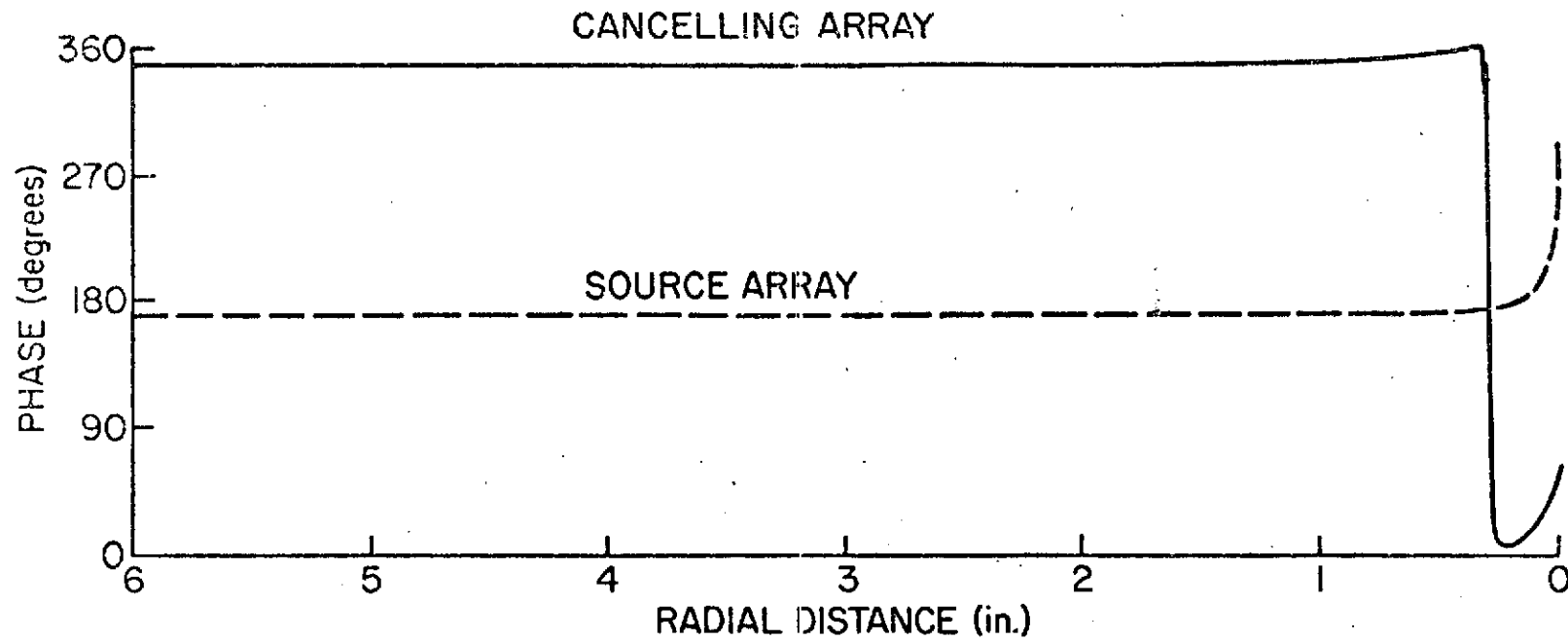


FIGURE 50

SPL versus Radial Distance at 8' from Plate for $m = 1$, $\mu = 0$

Mode at 750 Hz with Acoustic Parameters of each

Transducer set by use of Plate Microphone

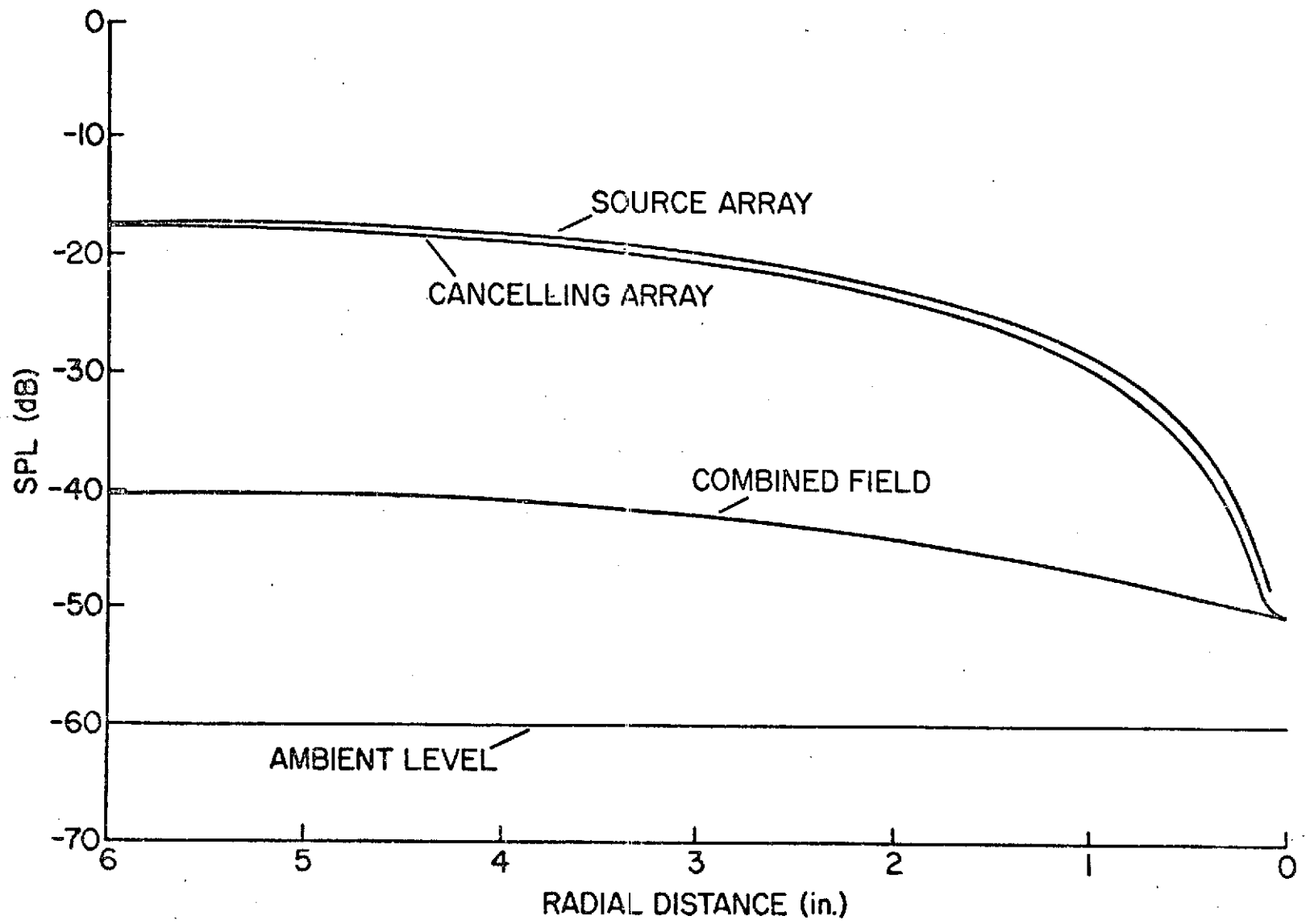
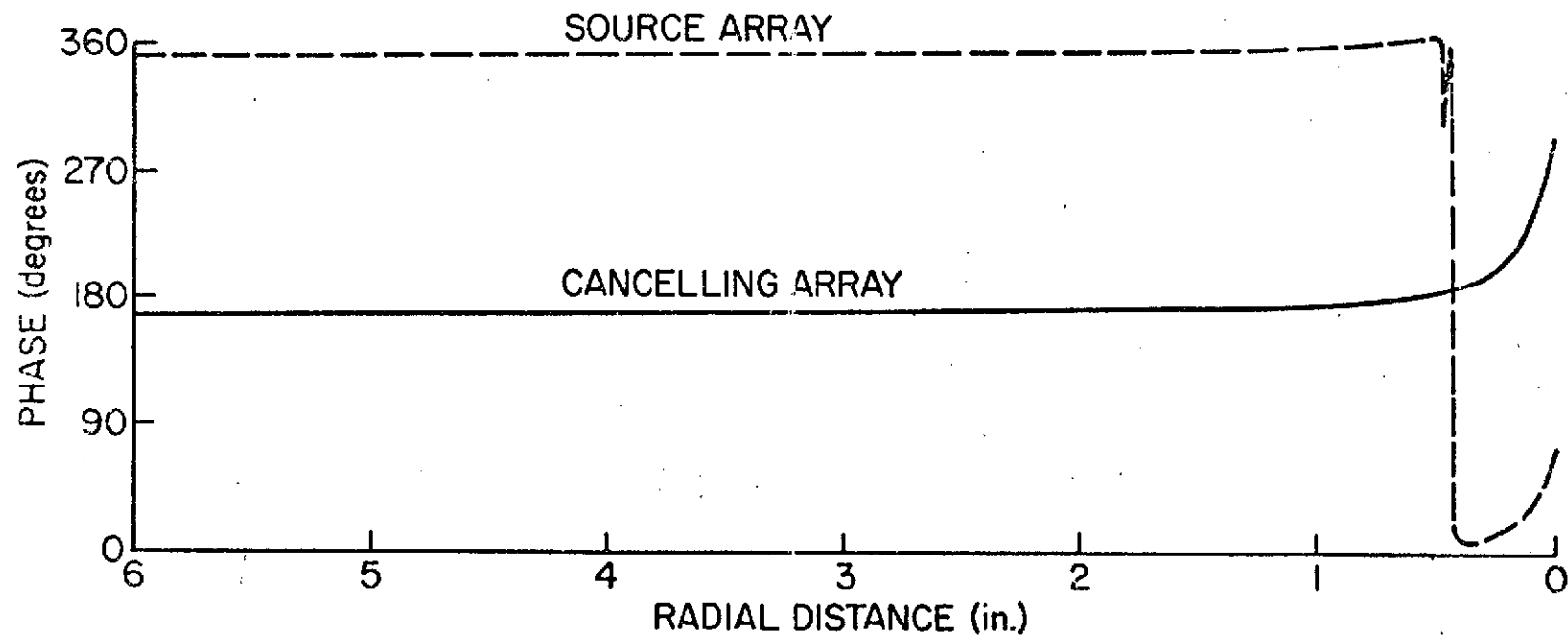


FIGURE 51

Phase versus Radial Distance at 8' from Plate for $m = 1$, $\mu = 0$
Mode at 750 Hz with Acoustic Parameters of
each Transducer set by use of Plate Microphone



array transducers did not produce an overall cancellation performance improvement (Figures 46 through 51).

Sufficient information had been obtained so preliminary experimental analysis was concluded. Satisfactory cancellation performance was observed to 1400 Hz for the fundamental spinning wave. The basic system parameters had been investigated and complications noted. Thus adequate knowledge of the system had been established for the synthesis of an automatic controller for in-duct cancellation.

III. Automatic Control Problem

3.1 Need for Automatic Control

The spinning modes of sound generated by a jet engine are dependent in part on relatively slowly time varying parameters. The set of circumferential modes which can be generated depend only on the blade-vane numbers. But, the predominant radial mode number associated with any given circumferential mode depends on the blade passage frequency, and duct diameter. The sound pressure levels associated with a given mode will vary, dependent largely upon throttle setting, air speed, and air density for any given engine configuration. Since the system is subject to time varying parameters, an acoustic cancellation system will require automatic control.

Application of the cancellation scheme to a jet engine poses a further complication. Because of the high acoustic amplitudes associated with fan noise, the linear acoustic approximation no longer holds and wave steepening occurs as the waves travel down the duct. An adaptive control may offer opportunities to compensate for this factor.

The automatic control of the Spinning Mode Synthesizer is of immediate concern. Objectives of this work are the attainment of effective parameter variation, rigorous evaluation of the synthesizer, and the introduction of complexities characteristic of jet engines. Open loop control of cancellation has been found to be insufficient in these areas.

The determination of the optimum input parameter setting to maximize cancellation of a particular spinning mode by open loop control is tedious. Open loop control does not allow sufficient test cases to ensure effective mode cancellation specifically for high frequencies.

The "point cancellation" effect discussed in Chapter II provides an additional barrier to productive experimentation. As suggested, a measurement system yielding a signal proportional to overall system performance would greatly accelerate the testing process. The synthesis of such a measurement system is a difficult problem. The minimization of "point cancellation" effects on the index of performance will most likely require an empirical design technique. This would be impeded by the lengthy experimentation time. Thus the need for effective parameter variation is firmly established.

An important measure of SMS cancellation performance is the range of circumferential modes and radial distribution over which effective cancellation can be achieved. It is essential to the evaluation of the SMS to determine the pertinent parameters and the functional relationships which result in undesirable system performance. The empirical determination of these relationships would be greatly aided by an efficient testing system.

Open loop control of the cancelling array inhibits introduction of complexities characteristic of jet engines. For example, there is often significant energy in more than one mode. The cancellation of multiple modes increases the dimension of the controller to

$$n' = c n$$

where n = dimension of the cancellation system for a
single acoustic mode

c = number of modes

In addition, the spinning modes are contaminated by broad band noise, turbulent air flow, a short, thin-walled duct, time varying parameters, etc. Manually controlled cancellation under any of these conditions would be very difficult. Thus, the development of automatic control is essential for the successful development of the cancellation concept. And, automatic control of the Spinning Mode Synthesizer is a basic necessity to the development of an effective in-duct mode cancellation device.

3.2 Statement of Control Problem

A control system is to be designed and developed for the automatic control of the Spinning Mode Synthesizer cancellation simulation. There are five general variables: the circumferential distribution of the spinning wave (m), the radial distribution of the spinning wave (μ), frequency (f), acoustic pressure amplitude (A), and acoustic phase (α_o). For a given m , μ is a function of frequency so μ does not require regulation or control. The cancelling array is driven from the same frequency oscillator as the source array, maintaining a frequency lock on the optimum frequency. The term frequency lock is used to describe the cancelling system state of being driven exactly at the frequency of the source array, eliminating all beating effects.

Each transducer has an associated acoustic pressure amplitude A_j which will be measured in terms of SPL_j , the sound pressure level near the transducer, and an acoustic phase α_{oj} , $j = 1,2,3,4$. The electrical inputs to the transducers are the directly controlled variables. The

electrical amplitude and phase will be designated by v_i and θ_i .

Schematically, the plant can be shown as follows:

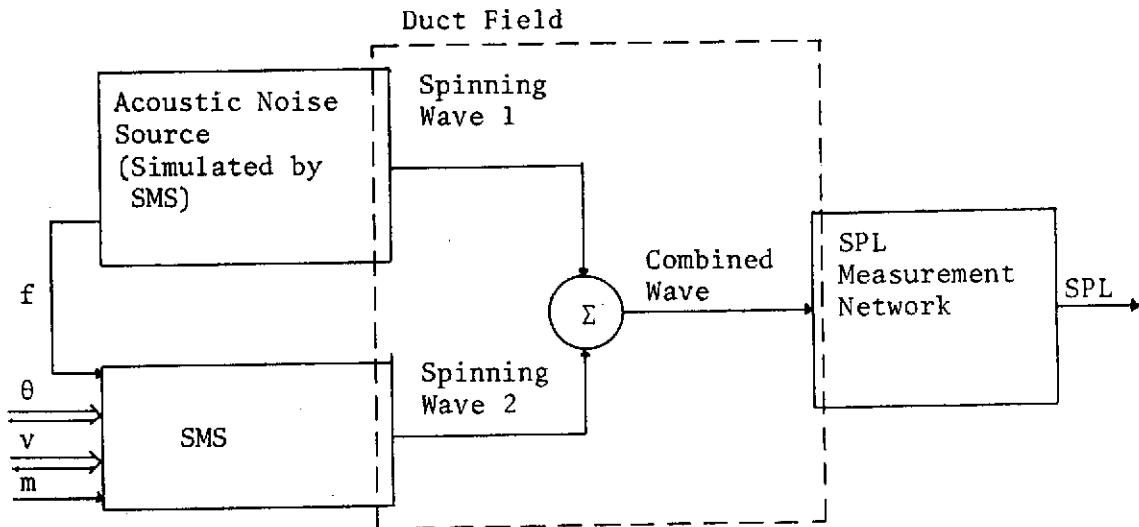


FIGURE 52

Plant Schematic

The plant is 10-dimensional: $f, m, \sum_{j=1}^4 (\theta_j, v_j)$. But frequency

is a variable controlled by a source array. The parameter m would be selected by the operator or by a pattern recognition system. So, once m is selected, the plant reduces to an 8-dimensional system with an 8-dimensional input and single output, or performance indicator.

3.3 Determination of System Model

Cylindrical coordinates for the SMS can be established as follows:

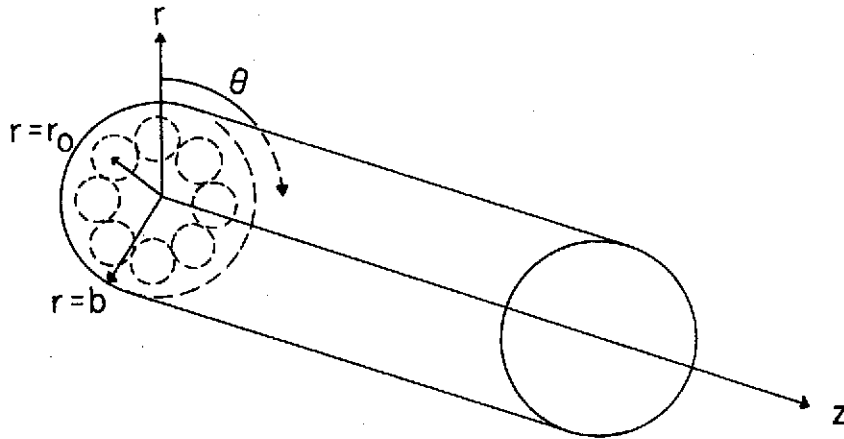


FIGURE 53

Cylindrical Coordinates of SMS

The analytical description of the pressure field inside a hard-walled, semi-infinite duct due to a general sinusoidal source at $z = 0$ has been developed (Appendix 1):

$$P(r, \theta, z, t) = + \sum_{m=0}^{\infty} \sum_{\mu=0}^{\infty} E_{m\mu} [G_{m\mu} e^{+im\theta} + H_{m\mu} e^{-im\theta}] J_m(k_{m\mu} r) e^{i(\gamma_{m\mu} z - \omega t)}$$

where

$E_{m\mu}$ = amplitude coefficients (Appendix 1)

$$G_{m\mu} = \int_0^{2\pi} \int_0^b r f(r, \theta, 0) J_m(k_{m\mu} r) e^{-im\theta} dr d\theta, m \neq 0$$

$$H_{m\mu} = \int_0^{2\pi} \int_0^b r f(r, \theta, 0) J_m(k_{m\mu} r) e^{im\theta} dr d\theta, m \neq 0$$

$$G_{0\mu} + H_{0\mu} = \int_0^{2\pi} \int_0^b r f(r, \theta, 0) J_0(k_{0\mu} r) dr d\theta, m = 0$$

and

$J_m(k_{m\mu} r)$ = Bessel function of the first kind of order m

$k_{m\mu}$ = eigenvalue of order μ for the m^{th} mode having

a hub-tip ratio $\sigma = 0$

$f(r, \theta, 0)$ = amplitude distribution of source

$$\gamma_{m\mu} = \sqrt{\left(\frac{\omega}{c}\right)^2 - k_{m\mu}^2}$$

m = circumferential distribution

μ = radial distribution

To complete the solution, the source must be specified. The two sets of n transducers will be approximated by two sets of n point sources. Both transducer arrays are located a distance r_0 from the z axis. The relative position of the transducers in the θ direction is given by

$$\theta_{0j} = \frac{2\pi}{n} (j - 1), \quad j = 1, 2, \dots, n$$

where θ_{0j} is the relative position of the j^{th} transducer. The Dirac delta function is used to mathematically provide the point source description in the r and θ directions. A point in cylindrical

coordinates is given by

$$g(r, \theta, z) = \frac{1}{r} \delta(r - r_0) \delta(\theta - \theta_0) \delta(z - z_0).$$

So, a point at r_0 and θ_{0j} in the plane $z = 0$ is given by

$$g_j(r, \theta, 0) = \frac{1}{r} \delta(r - r_0) \delta(\theta - \theta_{0j})$$

The cancelling array is offset by an angle Δ :

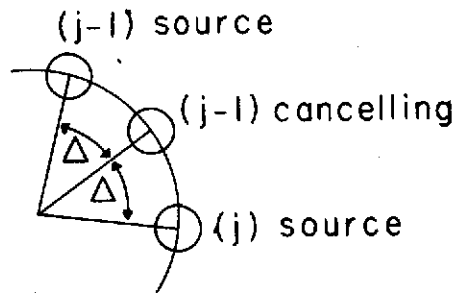


FIGURE 54

Angle Between Cancelling Array and Source Array

where $\Delta = \frac{1}{2} \left[\frac{2\pi}{n} (j - 1) - \frac{2\pi}{n} (j - 1) - 1 \right] = \frac{\pi}{n}$.

The acoustic phase of the source array, using the first transducer as a reference, is given by:

$$\phi_{0j} = \frac{2\pi r_0}{n} (j - 1), \quad j = 1, 2, \dots, n$$

where ϕ_{oj} is the acoustic phase of the j^{th} transducer and m_o is the desired circumferential distribution. The acoustic phases of the cancelling transducers will be given by α_{oj} , $j = 1, 2, \dots, n$, which are not yet determined. Let Q = source strength of source transducer, in cubic meters per second. Let q = source strength of cancelling transducer, in cubic meters per second. The source can then be defined by:

$$f(r, \theta, 0) = \sum_{j=1}^n \left[\frac{Q}{r} e^{i\phi_{oj}} \delta(r - r_o) \delta(\theta - \theta_{oj}) + \frac{q}{r} e^{i\alpha_{oj}} \delta(r - r_o) \delta(\theta - \theta_{oj} - \frac{\pi}{n}) \right]$$

Then,

$$\begin{aligned} G_{m\mu} &= \int_0^{2\pi} \int_0^b r \left\{ \sum_{j=1}^n \left[\frac{Q}{r} e^{i\phi_{oj}} \delta(r - r_o) \delta(\theta - \theta_{oj}) + \frac{q}{r} e^{i\alpha_{oj}} \delta(r - r_o) \delta(\theta - \theta_{oj} - \frac{\pi}{n}) \right] \right\} J_m(k_{m\mu} r) e^{-im\theta} dr d\theta \\ &= \int_0^b J_m(k_{m\mu} r) \delta(r - r_o) dr \cdot \sum_{j=1}^n \int_0^{2\pi} \left[Q e^{i\phi_{oj}} \delta(\theta - \theta_{oj}) + q e^{i\alpha_{oj}} \delta(\theta - \theta_{oj} - \frac{\pi}{n}) \right] e^{-im\theta} d\theta \\ &= J_m(k_{m\mu} r_o) \sum_{j=1}^n \left[Q e^{i\phi_{oj}} e^{-im\theta_{oj}} + q e^{i\alpha_{oj}} e^{-im(\theta_{oj} + \frac{\pi}{n})} \right] \end{aligned}$$

Similarly,

$$H_{m\mu} = J_m(k_{m\mu} r_o) \sum_{j=1}^n \left[Q e^{i\phi_{oj}} e^{im\theta_{oj}} + q e^{i\alpha_{oj}} e^{im(\theta_{oj} + \frac{\pi}{n})} \right].$$

Also,

$$\begin{aligned}
 G_{0\mu} + H_{0\mu} &= \int_0^b \int_0^{2\pi} r \left\{ \sum_{j=1}^n \left[\frac{Q}{r} e^{i\phi_{oj}} \delta(r - r_o) \delta(\theta - \theta_{oj}) \right. \right. \\
 &\quad \left. \left. + \frac{q}{r} e^{i\alpha_{oj}} \delta(r - r_o) \delta\left(\theta - \theta_{oj} - \frac{\pi}{n}\right) \right] \right\} J_0(k_{0\mu}r) dr d\theta \\
 &= \int_0^b J_0(k_{0\mu}r) \delta(r - r_o) dr \cdot \\
 &\quad \cdot \sum_{j=1}^n \int_0^{2\pi} \left[Q e^{i\phi_{oj}} \delta(\theta - \theta_{oj}) + q e^{i\alpha_{oj}} \delta\left(\theta - \theta_{oj} - \frac{\pi}{n}\right) \right] d\theta \\
 &= J_0(k_{0\mu}r_o) \sum_{j=1}^n \left[Q e^{i\phi_{oj}} + q e^{i\alpha_{oj}} \right]
 \end{aligned}$$

Now,

$$\begin{aligned}
 K_{m\mu} &= G_{m\mu} e^{im\theta} + H_{m\mu} e^{-im\theta} \\
 &= J_m(k_{m\mu}r_o) \sum_{j=1}^n \left\{ \left[Q e^{i(\phi_{oj} - m\theta_{oj})} + q e^{i(\alpha_{oj} - m(\theta_{oj} + \frac{\pi}{n}))} \right] \cdot \right. \\
 &\quad \left. \cdot e^{im\theta} + \left[Q e^{i(\phi_{oj} + m\theta_{oj})} + q e^{i(\alpha_{oj} + m(\theta_{oj} + \frac{\pi}{n}))} \right] e^{-im\theta} \right\}
 \end{aligned}$$

for $m \neq 0$. For $m = 0$,

$$K_{m\mu} = J_0(k_{0\mu}r_o) \sum_{j=1}^n \left[Q e^{i\phi_{oj}} + q e^{i\alpha_{oj}} \right].$$

an expression for $K_{m\mu}$ valid for all m can be given by:

$$\begin{aligned}
 K_{m\mu} &= \frac{\epsilon_m}{2} J_m(k_{m\mu}r_o) \sum_{j=1}^n \left\{ \left[Q e^{i(\phi_{oj} - m\theta_{oj})} + q e^{i(\alpha_{oj} - m(\theta_{oj} + \frac{\pi}{n}))} \right] \cdot \right. \\
 &\quad \left. \cdot e^{im\theta} + \left[Q e^{i(\phi_{oj} + m\theta_{oj})} + q e^{i(\alpha_{oj} + m(\theta_{oj} + \frac{\pi}{n}))} \right] e^{-im\theta} \right\}
 \end{aligned}$$

where $\epsilon_m = \begin{cases} 1 & \text{for } m = 0 \\ 2 & \text{for } m \geq 1. \end{cases}$

Thus the complete solution is given by

$$P(r, \theta, z, t) = + \sum_{m=0}^{\infty} \sum_{\mu=0}^{\infty} E_{m\mu} K_{m\mu} J_m(k_{m\mu} r) e^{i(\omega t - \gamma_{m\mu} z)}$$

where $K_{m\mu}$ is given above. Since $\phi_{oj} = m_o \theta_{oj}$, $K_{m_o \mu}$ can be written as:

$$K_{m_o \mu} = \frac{\epsilon_m}{2} J_{m_o}(k_{m_o \mu} r_o) \sum_{j=1}^n \left\{ [Q + q e^{i(\alpha_{oj} - \phi_{oj} - \frac{m_o \pi}{n})}] e^{im_o \theta} + [Q e^{2i\phi_{oj}} + q e^{i(\alpha_{oj} + \phi_{oj} + \frac{m_o \pi}{n})}] e^{-m_o \theta} \right\}$$

Maximum cancellation occurs when the magnitude of the real component of pressure is minimized with respect to α_{oj} and q . $\text{Re}[P(r, \theta, z, t)]$ can be evaluated as follows:

$$P(r, \theta, z, t) = \sum_{m=0}^{\infty} \sum_{\mu=0}^{\infty} E_{m\mu} \frac{\epsilon_m}{2} J_m(k_{m\mu} r_o) \sum_{j=1}^n \left\{ [Q e^{i(\phi_{oj} - m\theta_{oj})} + q e^{i(\alpha_{oj} - m(\theta_{oj} + \frac{\pi}{n}))}] e^{im\theta} + [Q e^{i(\phi_{oj} + m\theta_{oj})} + q e^{i(\alpha_{oj} + m(\theta_{oj} + \frac{\pi}{n}))}] e^{-im\theta} \right\} J_m(k_{m\mu} r) e^{i(\gamma_{m\mu} z - \omega t)}$$

$$P(r, \theta, z, t) = \sum_{m=0}^{\infty} \sum_{\mu=0}^{\infty} E_{m\mu} \frac{\epsilon_m}{2} J_m(k_{m\mu} r_o) J_m(k_{m\mu} r) \cdot \sum_{j=1}^n \left\{ Q e^{i(\phi_{oj} - m\theta_{oj} + m\theta + \gamma_{m\mu} z - \omega t)} + q e^{i(\alpha_{oj} - m\theta_{oj} - \frac{m\pi}{n} + m\theta + \gamma_{m\mu} z - \omega t)} + Q e^{i(\phi_{oj} + m\theta_{oj} - m\theta + \gamma_{m\mu} z - \omega t)} + \dots \right\}$$

$$+ q e^{i(\alpha_{oj} + m\theta_{oj} + \frac{m\pi}{n} - m\theta + \gamma_{m\mu} z - \omega t)}$$

Then,

$$\begin{aligned} \operatorname{Re}[P(r, \theta, z, t)] &= \left[\sum_{m=0}^{\infty} \sum_{\mu=0}^{\infty} E_{m\mu} \frac{\epsilon_m}{2} J_m(k_{m\mu} r_o) J_m(k_{m\mu} r) \cdot \right. \\ &\quad \cdot \sum_{j=1}^n \{ Q \cos(\phi_{oj} - m\theta_{oj} + m\theta + \gamma_{m\mu} z - \omega t) + \\ &\quad + q \cos(\alpha_{oj} - m\theta_{oj} - \frac{m\pi}{n} + m\theta + \gamma_{m\mu} z - \omega t) + \\ &\quad + Q \cos(\phi_{oj} + m\theta_{oj} - m\theta + \gamma_{m\mu} z - \omega t) + \\ &\quad \left. + q \cos(\alpha_{oj} + m\theta_{oj} + \frac{m\pi}{n} - m\theta + \gamma_{m\mu} z - \omega t) \right] \\ &\quad \text{for } m, \mu \text{ such that } k_{m\mu} \leq \frac{\omega}{c} \\ &- \left[\sum_{m=0}^{\infty} \sum_{\mu=0}^{\infty} (i E_{m\mu}) \frac{\epsilon_m}{2} J_m(k_{m\mu} r_o) J_m(k_{m\mu} r) e^{i\gamma_{m\mu} z} \cdot \right. \\ &\quad \cdot \sum_{j=1}^n \{ Q \sin(\phi_{oj} - m\theta_{oj} + m\theta - \omega t) + \\ &\quad + q \sin(\alpha_{oj} - m\theta_{oj} - \frac{m\pi}{n} + m\theta - \omega t) + \\ &\quad + Q \sin(\phi_{oj} + m\theta_{oj} - m\theta - \omega t) + \\ &\quad \left. + q \sin(\alpha_{oj} + m\theta_{oj} + \frac{m\pi}{n} - m\theta - \omega t) \right] \\ &\quad \text{for } m, \mu \text{ such that } k_{m\mu} > \frac{\omega}{c} \end{aligned}$$

$$\begin{aligned} \operatorname{Re}[P(r, \theta, z, t)] &= \sum_{m=0}^{\infty} \sum_{\mu=0}^{\infty} \epsilon_m J_m(k_{m\mu} r_o) J_m(k_{m\mu} r) \cdot \\ &\quad \cdot \left[E_{m\mu} \sum_{j=1}^n \{ Q \cos(\phi_{oj} + \gamma_{m\mu} z - \omega t) \cos(m\theta - m\theta_{oj}) + \right. \end{aligned}$$

$$\begin{aligned}
& + q \cos \left(\alpha_{oj} + \gamma_{m\mu} z - \omega t \right) \cos \left(m\theta - m\theta_{oj} - \frac{m\pi}{n} \right) \} \\
& \text{for } m, \mu \text{ such that } k_{m\mu} < \frac{\omega}{c} \\
& - [i E_{m\mu} e^{i\gamma_{m\mu} z} \sum_{j=1}^n \{ Q \sin (\phi_{oj} - \omega t) \cos (m\theta - m\theta_{oj}) + \\
& + q \sin (\alpha_{oj} - \omega t) \cos (m\theta - m\theta_{oj} - \frac{m\pi}{n}) \} \\
& \text{for } m, \mu \text{ such that } k_{m\mu} > \frac{\omega}{c}]
\end{aligned}$$

considering only propagating waves, i.e., $k_{m\mu} < \frac{\omega}{c}$, we have

$$\begin{aligned}
\text{Re}[P(r, \theta, z, t)] &= \sum_{m=0}^{\infty} \sum_{\mu=0}^{\infty} E_{m\mu} \epsilon_m J_m(k_{m\mu} r_o) J_m(k_{m\mu} r) \cdot \\
&\cdot \sum_{j=1}^n \{ Q \cos (\phi_{oj} + \gamma_{m\mu} z - \omega t) \cos (m\theta - m\theta_{oj}) \\
&+ q \cos (\alpha_{oj} + \gamma_{m\mu} z - \omega t) \cos (m\theta - m\theta_{oj} - \frac{m\pi}{n}) \} \\
&\hspace{15em} (3.3-A)
\end{aligned}$$

As $n \rightarrow \infty$, the two arrays approach "source rings", continuous arrays in the θ direction. For this case, $\text{Re}[P(r, \theta, z, t)]$ is zero term by term for all m and μ independent of r, θ, z , and t for $q = Q$ and $\alpha_{oj} = \phi_{oj} + (2\ell+1)\pi$, $\ell = 0, \pm 1, \pm 2, \dots$. In the other extreme, for small n the point source behavior of the arrays becomes significant. $\text{Re}[P]$ in general cannot be reduced to zero. As $m \rightarrow n$, significant multi-mode excitation can make cancellation impossible.

Consider the case of $n = 4$. As illustrated in Figure 55, there is good waveform phasing bias only for $m = 0$ and $m = 1$.

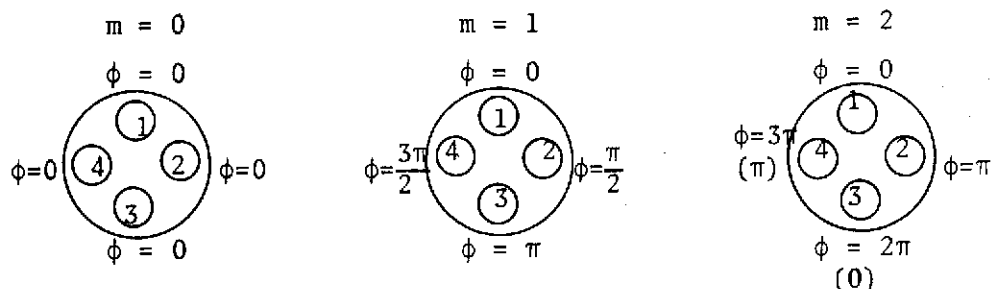


FIGURE 55

Acoustic Phases for $m = 0, 1,$ and 2 for $n = 4$

For $m = 2$, spinning waves of equal strength are excited in the clockwise and counter-clockwise directions. Also, the (1,3) and (2,4) transducer pairs generate plane waves of equal strength. Thus it can be deduced that for a single, well defined waveform, it is desirable to have $n \gg m$.

Assuming a single dominant acoustic mode of $m = m_0$ and $\mu = \mu(f)$, it is desired to determine the values of q and α_{0j} for maximum cancellation. One basic procedure is to take the respective partial derivatives and set them equal to zero, thus determining the maxima and minima. $\text{Re}[P]$ is the real component of a complex number, so both positive and negative values must be dealt with. The minimization of $(\text{Re}[P])^2$ provides a physically meaningful and analytically expedient means of minimizing the magnitude of P . The sound pressure level,

given by

$$\text{SPL} = 10 \log \left(\frac{p}{p_{\text{ref}}} \right)^2$$

is minimized by minimizing the rms pressure squared, p^2 . Since

$$p^2 = \overline{(\text{Re}[P])^2},$$

minimizing $(\text{Re}[P])^2$ minimizes the sound pressure level. Consider the determination of the extremum of $\{\text{Re}[P(m_0, \mu(f), r, \theta, z, t)]\}^2$ by evaluation of the partial derivations with respect to q and α_{oj} , $j = 1, 2, \dots, n$. The optimal values q^* and α_{oj}^* are then q and α_{oj} evaluated at the minima of $\{\text{Re}[P]\}^2$, if and only if these values are independent of r, θ, z and t .

The partial derivative of $\{\text{Re}[P]\}^2$ with respect to q is:

$$\frac{\partial}{\partial q} \{\text{Re}[P]\}^2 = 2 \text{Re}[P] \frac{\partial}{\partial q} \text{Re}[P] = 0$$

Either $\text{Re}[P] = 0$ or $\frac{\partial}{\partial q} \text{Re}[P] = 0$. For the acoustic phases,

$$\frac{\partial}{\partial \alpha_{oj}} \{\text{Re}[P]\}^2 = 2 \text{Re}[P] \frac{\partial}{\partial \alpha_{oj}} \text{Re}[P] = 0$$

If $\text{Re}[P] = 0$, there is only one equation while there are $(n + 1)$ unknowns. Thus if $\text{Re}[P(m_0, \mu(f), r, \theta, z, t)]$ is zero, this method of solution cannot be used to determine the optimal values q^* and α_{oj}^* . If $\text{Re}[P] \neq 0$, there are $(n + 1)$ equations.

$$\frac{\partial}{\partial q} \operatorname{Re}[P] = 0 \implies \sum_{j=1}^n \left\{ \cos(\alpha_{oj} + \gamma_{m_o \mu} z - \omega t) \cdot \cos(m_o \theta - m_o \theta_{oj} - \frac{m_o \pi}{n}) \right\} = 0$$

and

$$\frac{\partial}{\partial \alpha_{oj}} \operatorname{Re}[P] = 0 \implies \cos(\alpha_{oj} + \gamma_{m_o \mu} z - \omega t) \cos(m_o \theta - m_o \theta_{oj} - \frac{m_o \pi}{n}) = 0$$

But, the $(n + 1)$ equations give only space and time coordinates at which minima can occur in the sound field. Thus no usable information is yet obtainable about q and α_{oj} .

To obtain usable information, an index of performance is defined as follows:

$$IP = \frac{1}{2\ell\pi^2 b^2 Z} \int_0^{2\ell\pi} \int_0^Z \int_0^{2\pi} \int_0^b \{\operatorname{Re}[P(m, \mu)]\}^2 r dr d\theta dz d\omega t \quad (3.3-B)$$

This serves as an indicator of the time average pressure amplitude of the (m, μ) mode over the entire duct volume out to a distance Z . The minimization of this index of performance is thus physically meaningful since it is the objective of this system to reduce the overall sound pressure. Since direct dependence upon spatial coordinates is eliminated, meaningful results can be expected. The IP is evaluated as follows:

$$\{\operatorname{Re}[P(m, \mu)]\}^2 = E_{m\mu}^2 \epsilon_m^2 J_m^2(k_{m\mu} r_o) J_m^2(k_{m\mu} r) \cdot \left[\sum_{j=1}^n \{Q \cos(\phi_{oj} + \gamma_{m\mu} - \omega t) \cos(m\theta - m\theta_{oj})\} \right]$$

$$+ q \cos \left(\alpha_{oj} + \gamma_{m\mu} z - \omega t \right) \cos \left(m\theta - m\theta_{oj} - \frac{m\pi}{n} \right) \Big]^2$$

$$\int_0^b \{ \text{Re}[P(m,\mu)] \}^2 r dr = E_{m\mu}^2 \epsilon_m^2 J_m^2(k_{m\mu} r_0) [\cdot]^2 \int_0^b r J_m^2(k_{m\mu} r) dr$$

where $[\cdot]$ represents the bracketed term in the previous equation.

$$\int_0^b r J_m^2(k_{m\mu} r) dr = \left[\frac{1}{2k_{m\mu}^2} \right] \left[(k_{m\mu}^2 r^2 - m^2) J_m^2(k_{m\mu} r) + \right.$$

$$\left. + k_{m\mu}^2 r^2 (J_m'(k_{m\mu} r))^2 \right]_0^b \quad (\text{Ref. 10})$$

$$= \frac{1}{2k_{m\mu}^2} \left[(k_{m\mu}^2 b^2 - m^2) J_m^2(k_{m\mu} b) + (J_m'(k_{m\mu} b))^2 - m^2 J_m^2(0) \right]$$

$$= \frac{1}{2k_{m\mu}^2} (k_{m\mu}^2 b^2 - m^2) J_m^2(k_{m\mu} b)$$

$$\int_0^b \{ \text{Re}[P(m,\mu)] \}^2 r dr = E_{m\mu}^2 \frac{\epsilon_m^2}{2k_{m\mu}^2} (k_{m\mu}^2 b^2 - m^2) J_m^2(k_{m\mu} b) \cdot$$

$$\cdot J_m^2(k_{m\mu} r_0) [\cdot]^2$$

$$= F_{m\mu}^2 [\cdot]^2$$

where

$$F_{m\mu}^2 = \frac{1}{2} \left(E_{m\mu} \frac{\epsilon_m}{k_{m\mu}} \right)^2 (k_{m\mu}^2 b^2 - m^2) J_m^2(k_{m\mu} b) J_m^2(k_{m\mu} r_0)$$

Next,

$$\int_0^{2\pi} \int_0^b \{ \text{Re}[P(m,\mu)] \}^2 r dr d\theta = F_{m\mu}^2 \int_0^{2\pi} [\cdot]^2 d\theta$$

$$\begin{aligned}
&= F_{m\mu}^2 \int_0^{2\pi} \left[\sum_{j=1}^n \{ Q \cos (\phi_{oj} + \gamma_{m\mu} z - \omega t) \cos (m\theta - m\theta_{oj}) \right. \\
&\quad \left. + q \cos (\alpha_{oj} + \gamma_{m\mu} z - \omega t) \cos (m\theta - m\theta_{oj} - \frac{m\pi}{n}) \right]^2 d\theta \\
&= F_{m\mu}^2 \int_0^{2\pi} \left[\sum_{k=1}^n \sum_{j=1}^n \{ Q \cos (\phi_{ok} + \gamma_{m\mu} z - \omega t) \cos (m\theta - m\theta_{ok}) \right. \\
&\quad \left. + q \cos (\alpha_{ok} + \gamma_{m\mu} z - \omega t) \cos (m\theta - m\theta_{ok} - \frac{m\pi}{n}) \right] \cdot \\
&\quad \cdot \{ Q \cos (\phi_{oj} + \gamma_{m\mu} z - \omega t) \cos (m\theta - m\theta_{oj}) \\
&\quad \left. + q \cos (\alpha_{oj} + \gamma_{m\mu} z - \omega t) \cos (m\theta - m\theta_{oj} - \frac{m\pi}{n}) \right] d\theta \\
&= F_{m\mu}^2 \int_0^{2\pi} \left\{ \sum_{k=1}^n \sum_{j=1}^n [Q^2 \cos (\phi_{ok} + \gamma_{m\mu} z - \omega t) \cos (\phi_{oj} + \gamma_{m\mu} z - \omega t) \cdot \right. \\
&\quad \cdot \frac{1}{2} [\cos (2m\theta - m(\theta_{ok} + \theta_{oj})) + \cos m(\theta_{ok} - \theta_{oj}) + \\
&\quad \left. + q^2 \cos (\alpha_{ok} + \gamma_{m\mu} z - \omega t) \cos (\alpha_{oj} + \gamma_{m\mu} z - \omega t) \cdot \right. \\
&\quad \cdot \frac{1}{2} [\cos (2m\theta - m(\theta_{ok} + \theta_{oj}) - \frac{2m\pi}{n}) + \\
&\quad \left. + \cos m(\theta_{ok} - \theta_{oj})] + Qq \cos (\phi_{ok} + \gamma_{m\mu} z - \omega t) \cos (\alpha_{oj} + \gamma_{m\mu} z - \omega t) \cdot \right. \\
&\quad \cdot \frac{1}{2} [\cos (2m\theta - m(\theta_{oj} + \theta_{ok}) - \frac{m\pi}{n}) + \cos (m\theta_{ok} - m\theta_{oj} - \frac{m\pi}{n})] \\
&\quad \left. + Qq \cos (\phi_{oj} + \gamma_{m\mu} z - \omega t) \cos (\alpha_{ok} + \gamma_{m\mu} z - \omega t) \cdot \right. \\
&\quad \left. \cdot \frac{1}{2} [\cos (2m\theta - m(\theta_{ok} + \theta_{oj}) - \frac{m\pi}{n}) + \cos (m\theta_{ok} - m\theta_{oj} + \frac{m\pi}{n})] \right\} d\theta \\
&= F_{m\mu}^2 \sum_{k=1}^n \sum_{j=1}^n \{ \pi \cos m(\theta_{ok} - \theta_{oj}) [Q^2 \cos (\phi_{ok} + \gamma_{m\mu} z - \omega t) \cdot
\end{aligned}$$

$$\begin{aligned}
& \cdot \cos (\phi_{oj} + \gamma_{m\mu} z - \omega t) + q^2 \cos (\alpha_{ok} + \gamma_{m\mu} z - \omega t) \cdot \\
& \cdot \cos (\alpha_{ok} + \gamma_{m\mu} z - \omega t)] + \pi Q q \cos (m\theta_{ok} - m\theta_{oj} - \frac{m\pi}{n}) \cdot \\
& \cdot \cos (\phi_{ok} + \gamma_{m\mu} z - \omega t) \cos (\alpha_{oj} + \gamma_{m\mu} z - \omega t) + \\
& + \pi Q q \cos (m\theta_{ok} - m\theta_{oj} + \frac{m\pi}{n}) \cdot \\
& \cdot \cos (\phi_{oj} + \gamma_{m\mu} z - \omega t) \cos (\alpha_{ok} + \gamma_{m\mu} z - \omega t) \}
\end{aligned}$$

Integrating next with respect to (ωt) ,

$$\begin{aligned}
& \int_0^{2\pi} \int_0^{2\pi} \int_0^b \operatorname{Re}^2[P] r dr d\omega t = \\
& \int_0^{2\pi} F_{m\mu}^2 \pi \sum_{k=1}^n \sum_{j=1}^n \{ \cos m (\theta_{ok} - \theta_{oj}) \cdot \\
& \cdot [Q^2 \frac{1}{2} [\cos (\phi_{ok} + \phi_{oj} + 2\gamma_{m\mu} z - 2\omega t) + \cos (\phi_{ok} - \phi_{oj})] + \\
& + q^2 \frac{1}{2} [\cos (\alpha_{ok} + \alpha_{oj} + 2\gamma_{m\mu} z - 2\omega t) + \cos (\alpha_{ok} - \alpha_{oj})]] + \\
& + Qq \cos (m\theta_{ok} - m\theta_{oj} - \frac{m\pi}{n}) \frac{1}{2} [\cos (\phi_{ok} + \alpha_{oj} + 2\gamma_{m\mu} z - 2\omega t) + \\
& + \cos (\phi_{ok} - \alpha_{oj})] + Qq \cos (m\theta_{ok} - m\theta_{oj} + \frac{m\pi}{n}) \cdot \\
& \cdot \frac{1}{2} [\cos (\alpha_{ok} + \phi_{oj} + 2\gamma_{m\mu} z - 2\omega t) + \cos (\alpha_{ok} - \phi_{oj})] \} d\omega t \\
= & F_{m\mu}^2 \pi^2 \ell \sum_{k=1}^n \sum_{j=1}^n \{ \cos m (\theta_{ok} - \theta_{oj}) [Q^2 \cos (\phi_{ok} - \phi_{oj}) + \\
& + q^2 \cos (\alpha_{ok} - \alpha_{oj})] + Qq [\cos (m\theta_{oj} - m\theta_{oj} - \frac{m\pi}{n}) \cos (\phi_{ok} - \alpha_{oj} + \\
& + \cos (m\theta_{ok} - m\theta_{oj} + \frac{m\pi}{n}) \cos (\alpha_{ok} - \phi_{oj})] \}
\end{aligned}$$

Since the above expression is independent of z , it is the average with respect to z ; $\frac{1}{Z} \int_0^Z [\cdot] dz = [\cdot]$. Thus the index of performance is:

$$\begin{aligned} IP = & \frac{F_{m\mu}^2}{2b^2} \sum_{k=1}^n \sum_{j=1}^n \cos m(\theta_{ok} - \theta_{oj}) [Q^2 \cos(\phi_{ok} - \phi_{oj}) + \\ & + q^2 \cos(\alpha_{ok} - \alpha_{oj})] + Qq [\cos(m\theta_{ok} - m\theta_{oj} - \frac{m\pi}{n}) \cos(\phi_{ok} - \alpha_{oj}) + \\ & + \cos(m\theta_{ok} - m\theta_{oj} + \frac{m\pi}{n}) \cos(\alpha_{ok} - \phi_{oj})] \end{aligned}$$

To determine the optimal q 's and $\alpha_{oj(k)}$'s, the partials are evaluated and set equal to zero.

$$\begin{aligned} \frac{\partial}{\partial q} IP = & F_{m\mu}^2 \frac{1}{2b^2} \sum_{k=1}^n \sum_{j=1}^n \{2q [\cos m(\theta_{ok} - \theta_{oj}) \cos(\alpha_{ok} - \alpha_{oj})] + \\ & + Q [\cos(m\theta_{ok} - m\theta_{oj} - \frac{m\pi}{n}) \cos(\phi_{ok} - \alpha_{oj}) + \\ & + \cos(m\theta_{ok} - m\theta_{oj} + \frac{m\pi}{n}) \cos(\alpha_{ok} - \phi_{oj})] \} \end{aligned}$$

$$\begin{aligned} \frac{\partial}{\partial \alpha_{oi}} IP = & \frac{\partial}{\partial \alpha_{oi}} [2 F_{m\mu}^2 \frac{1}{2b^2} \sum_{\substack{k=1 \\ \neq i}}^n \cos m(\theta_{ok} - \theta_{oi}) \cdot \\ & \cdot [Q^2 \cos(\phi_{ok} - \phi_{oi}) + q^2 \cos(\alpha_{ok} - \alpha_{oi})] + \\ & + Qq [\cos(m\theta_{ok} - m\theta_{oi} - \frac{m\pi}{n}) \cos(\phi_{ok} - \alpha_{oi}) + \\ & + \cos(m\theta_{ok} - m\theta_{oi} + \frac{m\pi}{n}) \cos(\alpha_{ok} - \phi_{oi})] \} + \\ & + F_{m\mu}^2 \frac{1}{b^2} \{Q^2 + q^2 + 2Qq \cos \frac{m\pi}{n} \cos(\alpha_{oi} - \alpha_{oi}) \} \end{aligned}$$

$$= 2 F_{m\mu}^2 \frac{1}{2b^2} \sum_{k=1}^n \{q^2 \cos m (\theta_{ok} - \theta_{oj}) \sin (\alpha_{ok} - \alpha_{oj}) +$$

$$+ Qq [\cos (m\theta_{ok} - m\theta_{oi} - \frac{m\pi}{n}) \sin (\phi_{ok} - \alpha_{oi})]\}$$

For $n = 4$, the expanded form of the partials is as follows:

$$\frac{\partial}{\partial q} IP \implies 0 = 4q \{2 + \cos \frac{m\pi}{2} \cos (\alpha_{02} - \alpha_{01}) +$$

$$+ \cos m\pi \cos (\alpha_{03} - \alpha_{01}) + \cos m \frac{3\pi}{2} \cos (\alpha_{04} - \alpha_{01}) +$$

$$+ \cos \frac{m\pi}{2} \cos (\alpha_{03} - \alpha_{02}) + \cos m\pi \cos (\alpha_{04} - \alpha_{02}) +$$

$$+ \cos \frac{m\pi}{2} \cos (\alpha_{04} - \alpha_{03}) + 2Q \{ \cos \frac{m\pi}{4} [\cos \alpha_{01} +$$

$$+ \cos (\alpha_{02} - m_o \frac{\pi}{2}) + \cos (\alpha_{03} - m_o \pi) + \cos (\alpha_{04} - m_o \frac{3\pi}{2}) +$$

$$+ \cos (\alpha_{01} - m_o \frac{\pi}{2}) + \cos (\alpha_{02} - m_o \pi) + \cos (\alpha_{03} - m_o \frac{3\pi}{2})] +$$

$$+ \cos m \frac{3\pi}{4} [\cos \alpha_{02} + \cos (\alpha_{01} - m_o \pi) + \cos (\alpha_{03} - m_o \frac{\pi}{2}) +$$

$$+ \cos (\alpha_{02} - m_o \frac{3\pi}{2}) + \cos (\alpha_{04} - m_o \pi)] +$$

$$+ \cos m \frac{5\pi}{4} (\cos \alpha_{03} + \cos (\alpha_{01} - m_o \frac{3\pi}{2}) +$$

$$+ \cos (\alpha_{04} - m_o \frac{\pi}{2})) + \cos m \frac{7\pi}{4} \cos \alpha_{04} \}$$

$$\frac{\partial}{\partial \alpha_{01}} IP \implies 0 = q^2 [\cos m \frac{\pi}{2} \sin (\alpha_{02} - \alpha_{01}) + \cos m\pi \cdot$$

$$\cdot \sin (\alpha_{03} - \alpha_{01}) + \cos m \frac{3\pi}{2} \sin (\alpha_{04} - \alpha_{01})] +$$

$$+ Qq [-\cos m \frac{\pi}{4} \sin \alpha_{01} + \cos \frac{m\pi}{4} \sin (m_o \frac{\pi}{2} - \alpha_{01}) +$$

$$+ \cos m \frac{3\pi}{4} \sin (m_o \pi - \alpha_{01}) + \cos m \frac{5\pi}{4} \sin (m_o \frac{3\pi}{2} - \alpha_{01})]$$

$$\frac{\partial}{\partial \alpha_{02}} \text{IP} \Rightarrow 0 = q^2 [-\cos \frac{m\pi}{2} \sin (\alpha_{02} - \alpha_{01}) +$$

$$+ \cos \frac{m\pi}{2} \sin (\alpha_{03} - \alpha_{02}) + \cos m\pi \sin (\alpha_{04} - \alpha_{02})] +$$

$$+ Qq [\cos m \frac{\pi}{4} \sin (m_o \frac{\pi}{2} - \alpha_{02}) + 2 \cos \frac{m\pi}{4} \sin (m_o \pi - \alpha_{02}) +$$

$$+ \cos m \frac{3\pi}{4} \sin (-\alpha_{02}) + \cos m \frac{3\pi}{4} \sin (m_o \frac{3\pi}{2} - \alpha_{02})]$$

$$\frac{\partial}{\partial \alpha_{03}} \text{IP} \Rightarrow 0 = q^2 [-\cos m\pi \sin (\alpha_{03} - \alpha_{01}) - \cos \frac{m\pi}{2} \sin (\alpha_{03} - \alpha_{02}) +$$

$$+ \cos \frac{m\pi}{2} \sin (\alpha_{04} - \alpha_{03})] + Qq [\cos \frac{m\pi}{4} \sin (m_o \pi - \alpha_{03}) +$$

$$+ \cos \frac{m\pi}{4} \sin (m_o \frac{3\pi}{2} - \alpha_{03}) + \cos m \frac{3\pi}{4} \sin (m_o \frac{\pi}{2} - \alpha_{03}) -$$

$$- \cos m \frac{5\pi}{4} \sin \alpha_{03}]$$

$$\frac{\partial}{\partial \alpha_{04}} \text{IP} \Rightarrow 0 = q^2 [-\cos m \frac{3\pi}{2} \sin (\alpha_{04} - \alpha_{01}) - \cos m\pi \sin (\alpha_{04} - \alpha_{02}) -$$

$$- \cos \frac{m\pi}{2} \sin (\alpha_{04} - \alpha_{03})] + Qq [\cos \frac{m\pi}{4} \sin (m_o \frac{3\pi}{2} - \alpha_{04}) +$$

$$+ \cos m \frac{3\pi}{4} \sin (m_o \pi - \alpha_{04}) + \cos m \frac{5\pi}{4} \sin (m_o \frac{\pi}{2} - \alpha_{04}) -$$

$$- \cos m \frac{7\pi}{4} \sin \alpha_{04}]$$

For $m_o = 0$ and $m = 0$,

$$0 = q \{ \sin (\alpha_{01} - \alpha_{02}) + \sin (\alpha_{01} - \alpha_{02}) + \sin (\alpha_{01} - \alpha_{02}) \} + \sin \alpha_{01}$$

$$0 = q \{-\sin(\alpha_{01} - \alpha_{02}) + \sin(\alpha_{02} - \alpha_{03}) + \sin(\alpha_{02} - \alpha_{04})\} + 4Q \sin \alpha_{02}$$

$$0 = q \{-\sin(\alpha_{01} - \alpha_{03}) - \sin(\alpha_{02} - \alpha_{03}) + \sin(\alpha_{03} - \alpha_{04})\} + 4Q \sin \alpha_{03}$$

$$0 = a \{-\sin(\alpha_{01} - \alpha_{04}) - \sin(\alpha_{02} - \alpha_{04}) - \sin(\alpha_{03} - \alpha_{04})\} + 4Q \sin \alpha_{04}$$

$$0 = 2q \{2 = \cos(\alpha_{01} - \alpha_{02}) + \cos(\alpha_{01} - \alpha_{03}) + \cos(\alpha_{01} - \alpha_{04}) + \cos(\alpha_{02} - \alpha_{03}) + \cos(\alpha_{02} - \alpha_{04}) + \cos(\alpha_{03} - \alpha_{04})\}$$

The predicted solution, $q = Q$ and $\alpha_{01} = \alpha_{02} = \alpha_{03} = \alpha_{04} = (2\ell+1)\pi$, $\ell = 0, \pm 1, \pm 2, \dots$, satisfies the above relations. For this solution, the index of performance for the m^{th} mode is:

$$IP = \frac{F^2}{2b} \frac{m\mu}{2} \left[1 - \cos \frac{m\pi}{4} \right] \left[4 + 8 \cos \frac{m\pi}{2} + 4 \cos m\pi \right]$$

Hence,

$$IP = 0 \text{ except when } |m| = 4, 12, 20, 28, \dots \text{ where } IP = 32 \frac{F^2 m\mu Q^2}{b^2} .$$

Thus, complete cancellation of the $m = 0$ mode is expected. Significant sound pressure reduction should be obtained below the cutoff frequency for $m = 4$. Sound pressure level reduction problems can be expected at the cutoff frequencies of the radial distributions of the $|m| = 4, 12, 20, \dots$ modes because the $F_{m\mu}$ term in the index of performance has singularities at these frequencies. Physically, this results in duct resonances of the specified higher order circumferential modes. Near these frequencies the predicted optimal solution no longer holds because a higher order mode propagates. Optimization

over the entire set of modes ($\sum_{m=0}^{\infty} IP_m$) would be required to determine the optimal solution. However, excellent results are predicted for $f < 1913$ Hz, the cutoff frequency for the $m = 4$, $\mu = 0$ mode, utilizing the predicted solution. This accounts for the good experimental results obtained for low frequencies.

The generation of the $m = 4$, $\mu = 0$ mode is illustrated by the circumferential distribution shown in Figure 56,

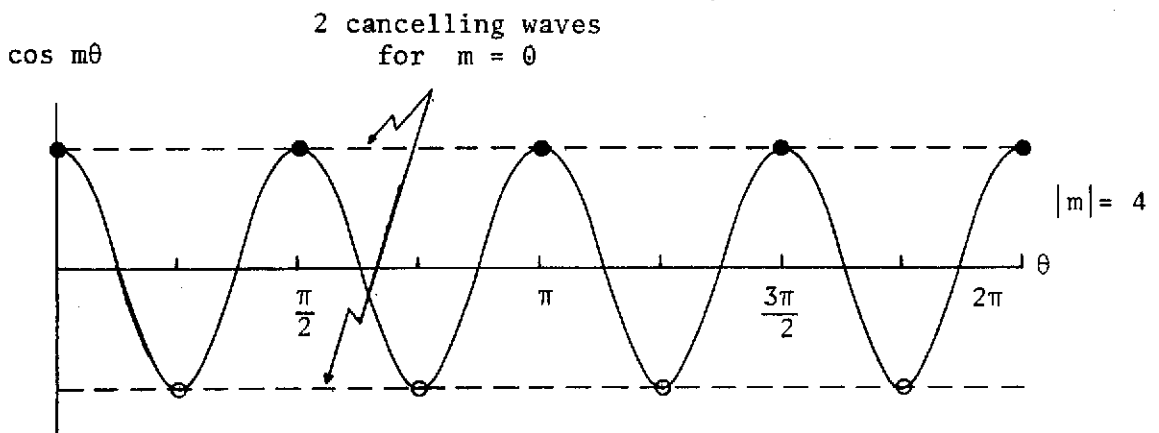


FIGURE 56

Generation of $m = 4$ Mode While Cancelling $m = 0$ Mode

where $t = \text{constant}$, the symbol \bullet designates the normalized amplitude of the source array transducers at time t , and the symbol \circ designates the normalized amplitude of the cancelling array transducers.

For $m_0 = 1$ and $m = 1$,

$$0 = q \{-\sin(\alpha_{01} - \alpha_{03})\} + \sqrt{2} Q \{\sin \alpha_{01} - \cos \alpha_{01}\}$$

$$0 = q \{-\sin(\alpha_{02} - \alpha_{04})\} + \sqrt{2} Q \{\sin \alpha_{02} - \cos \alpha_{02}\}$$

$$0 = q \{\sin(\alpha_{01} - \alpha_{03})\} + \sqrt{2} Q \{-\sin \alpha_{03} + \cos \alpha_{03}\}$$

$$0 = q \{-\sin(\alpha_{02} - \alpha_{04})\} + \sqrt{2} Q \{\sin \alpha_{04} + \cos \alpha_{04}\}$$

$$0 = 2q \{2 - \cos(\alpha_{01} - \alpha_{03}) - \cos(\alpha_{02} - \alpha_{04})\} + \\ + 2Q \{\cos \alpha_{01} + \sin \alpha_{01} - \cos \alpha_{02} + \sin \alpha_{02} - \cos \alpha_{03} \\ - \sin \alpha_{03} + \cos \alpha_{04} - \sin \alpha_{04}\}$$

The predicted solution, $q = Q$ and $\alpha_{01} = \frac{5\pi}{4}$, $\alpha_{02} = \frac{7\pi}{4}$, $\alpha_{03} = \frac{\pi}{4}$,

and $\alpha_{04} = \frac{3\pi}{4}$, satisfies the above relations. For this solution, the

index of performance for the m^{th} mode is:

$$IP = \frac{F^2 Q^2}{b^2} \{4(1 - \cos m\pi) + 4\sqrt{2} (\cos m \frac{3\pi}{4} - \cos m \frac{\pi}{4})\}$$

Hence,

$IP = 0$ except for $|m| = 3, 5, 11, 13, 19, 21 \dots$ where

$$IP = 16 \frac{F^2 Q^2}{b^2}$$

For reference, the IP for $q = 0$ is nonzero for $|m| = 1, 3, 5, 7, \dots$:

and is given by

$$IP = 4 \frac{F^2}{b^2}$$

Thus, cancellation difficulties can be expected for frequencies above 1511 Hz, the cutoff frequency for the $m = 3$, $\mu = 0$ mode. The generation of this mode is illustrated by the circumferential distribution

shown in Figure 57.

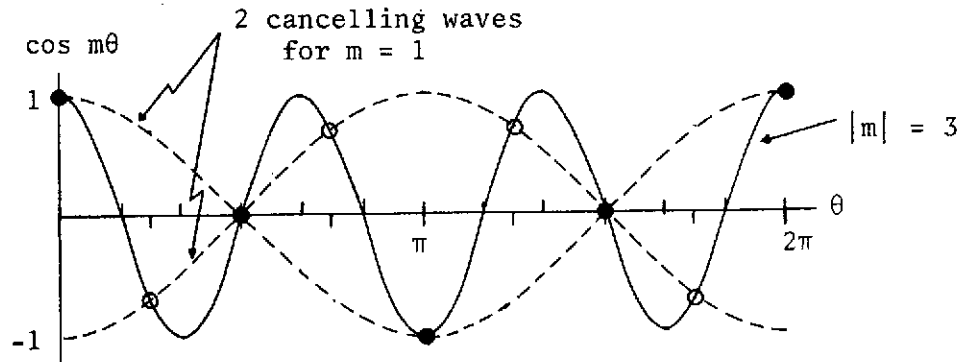


Figure 57

Generation of $m = 3$ Mode While Cancelling the $m = 1$ Mode

The symbol \bullet designates the normalized amplitude of the source array transducers, and the symbol \circ designates the normalized amplitude of the cancelling array transducers. Examination of Figure 21, the radial distribution of cancellation of the $m = 1$, $\mu = 0$ mode, illustrates this phenomenon. The radial distribution for the cancelled condition is a high sound pressure level $\mu = 0$ curve. This can be explained by the generation of an $m = 3$, $\mu = 0$ mode above 1511 Hz.

For $m_0 = 2$ and $m = 2$:

$$0 = q^2 \{ \sin(\alpha_{01} - \alpha_{02}) + \sin(\alpha_{01} - \alpha_{03}) - \sin(\alpha_{01} - \alpha_{04}) \}$$

$$0 = q^2 \{ \sin(\alpha_{01} - \alpha_{02}) - \sin(\alpha_{02} - \alpha_{03}) + \sin(\alpha_{02} - \alpha_{04}) \}$$

$$0 = q^2 \{ -\sin(\alpha_{01} - \alpha_{03}) + \sin(\alpha_{02} - \alpha_{03}) - \sin(\alpha_{03} - \alpha_{04}) \}$$

$$0 = q^2 \{ \sin(\alpha_{01} - \alpha_{04}) - \sin(\alpha_{02} - \alpha_{04}) + \sin(\alpha_{03} - \alpha_{04}) \}$$

$$0 = 4q \{ 2 - \cos(\alpha_{01} - \alpha_{02}) + \cos(\alpha_{01} - \alpha_{03}) - \cos(\alpha_{01} - \alpha_{04}) \\ - \cos(\alpha_{02} - \alpha_{03}) + \cos(\alpha_{02} - \alpha_{04}) - \cos(\alpha_{02} - \alpha_{04}) \}$$

The predicted solution, $q = Q$, and $\alpha_{01} = \frac{3\pi}{2}$, $\alpha_{02} = \frac{\pi}{2}$, $\alpha_{03} = \frac{3\pi}{2}$,

and $\alpha_{04} = \frac{\pi}{2}$ does not satisfy the last equation. The only physically

reasonable solution is $q = 0$. Therefore for $n = 4$ the $m = 2$

mode cannot be cancelled. The index of performance of the m^{th} mode

for $m_0 = 2$ and $q = 0$ is:

$$IP = \frac{2F_{m\mu}^2 Q^2}{b^2} [(1 + \cos m\pi) - 2 \cos \frac{m\pi}{2}]$$

Hence,

$IP = 0$ except for $|m| = 2, 6, 10, 14, \dots$ where

$$IP = 8 \frac{F_{m\mu}^2 Q^2}{b^2} .$$

Because of multiple mode excitation, $m_0 > 2$ will not be considered.

It is clear that for the generation of these modes, n must be increased from $n = 4$.

The following conclusions can be drawn from this analysis:

1) There exists a minimum number of transducers, n_{\min} , which can generate a single mode m_0 to a specified frequency f_{\max} . This number n_{\min} can be determined by proper manipulation of the equation for the index of performance developed in this section.

2) For a cancelling array interacting with a source array, as in our case, there is an additional restriction for a cancellable condition. There exists a minimum number of transducers, n'_{\min} , which can produce a cancelled condition for the m_0 mode to a specified frequency f_{\max} without the generation of higher order modes.

3) For the case of two interacting arrays, the second array can only impose further restrictions on the higher order modes which can be generated. Therefore, $n'_{\min} \leq n_{\min}$.

The number n_{\min} can be determined from the index of performance for $q = 0$.

$$\begin{aligned}
 IP &= \frac{F^2}{2b^2} \sum_{k=1}^n \sum_{j=1}^n \cos m (\theta_{ok} - \theta_{oj}) \cos (\phi_{ok} - \phi_{oj}) Q^2 \\
 &= \frac{F^2}{2b^2} Q^2 \left\{ n + 2 \sum_{j=1}^{n-1} (n-j) \cos \frac{2\pi m}{n} j \cos \frac{2\pi m_0}{n} j \right\} \quad (3.3-C)
 \end{aligned}$$

Hence, n is increased from a trial value until $IP = 0$ for all m except m_0 whose $\mu = 0$ cutoff frequency is below f_{\max} . The final value of n is n_{\min} .

The generation and cancelling of submodes of m_0 by a single array must also be considered. A large portion of acoustic power can be lost by this phenomenon. For example, consider the case of $n = 4$, $m_0 = 2$. As illustrated below, acoustic energy can be wasted in the generation of two cancelling plane waves as shown in Figure 58, where

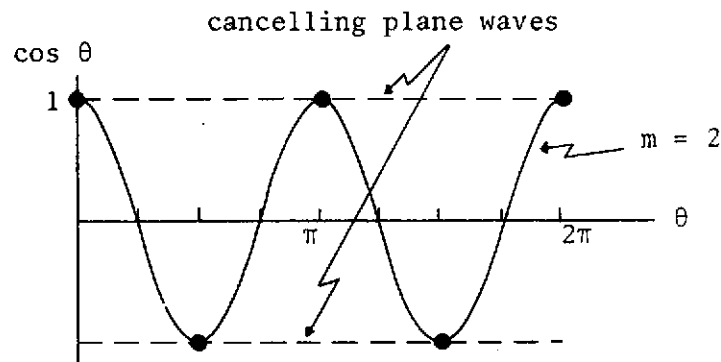


FIGURE 58

Generation of Cancelling Submodes

$t = \text{constant}$ and the symbol \bullet designates the normalized amplitude of the transducers at time t . Further testing would be required to verify the existence of this phenomenon. This particular case illustrates one additional problem. The relative positioning and phasing of transducers makes impossible the cancellation by an array displaced circumferentially $\frac{\pi}{n}$ radians. The cancelling array only provides a bias for the direction of spin and increases the sound pressure level. So, the additional restriction $n > 2m_0$ is required.

The range of m , μ , and frequency over which effective cancellation can be obtained can now be cataloged. Table 8 shows the results for $n = 4$. Upper frequency limits have been set approximately 100 Hz below the cutoff frequency of the higher order mode subject to excitation. This margin assures that the decay rate in the axial direction of the higher order mode is great enough to have little effect on the magnitude of sound pressure level reduction.

TABLE 8

m , μ , and f Range for Cancellation with $n = 4$

| F range | $\mu = 0$ | $\mu = 1$ | $\mu = 2$ |
|-----------|-------------|--------------|-----------|
| $m_0 = 0$ | 0 to 1378 | 1378 to 1800 | - |
| $m_0 = 1$ | 662 to 1400 | - | - |
| $m_0 = 2$ | - | - | - |

Examination of the experimental results of Chapter II substantiates the above figures. The actual results are slightly higher as a result of the duct resonant frequencies being slightly higher than predicted by theory.

The analysis of the wave equation has shown that the frequency range of propagation of a single, specified circumferential mode generated by a single array is finite and dependent upon the number of transducers. A circular transducer array given by equations 1.3-1

through 1.3-4 where n is finite and m is specified (m_0) can excite an infinite set of circumferential modes, $\{M\}$. The magnitudes of the elements of $\{M\}$ are given by the $|m|$ which yield a nonzero solution to the sound pressure level index of performance for a single array:

$$IP = \frac{F^2}{2b^2} \frac{Q^2}{m\mu} \left\{ n + 2 \sum_{j=1}^{n-1} (n-j) \cos \frac{2\pi m}{n} j \cos \frac{2\pi m_0}{n} j \right\} \quad (3.3-C)$$

For a given m_0 , the spacing of the elements of $\{M\}$ generally increases as n is increased. This is illustrated in Table 9 for $m_0 = 1$.

TABLE 9

$\{|M(n)|\}$ for $m_0 = 1$

| $m_0 = 1$ | $\{ M \}$ |
|-----------|--|
| $n = 1$ | $n > 1$ for equation 3.3-B to hold |
| $n = 2$ | {1, 3, 5, 7, 9, . . .} |
| $n = 3$ | {1, 2, 4, 5, 7, 8, 10, 11, . . .} |
| $n = 4$ | {1, 3, 5, 7, 9, . . .} |
| $n = 5$ | {1, 4, 6, 9, 11, 14, 16, . . .} |
| $n = 6$ | {1, 5, 7, 11, 13, 17, 19, . . .} |
| $n = 7$ | {1, 6, 8, 13, 15, 20, 22, 27, 29, . . .} |
| $n = 8$ | {1, 7, 9, 15, 17, 23, 25, . . .} |

The information in Table 9 was obtained by evaluation of the bracketed term in equation 3.3-B. A simpler approach yielding more information is available. Tyler and Sofrin (4) have derived a simple equation which yields the set of circumferential mode numbers which can be excited by rotor-stator interaction in a fan. The value of m is restricted to:

$$m = n' B + kv$$

where

m = circumferential mode number

n' = harmonic number

B = number of blades

$k = \dots -1, 0, 1, \dots$

v = number of vanes

A similar equation can be derived by analogy for a transducer array. The array is excited only at frequency ω , so the harmonic number n' is restricted to the fundamental. The transducers are stationary sources, so v is set equal to the number of transducers, n . The value of B is selected so that the individual rotor-stator interactions of the blade-vane system coincide with the positive maximum of the sinusoidal transducer outputs. Therefore B is simply m_0 . The rotor of the fan would have the same angular frequency as the acoustic frequency of the transducers. The equation can now be rewritten:

$$m = m_0 + kn \quad (3.3-E)$$

To illustrate the effectiveness of this equation, consider the case of $m_0 = 1$. Equation 3.3-E yields the sign of m (recall that a negative sign denotes spin in the opposite direction of the rotor). So, the set $\{M\}$ can be completely specified. Table 10 contains the new information.

TABLE 10

 $\{M(n)\}$ for $m_0 = 1$

| $m_0 = 1$ | $\{M\}$ |
|-----------|-------------------------------------|
| $n = 1$ | $\{0, +1, +2, +3, +4, \dots\}$ |
| $n = 2$ | $\{+1, +3, +5, +7, \dots\}$ |
| $n = 3$ | $\{1, -2, 4, -5, 7, -8, \dots\}$ |
| $n = 4$ | $\{1, -3, 5, -7, 9, -11, \dots\}$ |
| $n = 5$ | $\{1, -4, 6, -9, 11, -14, \dots\}$ |
| $n = 6$ | $\{1, -5, 7, -11, 13, -17, \dots\}$ |
| $n = 7$ | $\{1, -6, 8, -13, 15, -20, \dots\}$ |
| $n = 8$ | $\{1, -7, 9, -15, 17, -23, \dots\}$ |

Equation 3.3-E provides a very simple means for obtaining the minimum number of transducers in a single array necessary to generate a single, specified circumferential mode m_0 over a specified frequency range.

The blade-vane analogy can also be applied to the two array system with the cancelling array set for maximum cancellation by equations 1.3-7 and 1.3-8. The analysis of the transducer-duct system leads to a model of a rotor-stator source with $2n$ vanes, $(n + m_0)$ blades, and an angular rotor frequency of $\frac{1}{n+m_0}$ times the acoustic frequency of the transducers. The empirical relation yielding the circumferential modes which form the set $\{M\}$ is then given by:

$$m = m_0 + (2k + 1) n \quad (3.3-F)$$

The sets of $\{M\}$ for the four transducer array set for cancellation can now be easily specified:

TABLE 11

$\{M(m_0)\}$ for the 4 Transducer Arrays Set for Cancellation

| | $\{M\}$ |
|-----------|--------------------------------------|
| $m_0 = 0$ | $\{+4, +12, +20, +28, \dots\}$ |
| $m_0 = 1$ | $\{-3, 5, -11, 13, -19, 21, \dots\}$ |
| $m_0 = 2$ | $\{-2, 6, -10, 14, -18, 22, \dots\}$ |
| $m_0 = 3$ | $\{-1, 7, -9, 15, -17, 23, \dots\}$ |

The analysis of the sound field is hence complete. To complete the mathematical model of the system to be controlled, a measurement system must be produced which can generate a sound pressure level index of performance. Also, the transfer function for the transducers must be obtained.

An ideal measurement system for determining an overall sound pressure level for a sound field of unknown distribution would yield a function of the form:

$$\text{SPL}(t) = \frac{1}{\pi r^2 z} \int_r \int_\theta \int_z \text{SPL}(r, \theta, z, t) dz d\theta dr$$

which is similar to the index of performance which has been used. With a finite number of stationary probes, a sound pressure level indicator could be defined by:

$$\text{SPL}(t) = \frac{1}{w} \sum_{i=1}^w \beta_i \text{SPL}_i(t)$$

where w = number of probes

β_i = weighting factor related to position of probe

SPL_i = SPL at i^{th} position

$$= 20 \log p_i - 20 \log p_{\text{ref}} \text{ where } p_i \text{ is the RMS value of } P_i$$

determined by equation (3.3-A)

Such a system is physically realizable and can be designed to be relatively insensitive to the point cancellation effect. This form shall be assumed for the development of the controller.

The transducers must also be modeled. A ducted transducer has the following properties:

$$1) \text{ SPL}_j = k_1(f) + k_2(f) (20 \log V_j - 20 \log V_{\text{ref}})$$

where $k_1(f)$ and $k_2(f)$ are frequency-dependent parameters

V_j = electrical voltage across j^{th} transducer.

SPL_j = SPL near the j^{th} transducer.

$$2) \alpha_{oj} = \theta_j + k_3(f)$$

where α_{oj} = acoustic phase

θ_j = electrical phase

k_3 = frequency dependent parameter

The source strength q can be related to SPL_j :

$$q = f(\text{SPL}_j).$$

The plant can be modeled as shown in Figure 59. The difficulties associated with this plant can be easily seen by this model. As found in Chapter II, the functional relationships of k_1 , k_2 , and k_3 to frequency are too complex to be described analytically and provide an unreasonable function generation problem. In reality, $k_1(f)$, $k_2(f)$ and $k_3(f)$ also vary with the transducer and its location, though the frequency dependence is quite similar from point to point.

With the simulated source, Q and ϕ_{oj} are also dependent upon a similar set of k 's. In addition the relation for the pressure field is extremely complex.

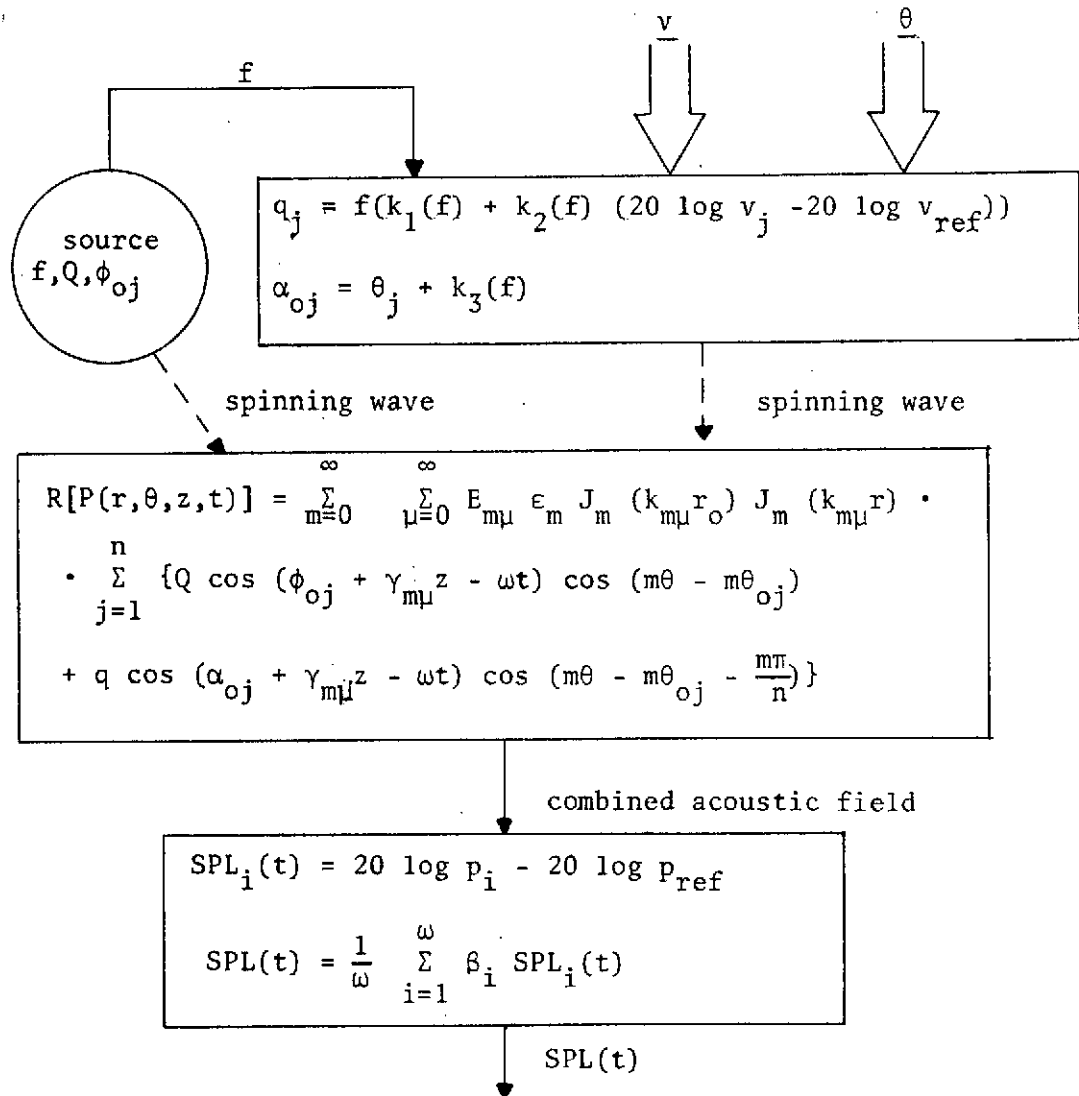


FIGURE 59

Mathematical Plant Model

Conventional optimal control techniques are not appropriate because of the complexity of the plant. Also, the sound field equations have been developed for a specified source, a transducer array. So, a conventional controller would be restricted to this type of simulated fan source. The application of adaptive control techniques would thus be appropriate and desirable. Then the SMS cancelling array could be applied to a variety of acoustic noise sources without modification.

The use of adaptive control had been proposed in the original research proposal. Because of the complexity of the transducer transfer function, the decision to design an adaptive controller was not made until the completion of experimentation. At this point, sufficient evidence had been gathered to support the adaptive design approach. The analysis presented in this section was developed parallel to the development of the controller. In addition to providing an understanding of the plant and providing background for future development, it gives further support to the original design proposal.

3.4 Synthesis of Adaptive Control Scheme

The model presented in the previous section does not entirely encompass the behavior of the plant. The relationship for $P(r, \theta, z, t)$ assumes symmetric waveforms due to a symmetric duct and ideal transducer outputs. Thus for the predicted solution \underline{q} and $\underline{\alpha}_0$ must be of the form:

$$\underline{q}(t) = q(t) [1, 1, 1, 1]^T \quad (3.4-1)$$

$$\underline{\alpha}_0(t) = \alpha_0(t) [1, 1, 1, 1]^T + [0, m \frac{\pi}{2}, m\pi, m \frac{3\pi}{2}]^T \quad (3.4-2)$$

where α_0 is in radians.

This also implies symmetric acoustic loading of the transducers so that $k_1(f)$, $k_2(f)$, and $k_3(f)$ are each uniformly alike for all transducers.

These assumptions reduce the dimensionality of the system from eight to two. So, the design of a controller based on these assumptions is an attractive proposition. Its justification is twofold:

- 1) the scope of concepts which can be effectively investigated would not be seriously limited by the suboptimal manipulation of the transducer array.
- 2) a two dimensional controller can serve as a rapid convergence initial stage of a multi-stage controller for optimal cancellation.

The two dimensional system offers obvious design, construction, and adaption advantages. So, the decision to design a 2-dimensional adaptive controller was made.

The plant controlled variables for the ideal plant can be defined by:

$$\underline{x}^T(t) = [x_1(t), x_2(t)] = [v(t), \theta(t)]$$

$$\text{such that } \underline{v}^T(t) = v(t) [1, 1, 1, 1]$$

$$\text{and } \underline{\theta}^T(t) = [0, \frac{\pi}{2}, \pi, \frac{3\pi}{2}] + [\theta, \theta, \theta, \theta]$$

where $v(t)$ = electrical voltage and $\theta(t)$ = electrical phase. The measurement system formulated in section 3.3,

$$\text{SPL}(t) = \frac{1}{w} \sum_{i=1}^w \beta_i \text{SPL}_i(t)$$

where w = number of probes

β_i = weighting factor related to position of probe

$\text{SPL}_i(t)$ = SPL at i^{th} position,

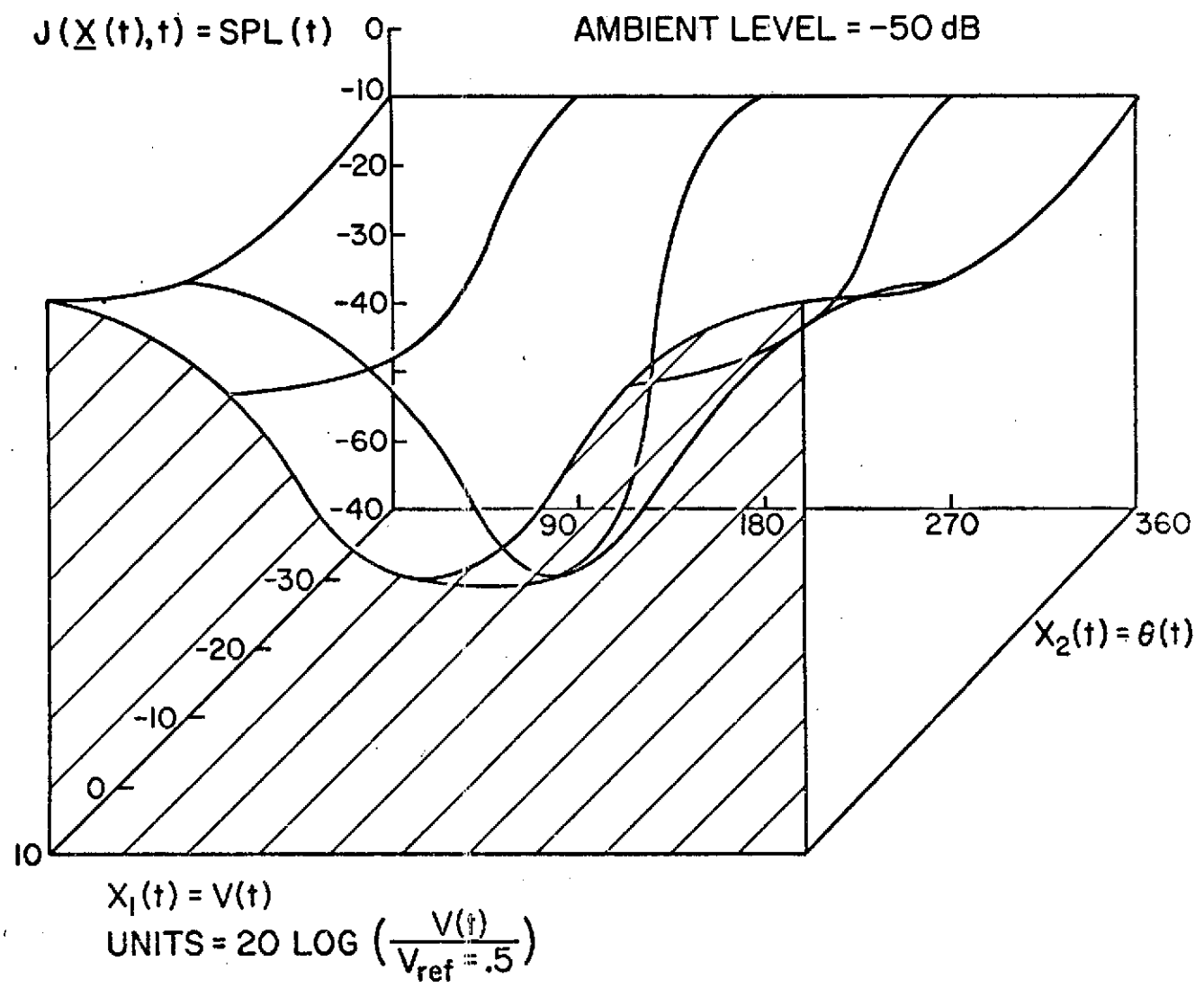
provides a meaningful index of performance or cost function. It shall be designated as $J(x(t), t)$, indicating its dependence on the plant controlled variables and time. Maximum cancellation occurs when $J(x(t), t)$ is minimized. The optimum inputs providing J_{\min} shall be designated by $X^*(t) = [X_1^*(t), X_2^*(t)]$.

The cost function with an arbitrarily located minimum would appear as in Figure 58. This applies for the predicted form of the solution when the system is operating under modal conditions satisfied by n_{\min} (see section 3.3). The following features are important:

- 1) 2-dimensional plant
- 2) unimodal cost function surface
- 3) time varying minimum
- 4) probably a noisy surface because of the SPL measurement algorithm.

Figure 60

A Hypothetical Realization of
the Cost Function Surface



An adaptive controller would use a search technique to locate the minimum and follow its time variation. There are many techniques applicable to our particular problem. Those considered for application are presented in the next chapter.

IV Adaptive Optimization Procedures for Multi-Dimensional, Unimodal, Noisy Systems

A literature search yielded several methods satisfying the multi-dimensional, unimodal, noisy signal requirements. McMurtry (11) has cataloged a representative set of these and other adaptive methods. Because of his organized approach to the presentation of method algorithms, his work serves as a basis for this chapter.

4.1 Method of Steepest Descent

Methods of steepest descent converge to the minimum of a surface by moving in the direction of steepest slope. A deterministic surface, $J(\underline{x})$, is assumed. But, adequate performance can often be obtained on systems contaminated by noise.

The method is discrete, and determines the gradient of the function $J(\underline{x})$ at each trial. The next step is made in the negative gradient direction. Given the gradient vector $\nabla_{\underline{x}} J(\underline{x})$ as

$$\nabla_{\underline{x}} J(\underline{x}) = \left[\frac{\partial J}{\partial x_1}, \frac{\partial J}{\partial x_2}, \dots, \frac{\partial J}{\partial x_n} \right]^T \quad (4.1-1)$$

the algorithm is

$$\underline{x}_{k+1} = \underline{x}_k - c_k \nabla_{\underline{x}} J(\underline{x}) \quad (4.1-2)$$

where c_k can be a constant or variable gain sequence. An adaptive adjustment procedure for c_k has been proposed by Eveleigh. Increased rate of convergence and decreased steady state error at x^* (where $\nabla_{\underline{x}} J(x^*) = 0$) can be expected from such a scheme.

A continuous controller based on this method could utilize the algorithm:

$$\frac{dx_i}{dt} = -K \frac{\partial J}{\partial x_i}, \quad i = 1, 2, \dots, n. \quad (4.1-3)$$

The gradient can be determined continuously by a perturbation technique.

4.2 Stochastic Approximation

Stochastic approximation methods, the stochastic analogs of the steepest descent method, may be employed to optimize systems corrupted by noise. This method can be applied to time-invariant systems. To establish notation, the problem is stated as follows: it is desired to minimize an unknown, deterministic function $J(\underline{x})$ where $\underline{x} = [x_1, \dots, x_n]^T$ are controlled variables. Contaminating the system output is a zero mean random process $N(\underline{x})$. Thus $E[J(\underline{x}) + N(\underline{x})] = J(\underline{x})$.

Consider the minimization of $J(\underline{x})$ by finding the zero of $\nabla_{\underline{x}} J(\underline{x})$ in the presence of noise. Let $\underline{Y}(\underline{x})$ be the noisy value of the gradient function where $E[\underline{Y}(\underline{x})] = \nabla_{\underline{x}} J(\underline{x})$. Thus $\underline{Y}(\underline{x})$ is a random vector. The algorithm is:

$$\underline{x}_{k+1} = \underline{x}_k - \delta_k \underline{Y}(\underline{x}_k) \quad (4.2-1)$$

where δ_k is a variable gain sequence. It can be shown that when the following conditions are satisfied

$$\begin{aligned} 1) \quad & \delta_k \geq 0 \\ 2) \quad & \sum_{k=1}^{\infty} \delta_k = \infty \\ 3) \quad & \sum_{k=1}^{\infty} \delta_k^2 < \infty \end{aligned} \quad (4.2-2)$$

- 4) $E [|| \underline{Y}(\underline{x}) ||^2] \leq A(1 + || \underline{x} - \underline{x}^* ||^2), A > 0$
 5) $\nabla_{\underline{x}} J(\underline{x})$ behaves linearly for \underline{x} near \underline{x}^*

the algorithm converges to \underline{x}^* (where $\nabla_{\underline{x}} J(\underline{x}^*) = 0$) in mean square and with probability one.

Kiefer - Wolfowitz methods enable the determination of the extremum of $J(\underline{x})$ when $\underline{Y}(\underline{x})$ is not available. For $M(\underline{x}) = J(\underline{x}) + N(\underline{x})$, a gradient can be determined by

$$\tilde{\nabla}_{\underline{x}} M(\underline{x}) = \sum_{j=1}^n e_j \frac{1}{2c_k} [M(\underline{x}_k + c_k e_j) - M(\underline{x}_k - c_k e_j)] \quad (4.2-3)$$

where e_j are unit vectors in the j^{th} direction and c_k is the distance on either side of \underline{x}_k at which measurements are made. The algorithm is:

$$\underline{x}_{k+1} = \underline{x}_k - \delta_k \tilde{\nabla}_{\underline{x}} M(\underline{x}) \quad (4.2-4)$$

It can be shown for the Dvoretzky conditions:

- 1) $\lim_{k \rightarrow \infty} \delta_k = 0$
- 2) $\lim_{k \rightarrow \infty} c_k = 0$
- 3) $\lim_{n \rightarrow \infty} \sum_{k=1}^n \delta_k = \infty$
- 4) $\lim_{n \rightarrow \infty} \sum_{k=1}^n \left(\frac{\delta_k}{c_k} \right)^2 < \infty$

$$5) |J(\underline{x}_{k+1}) - J(\underline{x}_k)| < A |\underline{x}_{k+1} - \underline{x}_k| + B < \infty$$

that the algorithm converges to \underline{x}^* (where $\tilde{\nabla}_{\underline{x}} (J(\underline{x}^*)) = 0$) in mean square and with probability one. Convergence acceleration techniques are available.

4.3 Adaptive Step Size Random Search

Schumer and Steiglitz developed a random search method that uses the optimum step size at each step. The proposed adaptive step size random search has been shown to approximate the optimum step size random search (OSSRS) for a hyperspherical surface only.

The algorithm is as follows: two steps are made in random directions of length s_k and $s_k(1+\alpha)$, $1 > \alpha > 0$, on the k^{th} iteration. s_{k+1} is set equal to the step size yielding the greatest improvement. If there is no improvement after a specified number of iterations, the step size is reduced. To ensure that s_k does not become too small, after a large number of iterations α is made much greater than one. This enables comparing s_k with a very large step.

4.4 Matyas' Method

Matyas considered adaptive optimization by the random variation of parameter magnitude and direction. Convergence of a random sequence of parameters for a stationary unimodal surface has been proven. The concept of directional adaptation, requiring memory, provides an algorithm for an increased rate of convergence:

$$\underline{x}_{k+1} = \underline{x}_k + \underline{d}_{k+1} + T_{k+1} \underline{\zeta}_{k+1} = \underline{x}_k + \underline{Y}_{k+1} \quad (4.4-1)$$

where T_{k+1} is a variable correlation matrix, $\underline{\zeta}_{k+1}$ is a random vector selected from a multivariate normal distribution with zero mean and unit correlation matrix, $\underline{Y}_{k+1} = \underline{d}_{k+1} + T_{k+1} \underline{\zeta}_{k+1}$, and \underline{d}_{k+1} is given by:

$$\underline{d}_{k+1} = [c_0(\underline{x}_k) + c_1(\underline{x}_k)] \left[\underline{d}_k + \sum_{i=1}^{k-1} h_{i,k-1} \delta_i \right] + c_1(\underline{x}_k) T_k \underline{\zeta}_k \quad (4.4-2)$$

where

$$0 \leq c_0(\underline{x}_k) \leq 1, c_1(\underline{x}_k) > 0, \text{ and } c_0(\underline{x}_k) + c_1(\underline{x}_k) > 1 \text{ if } \delta_k = 0$$

$$0 \leq c_0(\underline{x}_k) \leq 1, c_1(\underline{x}_k) \leq 0, \text{ and } |c_0(\underline{x}_k) + c_1(\underline{x}_k)| < 1 \text{ if } \delta_k = 1$$

(4.4-3)

and

$$h_{i,k-1} = \prod_{j=1}^{k-1} \delta_j.$$

Although requiring greater computing capability than the simpler methods already mentioned, the method can be easily implemented on a digital computer.

4.5 Gradient Biased Random Search

Pensa used the noisy gradient measurement (equation 4.2-3) as the bias vector $\underline{\zeta}_{k+1}$ in equation 4.4-1 of Matyas' method. The rate of convergence on a noisy unimodal surface is optimized by specifying the covariance matrix T_{k+1} . Convergence has been proven for a noisy unimodal surface.

V Perturbation Types Adaptive Controller

5.1 Perturbation Signals

The gradient of a cost function surface can be determined continuously by the perturbation, or small amplitude oscillation about the current value, of the input signals to the system. This in effect increases the dimension of the output by producing information about the system as it responds to the perturbations. Thus, for a single output, n -dimensional system with n perturbed inputs, the output can contain up to $n+1$ simultaneous, separable signals. Filtering provides the signal separation.

With signal perturbation, a continuous-time gradient technique can be applied. This would require only a relatively simple continuous controller, since discrete operations, memory, and logic, requiring a digital computer type controller, would not be needed. With conditions on the perturbation amplitudes to be discussed later, this technique can work well on noisy cost function surfaces. Therefore, it will be investigated in depth.

The plant to be controlled is a high frequency electrical-acoustical system. For practical experimental purposes, the acoustic frequency can be assumed to be greater than 600 Hz. So, equilibrium conditions and good signal separation can be obtained for perturbations to the system of less than about 100 Hz. Voltage perturbation will be realized as amplitude modulation of the high frequency signal. Phase perturbation will simply be modulation of the signal phase controller.

The following obtained from a perturbation signal can be analyzed as follows:

Let $J(X_i)$ be one dimension of a smooth, unknown cost function where X_i is slowly time varying for the time interval of investigation.

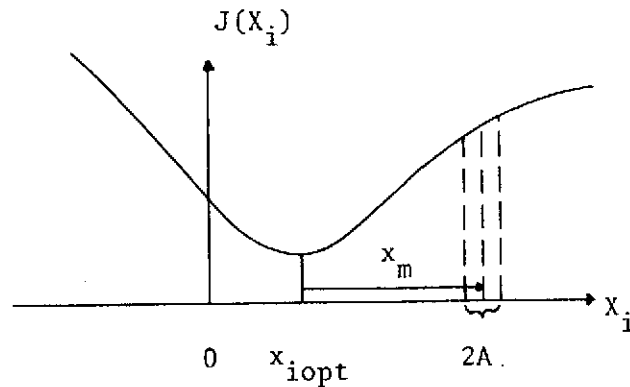


FIGURE 61

One Dimensional Perturbation

$$\text{The perturbed signal is: } X_i = x_{i\text{opt}} + x_m + A \sin \omega_1 t \quad (5.1-1)$$

$$\text{Let } x_k = X_i - x_{\text{opt}}. \text{ Then } x_k = x_m + A \sin \omega_1 t \quad (5.1-2)$$

Use a polynomial approximation for the unknown cost function in the region $x - c < x_k < x + c$, $c > A$:

$$J \approx a_0 + a_1 x_k + a_2 x_k^2 + \dots + a_n x_k^n \quad (5.1-3)$$

The slope of J at $x_k = x_m$ is:

$$\left. \frac{\partial J}{\partial x_k} \right|_{x_k = x_m} = a_1 + 2a_2 x_m + 3a_3 x_m^2 + \dots + n a_n x_m^{n-1} \quad (5.1-4)$$

The output $J(t)$ due to the input $x_k = x_m + A \sin \omega_1 t$ is:

$$\begin{aligned}
 J(t) &= a_0 + a_1 (x_m + A \sin \omega_1 t) + a_2 (x_m + A \sin \omega_1 t)^2 \\
 &\quad + a_3 (x_m + A \sin \omega_1 t)^3 + \dots + a_n (x_m + A \sin \omega_1 t)^n \tag{5.1-5} \\
 &= a_0 + a_1 (x_m + A \sin \omega_1 t) + a_2 (x_m^2 + 2A \sin \omega_1 t + \\
 &\quad + \frac{1}{2} A^2 (1 - \cos 2 \omega_1 t)) + a_3 (x_m^3 + 3x_m^2 A \sin \omega_1 t + \\
 &\quad + \frac{3}{2} x_m A^2 (1 - \cos 2 \omega_1 t) + \frac{1}{4} A^3 (3 \sin \omega_1 t - \sin 3 \omega_1 t)) \\
 &\quad + a_4 (x_m^4 + 4x_m^3 A \sin \omega_1 t + 3x_m^2 A^2 (1 - \cos \omega_1 t) + \\
 &\quad + x_m A^3 (3 \sin \omega_1 t - \sin 3 \omega_1 t) + \frac{1}{8} A^4 (3 - 4 \cos 2 \omega_1 t + \\
 &\quad + \cos 4 \omega_1 t)) + \dots + a_n (x_m + A \sin \omega_1 t)^n
 \end{aligned}$$

The component of $J(t)$ which varies at frequency ω_1 , which can be obtained by ideal filtering, is:

$$\begin{aligned}
 y &= (a_1 + 2a_2 x_m + 3a_3 x_m^2 + \frac{3}{4} a_3 A^2 + 4a_4 x_m^3 + a_4 x_m A^2 + \dots) \cdot \\
 &\quad \cdot A \sin \omega_1 t \tag{5.1-6}
 \end{aligned}$$

The amplitude of y is:

$$\begin{aligned}
 A_y &= A (a_1 + 2a_2 x_m + 3a_3 x_m^2 + \frac{3}{4} a_3 A^2 + 4a_4 x_m^3 + a_4 x_m A^2 + \dots) \\
 &\tag{5.1-7}
 \end{aligned}$$

Defining the parameter S to be

$$S = (a_1 + 2a_2 x_m + 3a_3 x_m^2 + \frac{3}{4} a_3 A^2 + 4a_4 x_m^3 + a_4 x_m A^2 + \dots),$$

it can be seen by comparison with Equation 5.1-4 that the slope of J at $x_k = x_m$ can be approximated by S :

$$\left. \frac{\partial J}{\partial x_k} \right|_{x_k = x_m} \approx S \quad (5.1-8)$$

The error is given by:

$$e = \frac{4}{3} a_3 A^2 + a_4 x_m A^2 + \dots \quad (5.1-9)$$

The error is due to the higher order terms of the polynomial approximation and is negligible for $x_m \gg A$. As $x_m \rightarrow 0$ however, A becomes a contributing factor to the steady state error.

For m independent perturbed inputs ($\omega_j \neq \ell\omega_i$ for all j, i and $\ell = 1, 2, 3 \dots$), m components of the cost function gradient can be determined. The response of the system will be limited by the time required to determine A_y . Error is accumulative only over the interval during which A_y is determined.

To minimize error in the determination of the gradient due to higher order components of the cost function surface and to minimize steady state error, it is desirable to minimize the perturbation amplitude, A . But, system irregularities, nonlinearities, and noise constrain the minimum value of A . It is therefore important to determine an A_{\min} as a function of the parameters of the non-ideal system characteristics.

Output signal separability is essential for complete perturbation measurability. So, each filtered perturbation output signal, y_i , must be independent of all other y_j , $j \neq i$. Thus, a 1-dimensional analysis can be applied to each of the perturbed system dimensions. Shown below is a realization of J versus x_i with random noise present for the i^{th} dimension at $f = f_1$ and x_j , $j \neq i$, fixed.

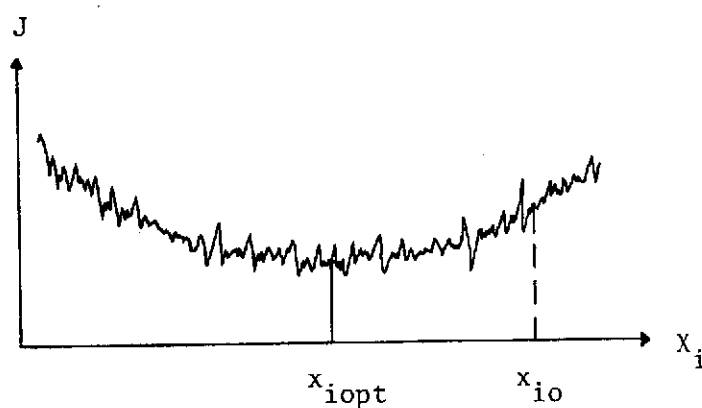


FIGURE 62

Realization of Cost Function in i^{th} Dimension

Of importance is the departure from a smooth, ideal function. This superimposed random process which is dependent upon x_i shall be denoted by the symbol $N(x_i)$. This random process was detected experimentally, and is dependent upon the acoustic frequency and the values of the other input parameters. The random process arises due to the point cancellation effect on a SPL measurement network. Individual microphone probes are effected independently because of localized distortions of the sound field due to an out-of-round duct, variation of

transducer-to-transducer response characteristics, etc. The measurement network combines these signals to obtain the "noisy" performance indicator, J . The output is dependent upon the acoustic frequency, which is a continuous variable from 600 Hz. to 6000 Hz., and the other parameter, X_j , which is continuous from 0 to $X_{j \text{ max}}$. Thus, there exists an infinite number of realizations, making deterministic analysis inapplicable.

We have for a single dimension

$$J(X_i) = f(X_i) + N(X_i)$$

where $X_i = x_{i0} + A \sin \omega t$

$$f(X_i) = \text{smooth deterministic function}$$

$$N(X_i) = \text{random component}$$

Since we are dealing with only 1 dimension, the i subscript will be temporarily dropped. The following qualifications will be used to establish a mathematical model for $N(x)$.

- 1) The rate of change of the acoustic frequency is slow enough that the realization of $N(x)$ remains unchanged for the time period for which $J(x)$ is being examined. This makes $n(X)$ slowly time varying in control systems context.
- 2) Each acoustic frequency has a unique realization of $N(x)$ and the selection of the acoustic frequency is not a deterministic process.
- 3) $N(X_i)$ is independent of $N(X_j)$ for all i, j and $i \neq j$.

It is therefore appropriate to model $N(x)$ as a random process $\{N\}$ such that

$$1) \quad P_N(X) = \frac{1}{\sqrt{2\pi} \sigma_N} e^{-\frac{1}{2} \left(\frac{X - \bar{X}}{\sigma_N}\right)^2} \quad (\text{Gaussian})$$

where σ_N is the standard deviation of the random process

2) $\{N(X)\}$ is white and of zero mean.

Thus:

$$\begin{aligned} E[J(X)] &= E[f(X)] + E[N(X)] \\ &= f(X) \end{aligned} \quad (5.1-11)$$

System nonlinearities may cause a vertical shift of the transfer (cost) function. Let the magnitude of this shift be " ℓ ". Define:

$$g(X) = f(X) + \ell. \quad (5.1-12)$$

$g(X)$ can be used as a new cost function surface without effecting the position of the minimum or the operation of the controller. Only the dc component associated with X_0 is changed, which is filtered out.

Now,

$$J(X) = g(X) + N(X) \quad (5.1-13)$$

Thus,

$$E[J(X)] = g(X) \quad (5.1-14)$$

Therefore, the expected value of an output signal is that obtained for a smooth transfer (or cost) function plus a constant. The analysis for a smooth, or ideal, cost function then applies to the expected signal.

Information is obtained from the ω_i frequency component of the output, where ω_i is the perturbation frequency in the i^{th} dimension. The processing of this signal introduces a bias due to $N(X)$. In particular, say the RMS value of the signal is used to determine its amplitude.

$$\begin{aligned} E[J^2(X)] &= E[g(X) + N(X)]^2 \\ &= E[g^2(X) + 2g(X)N(X) + N^2(X)] \\ &= g^2(X) + 0 + \sigma_N^2 \end{aligned} \quad (5.1-15)$$

From (5.1-6) and (5.1-8), the filtered output from a smooth cost function surface at the perturbation frequency is:

$$y \approx A \frac{dJ}{dX} \sin \omega_1 t = y_1 \quad (5.1-8a)$$

$$\text{Including the noise, } y_1 = A \frac{dJ}{dX} \sin \omega_1 t + N(X, \omega_1 t) \quad (5.1-16)$$

$$\text{where } N(X, \omega_1 t) = N(X(t) + A \sin \omega_1 t) \Big|_{\omega = \omega_1}$$

$$\begin{aligned} E[y_1^2(t)] &= E\left[A^2 \left(\frac{dJ}{dX}\right)^2 \sin^2 \omega_1 t + 2A \frac{dJ}{dX} \sin \omega_1 t N(X, \omega t) + N^2(X, \omega_1 t)\right] \\ &= A^2 \left(\frac{dJ}{dX}\right)^2 \sin^2 \omega_1 t + 0 + \sigma_N^2(\omega_1) \end{aligned} \quad (5.1-17)$$

The mean value can be determined:

$$\begin{aligned}
 \overline{y_1^2(t)} &= \frac{1}{\pi} \int_0^\pi y_1^2(t) dt \\
 &= \frac{1}{\pi} \int_0^\pi [A^2 \left(\frac{dJ}{dX}\right)^2 \sin^2 \omega_1 t + \sigma_N^2(\omega)] d\omega_1 t \\
 &= \frac{1}{\pi} [A^2 \left(\frac{dJ}{dX}\right)^2 \left(\frac{1}{2} \omega_1 t - \frac{1}{4} \sin^2 \omega_1 t\right) + (\omega_1 t) \sigma_N^2(\omega_1)]_0^\pi \\
 &= \frac{1}{2} A^2 \left(\frac{dJ}{dX}\right)^2 + \sigma_N^2(\omega_1) \tag{5.1-18}
 \end{aligned}$$

The RMS value is:

$$y_1(t)_{\text{RMS}} = \sqrt{\frac{1}{2} A^2 \left(\frac{dJ}{dX}\right)^2 + \sigma_N^2(\omega_1)} \tag{5.1-19}$$

$$\approx .707A \frac{dJ}{dX} + \frac{1}{2} \frac{\sigma_N^2(\omega_1)}{.707A \frac{dJ}{dX}} - \frac{1}{8} \frac{\sigma_N^4(\omega_1)}{\left(.707A \frac{dJ}{dX}\right)^3} \tag{5.1-20}$$

by a Binomial series expansion.

The information signal desired is $.707A \frac{\partial J}{\partial X_i}$ for the i^{th} dimension of an n dimensional system, so the higher order terms are errors.

For the error to be less than $N_e\%$, using the first predominant error

term gives

$$\frac{1}{2} \frac{\sigma_N^2(\omega_1)}{.707A \frac{\partial J}{\partial X_i}} \leq .01 N_e (.707) A \frac{\partial J}{\partial X_i}$$

$$\text{or } A \geq \frac{10 \sigma_N(\omega_1)}{\frac{\partial J}{\partial X_i} \sqrt{N_e}}$$

σ_N can be determined experimentally. So for N_e specified,

$$A_{\min} = \frac{10 \sigma_N(\omega_1)}{\frac{\partial J}{\partial X_i} \sqrt{N_e}} \quad (5.1-21)$$

For a constant amplitude perturbation system, the value of $\frac{\partial J}{\partial X}$ for which

A_{\min} violates E is specified. Thus, letting $S = \frac{\partial J}{\partial X_i}$ establishes

A_{\min} .

The $\sigma_N(\omega)$ obtained as a result of the "variation" of the cost function surface is a parameter of noise at frequency ω_1 . The output signal will also be contaminated by signal noise in the usual sense. There exists a random process, presumably Gaussian, of zero mean and standard deviation $\sigma_N'(\omega_1)$ which contains all signal noise. The minimum perturbation amplitude is then specified by:

$$A_{\min} = \frac{10 \sigma_N'(\omega_1)}{S \sqrt{N_e}} \quad (5.1-22)$$

5.2 Perturbation Circle

For a 2-dimensional perturbed input, single output system, filtering of the input yields the following information:

$$\frac{\partial J}{\partial X_i}(t) \cong \frac{A_{y1}(t)}{A_1}$$

$$\frac{\partial J}{\partial X_2}(t) \cong \frac{A_{y2}(t)}{A_2}$$

where A_1 and A_2 are the amplitudes of the input perturbations and $A_{y1}(t)$ and $A_{y2}(t)$ are the respective outputs.

To simplify the control system, the concept of a normalized system is introduced. Here, all quantities in the controller are proportional to those in the actual system by the proportionality constants α and β . But the proportionality constants are selected so that corresponding quantities in the controller have the same magnitude. For example, for the control variables X_1 and X_2 , let

$$X_1 \text{ max (controller)} = \alpha X_1 \text{ max (Actual)} = K \text{ volts}$$

$$X_2 \text{ max (controller)} = \beta X_2 \text{ max (actual)} = K \text{ volts}$$

Thus the controller inputs and outputs would be amplified or reduced, depending on the constants α and β .

Using the proportionality constants α and β , we can let

$A_1 = A_2 = A$. Then,

$$\frac{\partial J}{\partial X_1}(t) \cong \frac{A_{y1}(t)}{A}$$

$$\frac{\partial J}{\partial X_2}(t) \cong \frac{A_{y2}(t)}{A}$$

The angle of the negative gradients direction of J on the (X_1, X_2) plane with respect to the positive X_1 axis, γ^* , can be obtained from

the definition of the gradient:

$$\sin \gamma^* = \frac{-\frac{\partial J}{\partial X_2}}{\left(\frac{\partial J}{\partial X_1}\right)^2 + \left(\frac{\partial J}{\partial X_2}\right)^2} \cong \frac{-A_{y2}(t)}{A_{y1}^2(t) + A_{y2}^2(t)} \quad (5.2-1a)$$

$$\cos \gamma^* = \frac{-\frac{\partial J}{\partial X_1}}{\left(\frac{\partial J}{\partial X_1}\right)^2 + \left(\frac{\partial J}{\partial X_2}\right)^2} \cong \frac{-A_{y1}}{A_{y2}^2(t) + A_{y1}^2(t)} \quad (5.2-1b)$$

For a gradient method, the direction of the negative gradient, γ^* , is the desired direction of movement to converge on the minimum.

If $\sin \gamma^*$ and $\cos \gamma^*$ are to be found continuously as a function of time, the system must be perturbed simultaneously in the X_1 and X_2 directions. For simplicity, it would be desirable to develop a system utilizing a single perturbation frequency. In addition, perturbation of both inputs at a single maximum frequency will reduce the system time response. This could be accomplished by a perturbation "circle" which could be created by the inputs:

$$X_1(t) = x_1(t) + A \cos \omega_1 t \quad (5.2-2a)$$

$$X_2(t) = x_2(t) + A \sin \omega_1 t \quad (5.2-2b)$$

System time delays can be modeled by:

$$X_1(t) = x_1(t) + A \cos (\omega_1 t - \beta_1) \quad (5.2-3a)$$

$$X_2(t) = x_2(t) + A \sin (\omega_1 t - \beta_2) \quad (5.2-3b)$$

As $|\beta_1 - \beta_2| \rightarrow \frac{\pi}{2}$, the perturbation circle collapses to a single dimension perturbation, as illustrated in Figure 63.

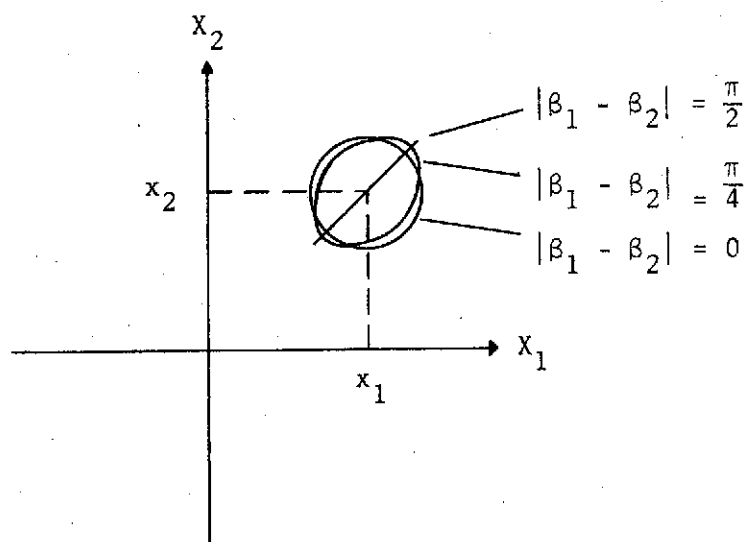


FIGURE 63

Two Dimensional, Single Frequency Perturbation

This would result in incomplete observability, and thus, incomplete convergence. The phase angles β_1 and β_2 can be measured. With calibrated time delays on the perturbation signals, β_1 and β_2 can be increased to $2n\pi$, $n = 1, 2, 3, \dots$, which has the effect of eliminating the time delays from the perturbation analysis.

For analysis purposes, assume the x_1, x_2 coordinate system has been centered on the cost function minimum. Then, in the region of (x_1, x_2) , the following polynomial approximation applies:

$$J \cong \sum_{s=1}^2 a_{s0} + a_{s1} x_s + a_{s2} x_s^2 + \dots + a_{sn} x_s^n \quad (5.2-4)$$

The output $J(t)$ due to the input

$$\begin{aligned} \underline{X}(t) &= x_1 + A \cos \omega_1 t \\ &= x_2 + A \sin \omega_1 t \end{aligned}$$

is:

$$\begin{aligned} J(t) &= a_{10} + a_{11} (x_1 + A \cos \omega_1 t) + a_{12} (x_1 + A \cos \omega_1 t)^2 + \\ &+ a_{13} (x_1 + A \cos \omega_1 t)^3 + \dots + a_{1n} (x_1 + A \cos \omega_1 t)^n + \\ &+ a_{20} + a_{21} (x_2 + A \sin \omega_1 t) + a_{22} (x_2 + A \sin \omega_1 t)^2 + \\ &+ a_{23} (x_2 + A \sin \omega_1 t)^3 + \dots + a_{2n} (x_2 + A \sin \omega_1 t)^n \\ &= (a_{10} + a_{20}) + a_{11} (x_1 + A \cos \omega_1 t) + a_{21} (x_2 + A \sin \omega_1 t) + \\ &+ a_{12} [x_1^2 + 2 A x_1 \cos \omega_1 t + \frac{1}{2} A^2 (1 + \cos 2 \omega_1 t)] + \\ &+ a_{22} [x_2^2 + 2 A x_2 \sin \omega_1 t + \frac{1}{2} A^2 (1 - \cos 2 \omega_1 t)] + \\ &+ a_{13} [x_1^3 + 3 x_1^2 A \cos \omega_1 t + \frac{3}{2} x_1 A^2 (1 + \cos 2 \omega_1 t) + \\ &+ \frac{1}{4} A^3 (3 \cos \omega_1 t + \cos 3 \omega_1 t)] + a_{23} [x_2^3 + 3 x_2^2 A \sin \omega_1 t + \end{aligned}$$

$$\begin{aligned}
& + \frac{3}{2} x_2 A^2 (1 - \cos 2 \omega_1 t) + \frac{1}{4} A^3 (3 \sin \omega_1 t - \sin 3 \omega_1 t)] + \\
& + a_{14} [x_1^4 + 4 x_1^3 A \cos \omega_1 t + 3 x_1^2 A^2 (1 + \cos 2 \omega_1 t) + \\
& + x_1 A^3 (3 \cos \omega_1 t + \cos 3 \omega_1 t) + \frac{1}{8} A^4 (3 + 4 \cos 2 \omega_1 t + \\
& + \cos 4 \omega_1 t)] + a_{24} [x_2^4 + 4 x_2^3 A \sin \omega_1 t + \\
& + 3 x_2^2 A^2 (1 - \cos 2 \omega_1 t) + x_2 A^3 (3 \sin \omega_1 t - \sin 3 \omega_1 t) + \\
& + \frac{1}{8} A^4 (3 - 4 \cos 2 \omega_1 t + \cos 4 \omega_1 t)] + \dots + \\
& + a_{1n} (x_1 + A \cos \omega_1 t)^n + a_{2n} (x_2 + A \sin \omega_1 t)^n \quad (5.2-5)
\end{aligned}$$

The component of $J(t)$ at frequency ω_1 , which can be obtained by filtering, is:

$$\begin{aligned}
y(t) = & (a_{11} + 2a_{12} x_1 + 3a_{13} x_1^2 + \frac{3}{4} a_{13} A^2 + 4a_{14} x_1 A^2 + \dots) \cdot \\
& \cdot A \cos \omega_1 t + (a_{21} + 2a_{22} x_2 + 3a_{23} x_2^2 + \frac{3}{4} a_{23} A^2 + 4a_{24} x_2^3 + \\
& + a_{24} x_2 A^2 + \dots) A \sin \omega_1 t = (A_{y1} \cos \omega_1 t + A_{y2} \sin \omega_1 t) \quad (5.2-6)
\end{aligned}$$

A_{y1} and A_{y2} are proportional to the slopes in the X_1 and X_2 direction, as shown in Section 5.1.

The single separation and analysis is illustrated by the following controller operation outline:

The controlled variables are given by:

$$\underline{X}(t) = \begin{bmatrix} x_1(t) + A \cos \omega_1 t \\ x_2(t) + A \sin \omega_1 t \end{bmatrix}$$

Let $\dot{\underline{X}}(t) \cong k e^{j\gamma^*}$ where k is the amplitude of $\dot{\underline{X}}(t)$ due to the sinusoidal perturbation. In vector form, $\dot{\underline{X}}(t)$ is given by

$$\dot{\underline{X}} \cong \begin{bmatrix} k \cos \gamma^* \\ k \sin \gamma^* \end{bmatrix}$$

The ideal filtered output is:

$$\begin{aligned} y(t) &= A_y(t) \sin(\omega_1 t + \phi) \\ &= A_{y1}(t) \cos \omega t + A_{y2}(t) \sin \omega_1 t \end{aligned}$$

Multiply $Y(t)$ by $1 \cdot \cos \omega_1 t$ to obtain:

$$\begin{aligned} u_1(t) &= y(t) \cdot \cos \omega_1 t = \frac{1}{2} A_{y1}(t) (1 + \cos 2 \omega_1 t) + \\ &+ \frac{1}{2} A_{y2}(t) \sin 2 \omega_1 t \end{aligned}$$

Filtering $u_1(t)$ with a low pass filter yields:

$$z_1(t) = \frac{1}{2} A_{y1}(t)$$

Multiplying $y(t)$ by $1 \cdot \sin \omega_1 t$ yields:

$$u_2(t) = \frac{1}{2} A_{y1}(t) \sin 2 \omega_1 t + \frac{1}{2} A_{y2}(t) (1 - \cos 2 \omega_1 t)$$

Filtering $u_2(t)$ with a low pass filter yields:

$$z_2(t) = \frac{1}{2} A_{y2}(t)$$

Equations (5.2-1a) and 5.2-1b) are

$$\sin \gamma^*(t) = \frac{-A_{y2}(t)}{\sqrt{A_{y1}^2(t) + A_{y2}^2(t)}}$$

$$\cos \gamma^*(t) = \frac{-A_{y1}(t)}{\sqrt{A_{y1}^2(t) + A_{y2}^2(t)}}$$

$A_y(t) = \sqrt{A_{y1}^2(t) + A_{y2}^2(t)}$, which is the amplitude of $y(t)$. The full wave rectified, low pass filtered signal $y(t)$ yields

$$z_3(t) = \frac{1}{2} A_y(t)$$

Then,

$$\sin \gamma^*(t) = -\frac{z_2(t)}{z_3(t)}$$

$$\cos \gamma^*(t) = -\frac{z_1(t)}{z_3(t)}$$

So,

$$\dot{\underline{X}} = K \begin{bmatrix} \frac{z_1(t)}{z_3(t)} \\ -\frac{z_2(t)}{z_3(t)} \\ \frac{z_2(t)}{z_3(t)} \\ -\frac{z_1(t)}{z_3(t)} \end{bmatrix}$$

and

$$\underline{X}(t) = \int_0^t \dot{\underline{X}}(t) dt$$

To study the sensitivity of the system to small variations in time delays, let

$$\underline{X}(t) = \begin{bmatrix} x_1(t) + A \cos (\omega_1 t - \alpha_1) \\ x_2(t) + A \sin (\omega_1 t - \alpha_2) \end{bmatrix}$$

where α_1 and α_2 are small (less than .1 radians). The filtered output of the system at frequency ω_1 due to $\underline{X}(t)$ would be:

$$\begin{aligned} y(t) &= A_{y1} \cos (\omega_1 t - \alpha_1) + A_{y2} \sin (\omega_1 t - \alpha_2) \\ &= A_{y1} [\cos \omega_1 t \cos \alpha_1 + \sin \omega_1 t \sin \alpha_1] + \\ &\quad + A_{y2} [\sin \omega_1 t \cos \alpha_2 - \cos \omega_1 t \sin \alpha_2] \\ &= [\cos \alpha_1 A_{y1} - \sin \alpha_2 A_{y2}] \cos \omega_1 t + \\ &\quad + [\sin \alpha_1 A_{y1} + \cos \alpha_2 A_{y2}] \sin \omega_1 t \\ &\approx [A_{y1} - \alpha_2 A_{y2}] \cos \omega_1 t + [\alpha_1 A_{y1} + A_{y2}] \sin \omega_1 t \end{aligned}$$

The two coefficients obtained by the signal separation scheme would be:

$$A'_{y1} = A_{y1} - \alpha_2 A_{y2}$$

$$A'_{y2} = A_{y2} + \alpha_1 A_{y1}$$

The control system would generate $\sin \gamma^*$ and γ^* directly from these coefficients. For this error analysis, it will be useful to determine

$|\gamma' - \gamma^*|$, the change in the indicated negative gradient direction due to α_1 and α_2 . γ' is the aberrant value of the negative gradient direction. For illustration purposes, α_1 and α_2 will be examined separately.

$$\tan \gamma^* = \frac{A_{y2}}{A_{y1}}$$

$$\tan \gamma' = \frac{A'_{y2}}{A'_{y1}} = \frac{A_{y2} + \alpha_1 A_{y1}}{A_{y1} - \alpha_2 A_{y2}}$$

$$\begin{aligned} \tan \gamma' &= \frac{\frac{A_{y2}}{A_{y1}} + \alpha_1}{1 - \alpha_2 \frac{A_{y2}}{A_{y1}}} \\ &= \frac{\tan \gamma^* + \alpha_1}{1 - \alpha_2 \tan \gamma^*} \end{aligned}$$

For $\alpha_2 = 0$, $\tan \gamma' = \tan \gamma^* + \alpha_1$. The greatest error would occur as γ^* approaches 0 or π , where $|\gamma' - \gamma^*|$ approaches α_1 . $|\gamma' - \gamma^*|$ goes to zero as γ^* approaches $\frac{\pi}{2}$ or $\frac{3\pi}{2}$. Similarly, for $\alpha_1 = 0$, $\cot \gamma' = \cot \gamma^* - \alpha_2$. The greatest error occurs as γ^* approaches $\frac{\pi}{2}$ or $\frac{3\pi}{2}$, where $|\gamma' - \gamma^*|$ approaches α_2 . $|\gamma' - \gamma^*|$ approaches zero as γ^* approaches 0 or π . We now have an indication of the magnitude of error which is expected to be encountered.

The stochastic aspects of this controller can be considered by the following simplified analysis:

Let $y(t) = A \sin(\omega_1 t + \phi) + N(t)$ where $N(t)$ is the component at frequency ω of a white, Gaussian process with zero mean.

$$y(t) = A_{y1} \cos \omega_1 t + A_{y2} \sin \omega_1 t + N(t)$$

Let $U_1(t) = y(t) \cos \omega_1 t$

$$\begin{aligned} &= A_{y1} \cos^2 \omega_1 t + A_{y2} \sin \omega_1 t \cos \omega_1 t + N(t) \cos \omega_1 t \\ &= \frac{1}{2} A_{y1} (1 + \cos 2\omega_1 t) + \frac{1}{2} A_{y2} \sin 2\omega_1 t + N(t) \cos \omega_1 t \end{aligned}$$

$$\begin{aligned} E[U_1(t)] &= E\left[\frac{1}{2} A_{y1} (1 + \cos 2\omega_1 t) + \frac{1}{2} A_{y2} \sin 2\omega_1 t\right] \\ &\quad + E[N(t)]E[\cos \omega_1 t] \\ &= \frac{1}{2} A_{y1} (1 + \cos 2\omega_1 t) + \frac{1}{2} A_{y2} \sin 2\omega_1 t \end{aligned}$$

Similarly, $E[U_2(t) = y(t) \sin \omega_1 t] = \frac{1}{2} A_{y1} \sin 2\omega_1 t + \frac{1}{2} A_{y2} (1 - \cos 2\omega_1 t)$

Thus, the expected values of the information signals are their deterministic components. The variance of the random component is:

$$\begin{aligned} E\left[(N(t) \begin{Bmatrix} \cos \omega_1 t \\ \sin \omega_1 t \end{Bmatrix})^2\right] &= E[N^2(t)]E\left[\begin{Bmatrix} \cos \omega_1 t \\ \sin \omega_1 t \end{Bmatrix}^2\right] \\ &= \frac{1}{2} \sigma_N^2 \end{aligned}$$

where σ_N^2 is the variance of $N(t)$.

Thus the information signal $\frac{1}{2} A_{y2}$ has a variance of approximately $\frac{1}{2} \sigma_N^2$. This provides adequate information about the stochastic aspects of the controller.

5.3 Analog Simulation of Control System

The circular perturbation system was simulated on the analog computer. The system flow chart is shown in figure 66. An available single output variable frequency sine wave generator provided the perturbation signal. The complement signal $(\cos \omega_1 t)$ was obtained by a simple approximate derivative circuit. It is recommended that the hard-wired unit be a single frequency oscillator providing both signals. Special purpose elements are given in figure 67. The plant was modeled as a quadratic cost function surface to enable comparison of performance with other adaptive methods. Since phase response of the plant is equal in the two parameter dimensions, the two pure time delays were placed parallel to the plant.

$$\begin{aligned}
 J &= \frac{1}{2} (x_1^2(t) + x_2^2(t)). \\
 &= \frac{1}{2} (x_1^2(t) + 2Ax_1(t)\cos\omega_1 t + A^2\cos^2\omega_1 t + 2Ax_2(t)\sin\omega_1 t + A^2\sin^2\omega_1 t) \\
 &= \frac{1}{2} (x_1^2 + x_2^2 + A^2 + 2A(x_1(t)\cos\omega_1 t + x_2(t)\sin\omega_1 t))
 \end{aligned}$$

Since $z_3(t) = \frac{1}{2} A_y(t)$ forms the denominator for two division operations, we must guarantee that it never goes to zero to prevent circuit overloading. This can be accomplished by the introduction of a bias voltage. To minimize performance degradation, it is desirable to activate the bias voltage only when $z_3(t)$ is small. Noting that such a bias voltage increases system damping, the following algorithm has been formulated:

$$z_3^i(t) = z_3(t) \quad \text{for } z_3(t) > B$$

$$= m z_3(t) + (1-m)B \quad \text{for } z_3(t) \leq B$$

This is illustrated in figure 64.

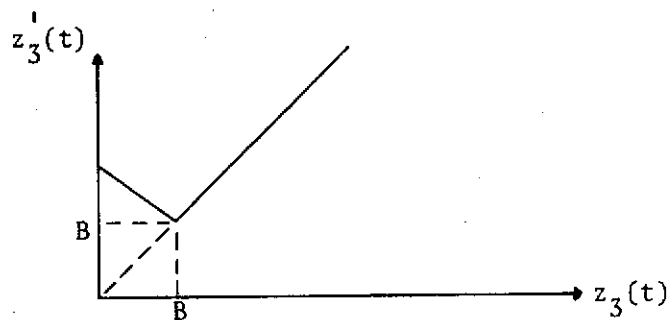


FIGURE 64

Bias Voltage

The slope m of the segment for $z_3(t) < B$, and B , the switching point, add two parameters which are to be manipulated for optimal system performance.

There are two aspects to be considered in the formulation of a performance criterion. First is that of steady state error, e_{ss} . For the quadratic plant, e_{ss} occurs when $X_1(t) = X_2(t) = 0$. Then,

$$e_{ss} = \frac{1}{2} A^2. \quad (5.3-1)$$

This non-zero steady state error is inherent in circular perturbation. The concept is illustrated in figure 65.

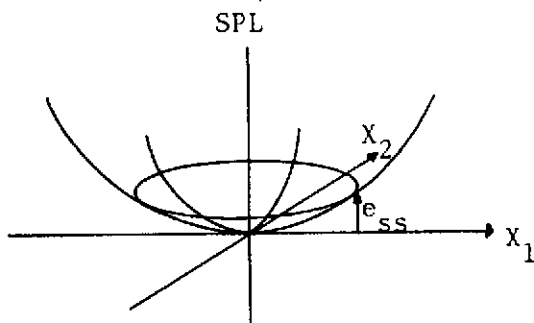


FIGURE 65

Steady State Error Due to Circular Perturbation

Let $e_{ss} = IP_1$. Second is the convergence performance. Let $IP_2 = \int_0^{\infty} (e(t) - e_{ss})^2 dt$ serve as a convergence performance where:

$$e(t) = \frac{1}{2} (x_1^2(t) + x_2^2(t) + A^2 + 2A(x_1(t)\cos\omega_1 t + x_2(t)\sin\omega_1 t))$$

The inclusion of the sinusoidal components accounts for the performance degradation due to the perturbation of the plant. The total performance criteria can then be given by:

$$\begin{aligned} IP &= a_1 IP_1 + a_2 IP_2 \\ &= a_1 e_{ss} + a_2 \int_0^{\infty} (e(t) - e_{ss})^2 dt \end{aligned}$$

where a_1 and a_2 are weighting factors.

Optimization is to be accomplished by varying four parameters: A, the perturbation amplitude, K, the velocity gain, B, the switching level, and m, the slope of the damping bias voltage. Optimal values of these parameters were selected by forming a sample test array and observing general trends.

For K small enough so that the system comes to rest at the minimum, e_{ss} was found to depend only on A , as predicted by equation 5.3-1:

$$e_{ss} = \frac{1}{2} A^2.$$

Calculated versus simulated steady state errors are shown in Table 12.

TABLE 12
Steady State Error

| A | $e_{ss} = \frac{1}{2} A^2$ | e_{ss} (simulated) |
|-----|----------------------------|----------------------|
| .01 | .00005 | .0003 |
| .05 | .00125 | .0012 |
| .10 | .0050 | .0049 |

All quantities are given in machine units, the operational units of the analog computer. Note: the maximum is one machine unit which corresponds to ten volts. Thus, a machine unit corresponds to the normalized units on which this system is based. Steady state error shall be considered important and therefore weighted heavily. Therefore A will be minimized to the limit allowed by system noise. Values of K for which the system does not come to rest at the minimum will be considered unacceptable.

To reduce the dimension of the test set, A was set to .01 machine units. Tests were then conducted in real time over the

23

23

sample space defined by K , B and M . The system was allowed to come to equilibrium at a selected initial input parameter setting, $\underline{x}(0) = (.8, .8)$. Then the adaptive controller was set in operation by switching the mode of the input parameter velocity integrators from initial conditions (IC) to operate (refer to Figure 66). The performance indicator network was activated simultaneously. A sample test set is given in Table 13.

The parameters $m = 0$, $\beta = .0050$, and $K = 10$ were selected because of the observed performance, consistency, and stability characteristics. The index of performance weighting factors a_1 and a_2 in

$$IP = a_1 IP_1 + a_2 IP_2$$

were not formally set. The steady state error, IP_1 , was considered separately and given intuitive weighting far exceeding that of IP_2 . The results obtained for IP_2 are considered satisfactory despite this disproportionate weighting.

Results for the selected parameters are shown in Figures 68 to 70. A was maintained at .01 as a base for further testing. As shown in Figure 69, two-thirds reduction of the cost function J for the test initial conditions was obtained in .08 seconds. Steady state operation was obtained in .6 seconds. These are promising results for the application of automatic control to the SMS.

Also subject to evaluation was the system response to a load change. This was simulated by changing the location of the minimum on the (x_1, x_2) plane. So that comparative data could be obtained,

FIGURE 66
Schematic for Analog Simulation of
Circular Perturbation System

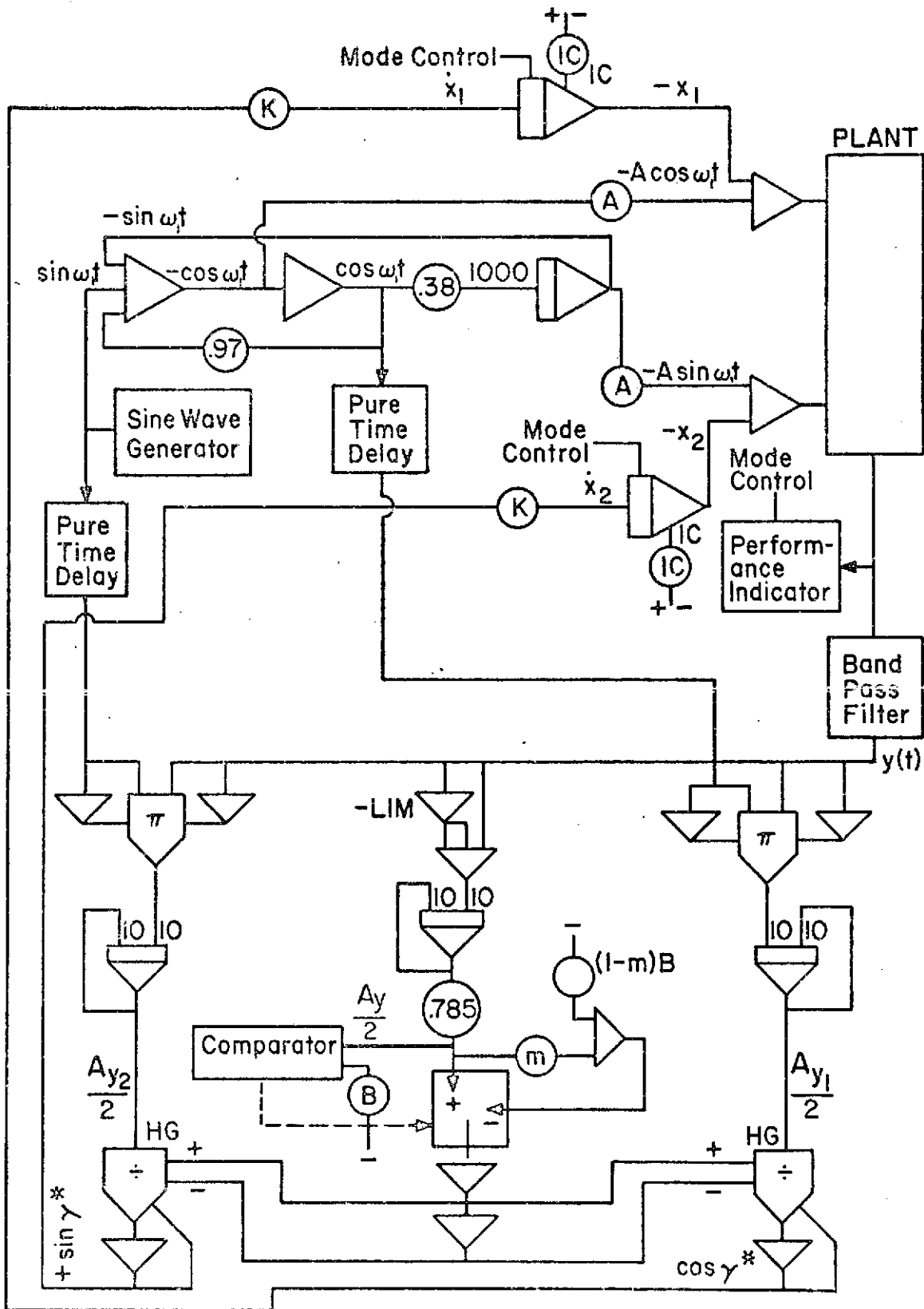
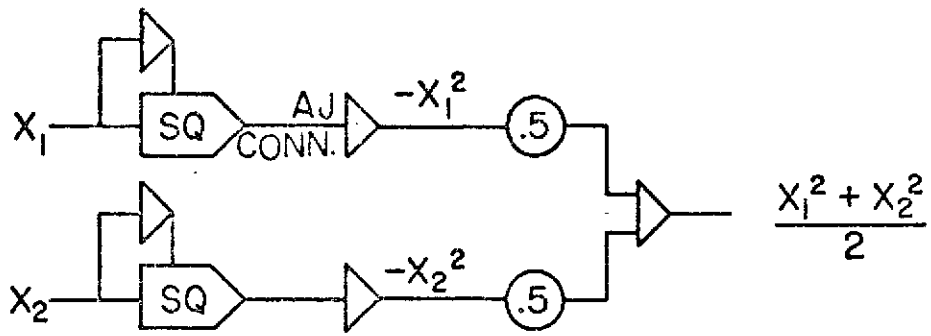
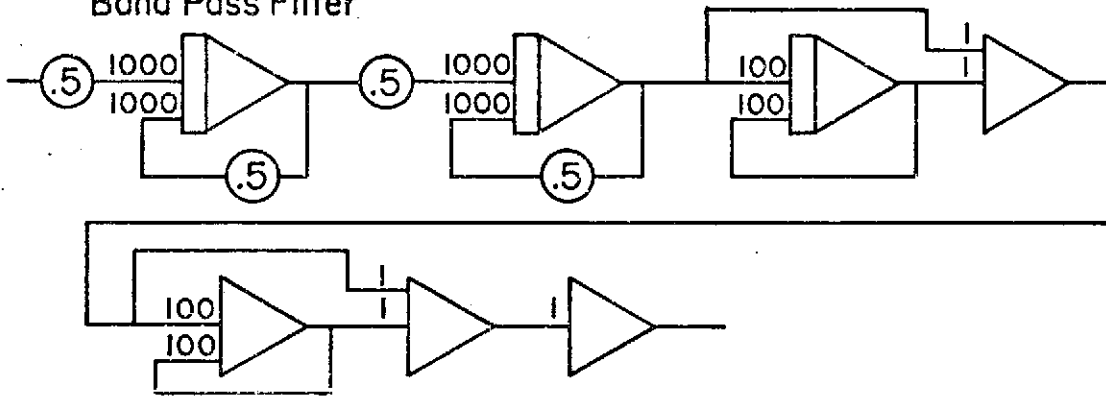


FIGURE 67
Details of Special Elements

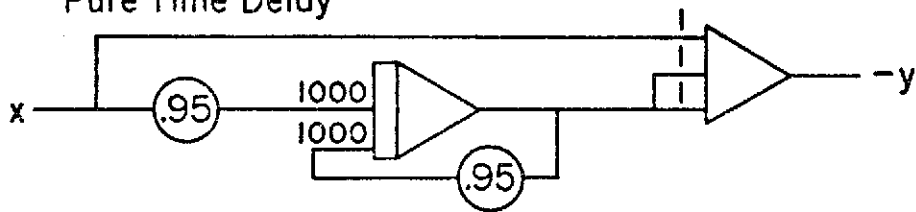
Quadratic Plant



Band Pass Filter



Pure Time Delay



Performance Indicator

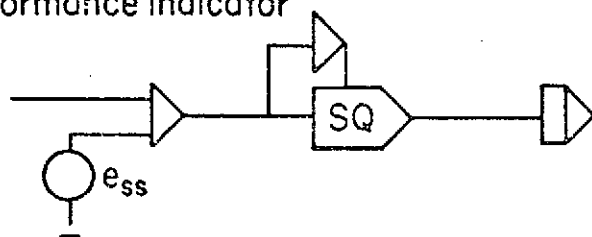


TABLE 13
Sample Test Set

Initial conditions: $x_1(0) = x_2(0) = .8$ machine units

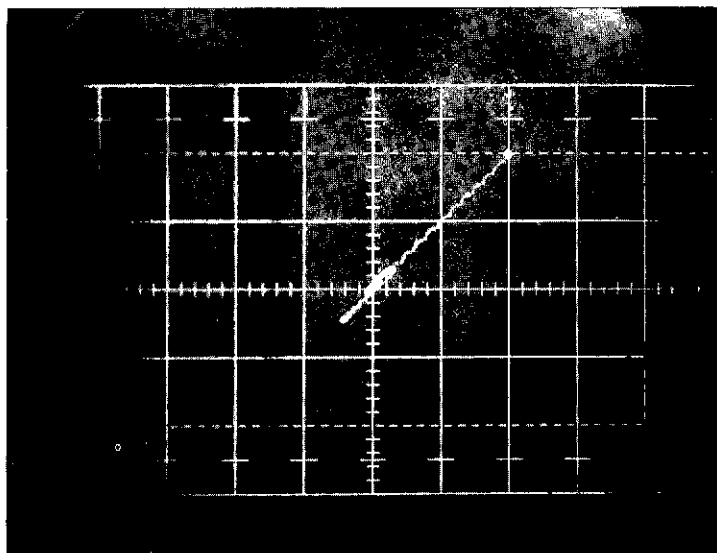
| A = .01 | K | IP_1 | \overline{IP}_2 |
|-----------|----|--------|-------------------|
| m = 0 | 1 | .0003 | .0967 |
| B = .0010 | 5 | .0003 | .0254 |
| m = 0 | 1 | .0003 | .0979 |
| B = .0050 | 5 | .0003 | .0265 |
| | 10 | .0003 | .0138 |
| m = 0 | 1 | .0003 | .1725 |
| B = .0100 | 5 | .0003 | .0354 |
| | 10 | .0003 | .0153 |
| m = -10 | 1 | .0003 | .0951 |
| B = .0010 | 5 | .0003 | .0258 |
| | 10 | .0003 | .0139 |
| m = -10 | 1 | .0005 | .1332 |
| B = .0050 | 5 | .0005 | .0262 |
| | 10 | .0005 | .0139 |
| m = -10 | 1 | .0005 | .1960 |
| B = .0100 | 5 | .0005 | .0402 |
| | 10 | .0005 | .0154 |

FIGURE 68

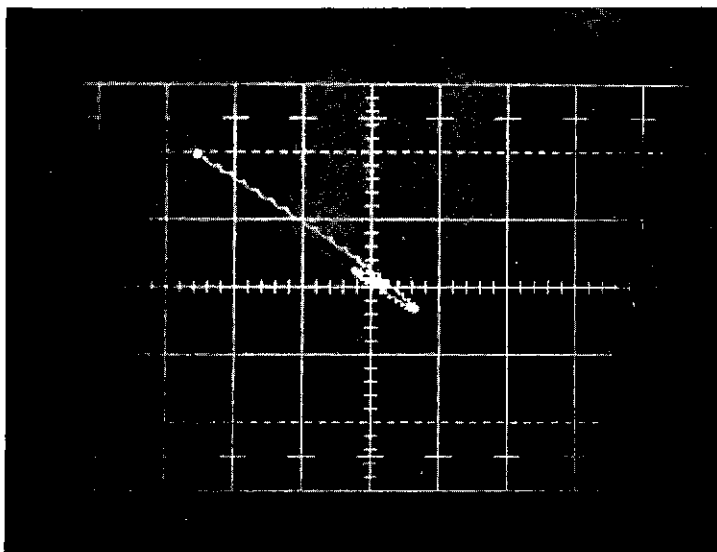
$x(t)$ for $\underline{x}(0) = \begin{bmatrix} 8 \\ 8 \end{bmatrix}$ volts

FIGURE 69

$x(t)$ for $\underline{x}(0) = \begin{bmatrix} -9 \\ 8 \end{bmatrix}$ volts

X_2 

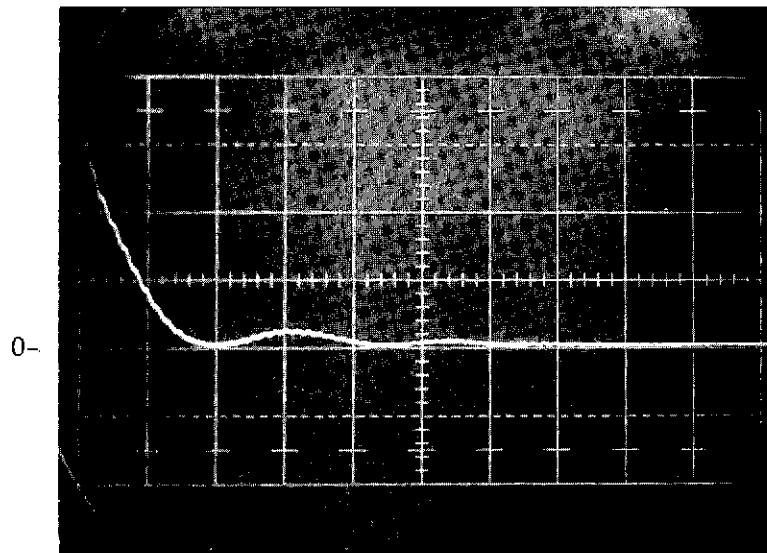
Scale = 4 volts/cm

 X_2 

Scale = 4 volts/cm

FIGURE 70

$J(t)$ for $\underline{x}(0) = \begin{bmatrix} 8 \\ 8 \end{bmatrix}$ volts



0

Ordinate = J(SPL)

Scale = 2 volts/cm

Absicca = Time

Scale = .1 sec/cm

the load change was modeled as a step change from the minimum at $X = (0,0)$ to a minimum location at $X = (.8,.8)$. The parabolic surface contour was maintained. Since the final value for the load change test was the initial value for the "convergence" tests, a meaningful comparison of the two types of response could be obtained.

Circuit overloading and instability resulted except for very small K and large B . Examination of the system indicates that the two dividers which yield $\sin \gamma^*$ and $\cos \gamma^*$ overload when the step change is made. This can be attributed to incompatible step change response of the parallel circuits providing the numerators and denominators of the two dividers. The circuit providing the denominators responds slower than the other two circuits (refer to Figure 66). This allows the numerator to exceed denominator, thus overloading the division circuits.

Various corrective measures were tried, such as increasing the damping in the numerator circuits to obtain compatible step response. But, acceptable performance to load change could not be obtained. Therefore, modification of the control scheme is necessary.

$$\begin{aligned}
 J(t) &= J_{dc}(t) + A_y \sin(\omega_1 t + \phi) \\
 &= J_{dc}(t) + A_{y1} \cos \omega_1 t + A_{y2} \sin \omega_1 t
 \end{aligned}$$

For the outside loop,

$$\begin{aligned}
 Y_7(t) &= (J_{dc}(t) + A_{y1} \cos \omega_1 t + A_{y2} \sin \omega_1 t) \cos \omega_1 t \\
 Y_7(t) &= J_{dc}(t) \cos \omega_1 t + \frac{1}{2} A_{y1} (1 + \cos 2\omega_1 t) + \frac{1}{2} A_{y2} \sin 2\omega_1 t
 \end{aligned}$$

$Y_7(t)$ is operated on by $G_2(s)$. Assuming for now that $G_2(s) = 1$, $Y_8(t) = Y_7(t)$. $Y_8(t)$ is then integrated.

$$Y_8(t) = K \int_0^t Y_8(t) dt$$

For $J_{dc}(t)$ slowly time varying,

$$Y_9(t) = K \left(\frac{A_{y1}}{2} t + \frac{J_{dc}(t)}{\omega_1} \sin \omega_1 t + \frac{A_{y1}}{4\omega_1} \sin 2\omega_1 t - \frac{A_{y2}}{4\omega_1} \cos 2\omega_1 t \right).$$

Note that integration attenuates the sinusoidal components by the amount of their frequency. $K \frac{A_{y1}}{2} t$ is the desired signal, so an improved signal would be obtained with $G_2(s)$ being a low pass filter. For our specific application, let

$$G_2(s) = G_4(s) = \frac{1}{s+10}.$$

A similar analysis holds for the inside loop. Again, let

$$G_2(s) = G_4(s) = \frac{1}{s+10}.$$

For this system, the control gain in the system dimensions is proportional to the magnitude of the respective gradient components.

This system more closely approximates the classical perturbation type gradient controller than the trigonometric form investigated in the previous section. The classical features will be investigated in section 5.5 to provide a basis for evaluation of system performance.

The modified circular perturbation controller does not contain division circuits, so the circuit overloading due to load change experienced in the previous controller is not expected. Because of the different nature of this controller, it is difficult to predict its relative performance.

This system was simulated on the analog computer. The flow chart is shown in Figure 72. For the quadratic plant the phase shift is zero so

$$G_1(s) = G_3(s) = 1.$$

A was set at .05 machine units to reduce noise effects. This was necessary because there is less signal filtering in this circuit than previously. $K = 300$ was found to optimize both convergence performance and load change performance. A sample data set is given in Table 14. The steady state error was .0009 due to the increased perturbation amplitude. Instability did not occur until $K = 800$.

The index of performance shows that load change stability of the modified system was obtained at the expense of initial convergence response degradation. Two thirds reduction for the convergence testcase now requires .26 seconds as opposed to .08 seconds.

FIGURE 72

Schematic of Modified Perturbation System

TABLE 14

Test Set for Modified Controller

Convergence Test

$$A = .05$$

$$\text{Initial Parameter Setting : } \underline{X}(0) = (0.8, 0.8)$$

$$\text{Optimal Parameter Setting : } \underline{X}^*(T) = (0.0, 0.0)$$

| K | IP ₁ | \overline{IP}_2 |
|-----|-----------------|-------------------|
| 100 | .0009 | .0679 |
| 200 | .0009 | .0437 |
| 300 | .0009 | .0366 |
| 400 | .0009 | .0401 |

Load Change Test

$$A = .05$$

$$\text{Initial Optimal Parameter Setting : } \underline{X}^*(0) = (0.0, 0.0)$$

$$\text{Final Optimal Parameter Setting : } \underline{X}^*(T) = (.8, .8)$$

Functional Change : Step

| K | IP ₁ | \overline{IP}_2 |
|-----|-----------------|-------------------|
| 100 | .0009 | .0847 |
| 200 | .0009 | .0673 |
| 300 | .0009 | .0670 |
| 400 | .0009 | .0966 |

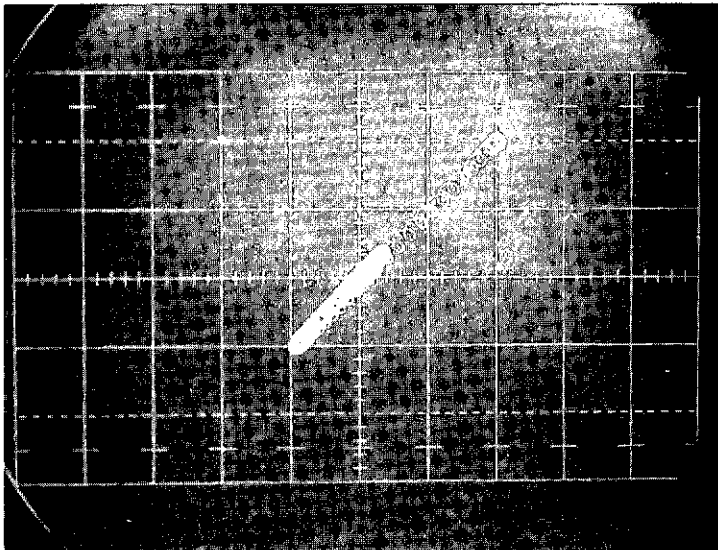
The same reduction for the load change test requires .40 seconds. But, this is still adequate system performance. Examples of system response are given in Figures 73 to 76.

FIGURE 73

Optimal Convergence Response

FIGURE 74

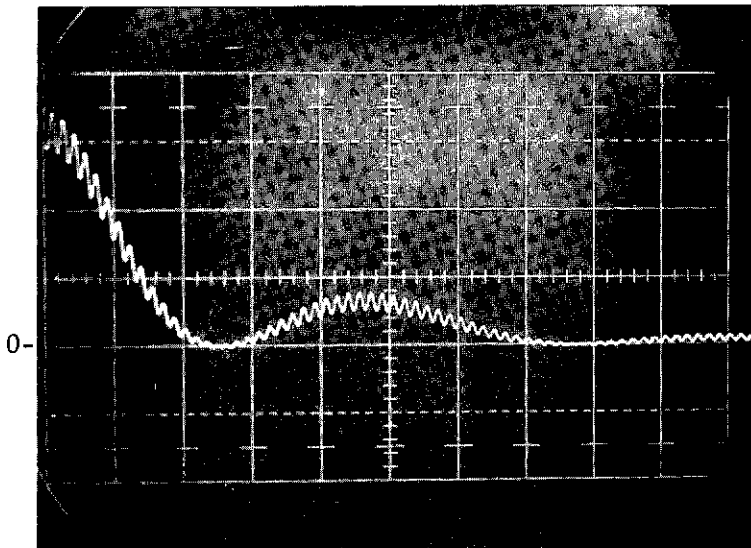
Optimal Convergence Response

x_2  $-x_1$

Scale = 4 volts/cm

$$\underline{x}^T (t=0) = [8, 8] \text{ volts}$$

$$\underline{x}^T (t \rightarrow \infty) = [0, 0] \text{ volts}$$



0

Ordinate = SPL

Scale = 2 volts/cm

SPL (t=0) = .64 volts

SPL (t $\rightarrow\infty$) = .009 volts

Absicca = Time

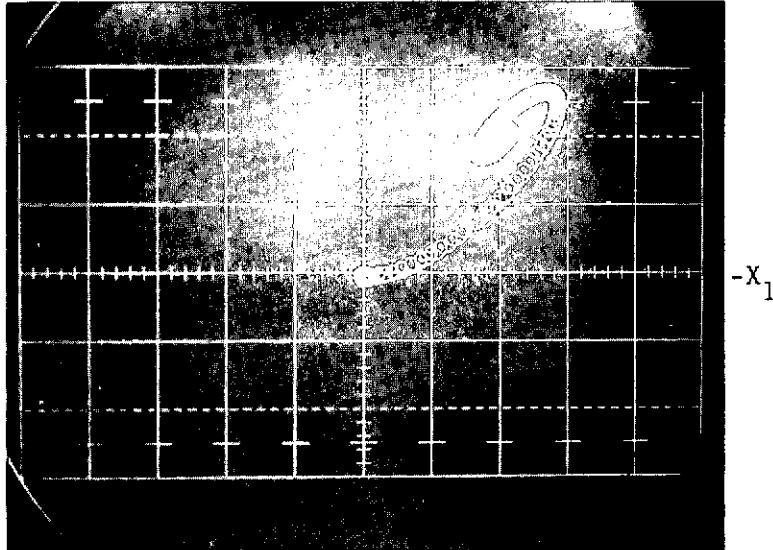
Scale = .2 sec/cm

FIGURE 76

Optimal Load Change Response

FIGURE 77

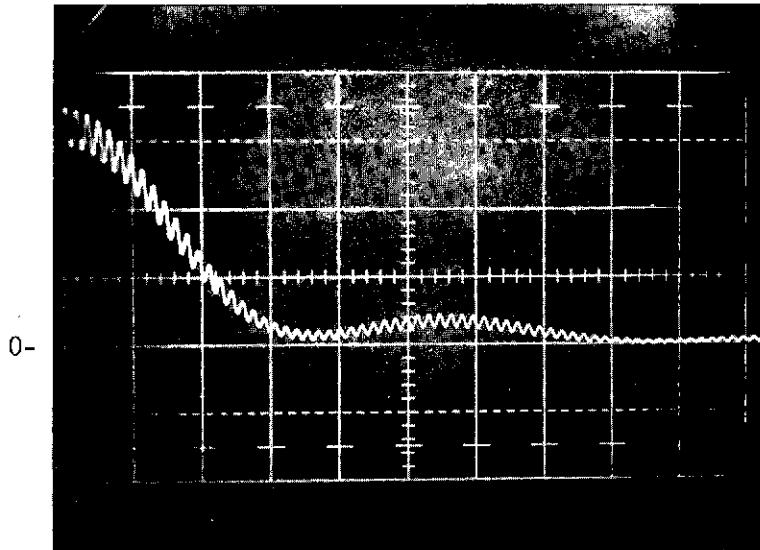
Optimal Load Change Response

x_2 

Scale = 4 volts/cm

$$\underline{x}^{*T}(t=0^-) = [0,0] \text{ volts}$$

$$\underline{x}^{*T}(t=0^+) = [8,8] \text{ volts}$$



0

Ordinate = SPL

Scale = 2 volts/cm

SPL ($t=0^+$) = .64 voltsSPL ($t \rightarrow \infty$) = .009 volts

Absicca = Time

Scale = .2 sec/cm

5.5 Classical Perturbation Controller Features

Eveleigh (9) provides the basic form of a classical single dimensional perturbation controller. Figure 77 shows the system with notation consistent with that of this chapter.

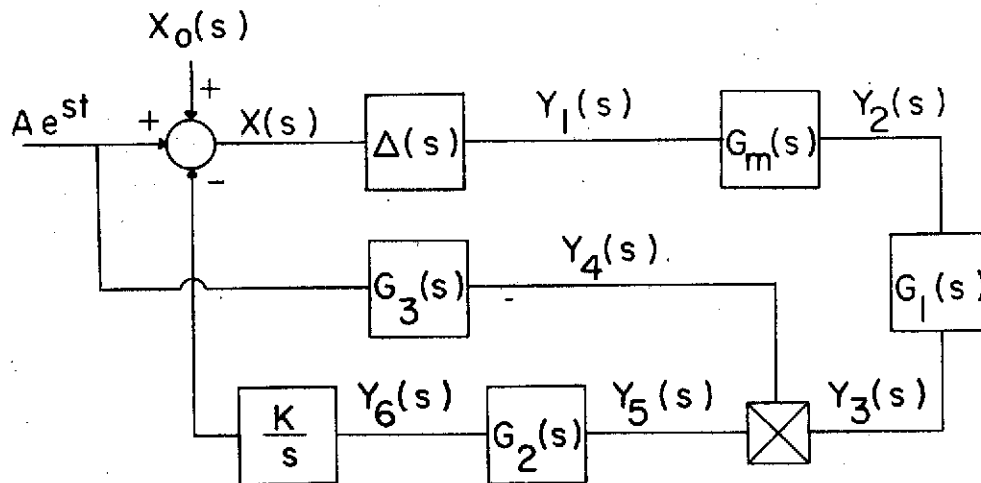


FIGURE 77

Single Dimensional Perturbation Adaptive Controller

The plant is represented by $\Delta(x)$. A linear filter $G_m(s)$ represents the index of performance measurement process. $G_1(s)$ is generally a narrowband filter centered at frequency ω_1 . Experimental evidence (9) shows that a reasonable form for $G_1(s)$ is

$$G_1(s) = \frac{\omega_1^2 s}{s^2 + \omega_1 s + \omega_1^2} = \frac{L[y_3(t)]}{L[y_2(t)]}$$

$G_3(s)$ is chosen to provide a phase shift at ω_1 equal to that across

$\Delta(x)$, $G_m(s)$, and $G_1(s)$. The signal at Y_5 is approximately

$$\pm A_y \sin^2 \omega_1 t = \pm \frac{A_y}{2} (1 - \cos 2\omega_1 t).$$

Since the desired signal is A_y , $G_2(s)$ is chosen as a low pass filter. The integration provides a type-one adaptive loop, allowing the system to follow changes in the optimum parameter setting with no steady state error.

Other than the concept of the perturbation circle, the narrow-band filter $G_1(s)$ is the only basic difference between the classical form and the controller developed in Section 5.3. This filter was incorporated into the controller so that performance data could be obtained. The filter circuitry was developed by the "M" method:

$$G_1(s) = \frac{\omega_1^2 s}{s^2 + \omega_1 s + \omega_1^2} = \frac{Y(s)}{X(s)}$$

then,

$$\frac{Y(s)}{\omega s} = \frac{\omega_1 X(s)}{s^2 + \omega_1 s + \omega_1^2} = M(s)$$

$$(s^2 + \omega_1 s + \omega_1^2) M(s) = \omega_1 X \implies \frac{s^2}{\omega_1} M(s) = \omega_1 X(s) - sM(s) - \omega_1 M(s)$$

and $Y = \omega_1 s M(s)$.

The circuit can then be shown as in Figure 78.

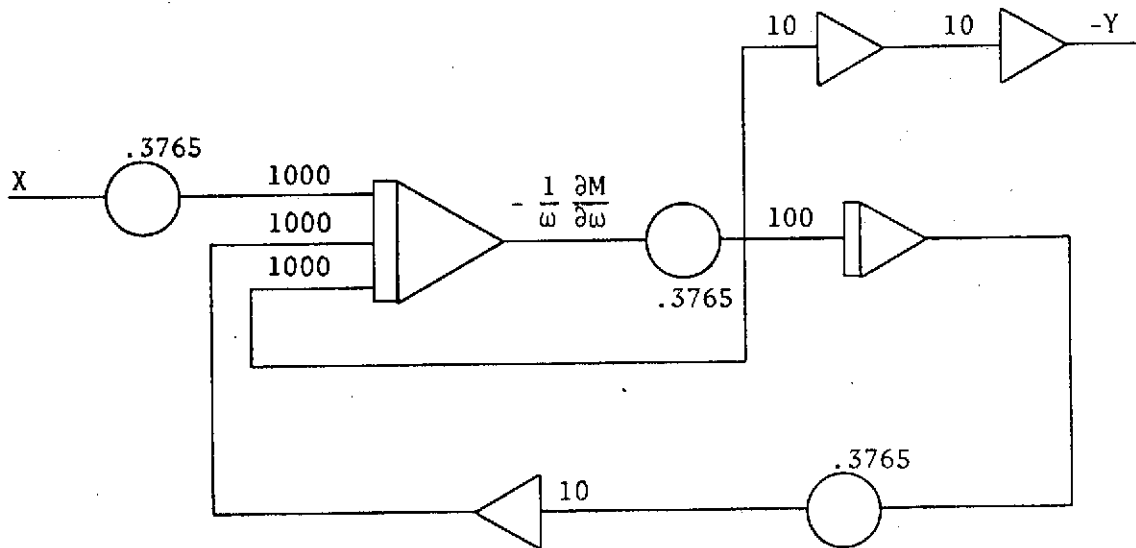


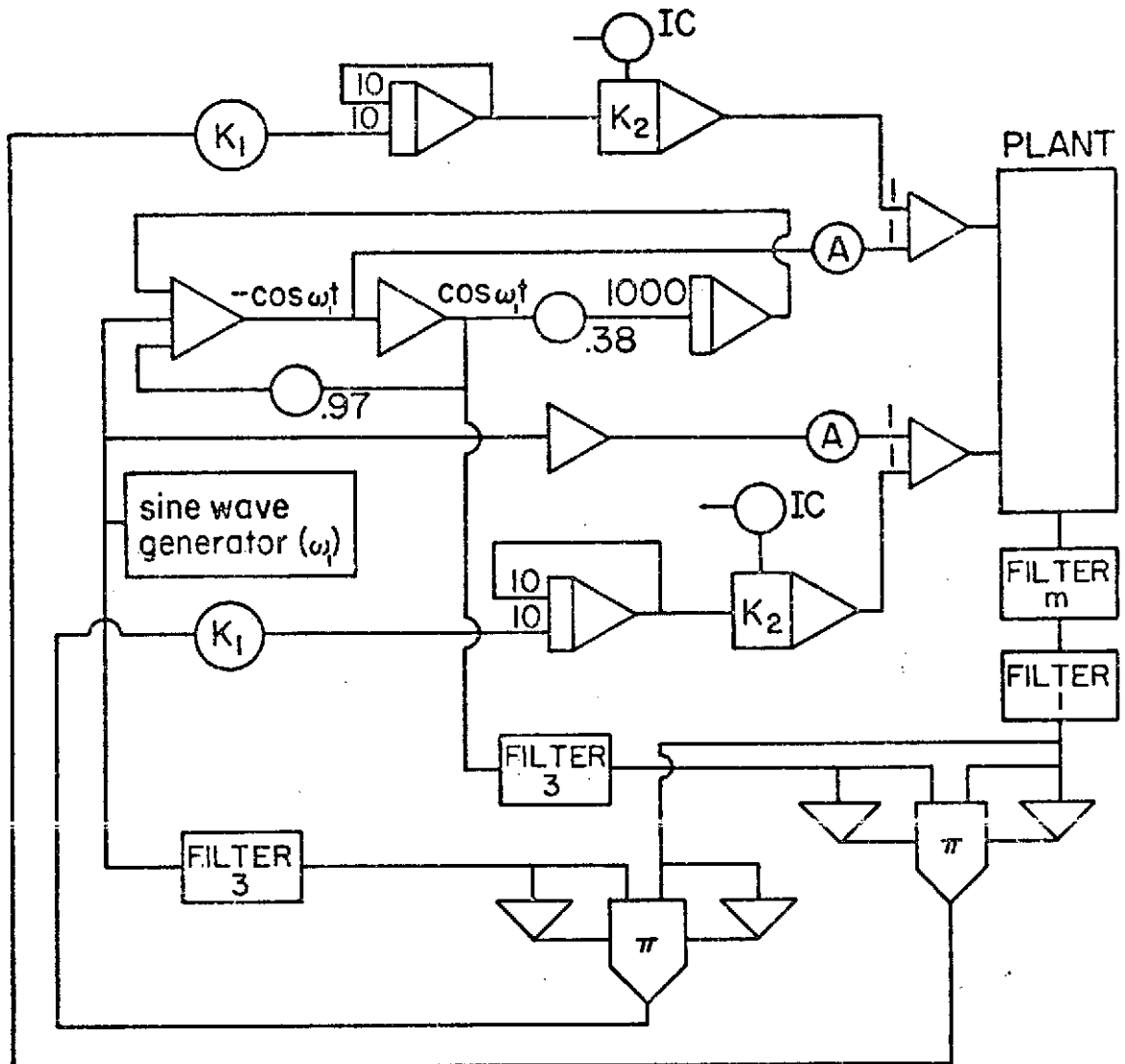
FIGURE 78

Implementation of Narrowband Filter $G_1(s)$

The high gains are due to $\omega = (60 \text{ Hz}) (2\pi) = 376.5 \text{ rad/sec.}$

The system of Section 5.4 was modified to include $G_1(s)$ and various low order low pass filters for $G_m(s)$ and $G_3(s)$. This revised system is shown in Figure 79. The performance index IP_2 was found to be an order of magnitude greater than that of the original system for all combinations. This occurred as a result of lightly damped system response due to $G_1(s)$, necessitating the use of low gains. Thus, this system modification is rejected.

FIGURE 79
Schematic for Analog Simulation of
Modified Perturbation System with
Bandpass Filter



Case I

$$G_m(s) = G_3(s) = 1$$

Case II

$$G_m(s) = G_3(s) = \frac{376.5}{s+376.5}$$

Case III

$$G_m(s) = G_3(s) = \left(\frac{376.5}{s+376.5} \right)^2$$

VI Discussion of Results

The development and analysis of the wave equation for the Spinning Mode Synthesizer has verified the predicted optimal solution. The optimal solution for the minimization of a ducted spinning mode generated by a circular transducer array given by

$$\begin{aligned} Z_{oj} &= \text{axial position of } j^{\text{th}} \text{ transducer} \\ &= Z_o, \quad j = 1, 2, \dots, n \end{aligned}$$

$$\begin{aligned} r_{oj} &= \text{radial distance of } j^{\text{th}} \text{ transducer} \\ &= r_o, \quad j = 1, 2, \dots, n \end{aligned} \quad (1.3-1)$$

$$\begin{aligned} \theta_{oj} &= \text{angular position of } j^{\text{th}} \text{ transducer} \\ &= \frac{2\pi}{n} (j-1), \quad j = 1, 2, \dots, n \end{aligned} \quad (1.3-2)$$

$$\begin{aligned} Q_{oj} &= \text{source strength of } j^{\text{th}} \text{ transducer} \\ &= Q_o, \quad j = 1, 2, \dots, n \end{aligned} \quad (1.3-3)$$

$$\begin{aligned} \phi_{oj} &= \text{acoustic phase of } j^{\text{th}} \text{ transducer} \\ &= \frac{2\pi m}{n} (j-1), \quad j = 1, 2, \dots, n \end{aligned} \quad (1.3-4)$$

by a circular cancelling transducer array positioned at

$$\begin{aligned} Z_{oj} &= Z_o, \quad j = 1, 2, \dots, n \\ r_{oj} &= r_o, \quad j = 1, 2, \dots, n \end{aligned} \quad (1.3-5)$$

$$\theta_{oj} = \frac{2\pi}{n} (j-1) + \frac{\pi}{n}, \quad j = 1, 2, \dots, n \quad (1.3-6)$$

is the predicted solution

$$\begin{aligned} q_{oj} &= \text{source strength of } j^{\text{th}} \text{ transducer} \\ &= Q_o, \quad j = 1, 2, \dots, n \end{aligned} \quad (1.3-7)$$

$$\begin{aligned}\alpha_{oj} &= \text{acoustic phase of } j^{\text{th}} \text{ transducer} \\ &= \frac{m\pi}{n} (2j-1) + \pi, \quad j = 1, 2, \dots, n\end{aligned}\quad (1.3-8)$$

The optimal solution has been shown to provide cancellation for a finite range of m, μ , and frequency which is governed by the set $\{M\}$. Table 11 is repeated for basis of discussion.

TABLE 11

$\{M(m_o)\}$ for the 4 Transducer Array Set for Cancellation

| | $\{M\}$ |
|-----------|--|
| $m_o = 0$ | $\{\pm 4, \pm 12, \pm 20, \pm 28, \dots\}$ |
| $m_o = 1$ | $\{-3, 5, -11, 13, -19, 21, \dots\}$ |
| $m_o = 2$ | $\{-2, 6, -10, 14, -18, 22, \dots\}$ |
| $m_o = 3$ | $\{-1, 7, -9, 15, -17, 23, \dots\}$ |

Cancellation is effective until the lowest cutoff frequency of the lowest order circumferential mode in the set $\{M\}$ is reached. Thus it was predicted that effective sound pressure level reduction could be obtained only over the frequency ranges shown in Table 15.

TABLE 15

Frequency Range of Effective Cancellation

| f range | $\mu = 0$ | $\mu = 1$ | $\mu = 2$ | . . . |
|-----------|-------------|--------------|-----------|-------|
| $m_0 = 0$ | 0 to 1378 | 1378 to 1913 | - | - |
| $m_0 = 1$ | 662 to 1511 | - | - | - |
| $m_0 = 2$ | - | - | - | - |
| $m_0 = 3$ | - | - | - | - |
| . | - | - | - | - |
| : | | | | |
| . | | | | |

0 Hz = cutoff frequency of $m = 0, \mu = 0$ mode
 1378 Hz = cutoff frequency of $m = 0, \mu = 1$ mode
 1913 Hz = cutoff frequency of $m = 4, \mu = 0$ mode
 662 Hz = cutoff frequency of $m = 1, \mu = 0$ mode
 1511 Hz = cutoff frequency of $m = 3, \mu = 0$ mode

Note: These results are valid for a 12 inch diameter duct.

A frequency margin of about 100 Hz to 200 Hz below the upper frequency limits is considered adequate to assure minimal degradation of sound pressure level reduction due to low decay rates in the axial direction of the limiting higher order mode.

Satisfactory sound pressure level reduction has been obtained for the $m_0 = 1$ circumferential mode below 1400 Hz, substantiating the predicted frequency limit. Figure 21, which gives the results for a test case at 1560 Hz, provides evidence of the generation of an $m = 3$ mode above its cutoff frequency of 1511 Hz. The radial distribution of the spinning modes generated by the individual arrays is characteristic of the waveform between the $\mu = 0$ and $\mu = 1$ cutoff frequencies, having some characteristics of both distributions. But, the cancelled radial distribution is clearly that of a $\mu = 0$ spinning mode. This is strong evidence of the propagation of an $m = -3$, $\mu = 0$ mode. The reduced level of this mode is expected due to energy loss to the cancelled $m = 1$, $\mu = 0$ mode.

Examination of the relative acoustic phases of the transducers gives further evidence to the generation of a higher order mode. Table 16 gives the acoustic phases for generation and optimal cancellation of the $m_0 = 1$ mode.

TABLE 16

Acoustic Phases for Optimal Cancellation of the $m_0 = 1$ Mode

| transducer | 1 | 2 | 3 | 4 | 5 | 6 | 7 | 8 |
|----------------------|---|------------------|-----------------|------------------|-------|-----------------|------------------|------------------|
| Acoustic phase (rad) | 0 | $\frac{5\pi}{4}$ | $\frac{\pi}{2}$ | $\frac{7\pi}{4}$ | π | $\frac{\pi}{4}$ | $\frac{3\pi}{2}$ | $\frac{3\pi}{4}$ |

Evaluation of equation 1.3-4 for $n = 8$ and $m = -3$ yields the identical acoustic phases! Therefore, the combined arrays behave as an $m = -3$ generator. This phenomenon can be verified for all m which are elements of $\{M\}$ given in Table 11.

Sound pressure level reduction of the plane wave within the specified frequency range had been verified by test cases. The propagation of a higher order mode above 1800 - 1900 Hz is illustrated by Figure 80. An $m_0 = 0, \mu = 1$ mode was generated at 2000 Hz, which is above the $m = 4, \mu = 0$ cutoff frequency at 1913 Hz. The cancelled radial distribution is clearly that of a $\mu = 0$ spinning mode. Thus, the $m = \pm 4, \mu = 0$ mode predicted by equation 3.3-F has been generated.

A mode $m = -2$ has been predicted to propagate instead of a cancelled distribution when sound pressure level reduction of the $m_0 = 2$ mode is attempted by the optimal solution. This was verified and is illustrated in Figure 81. The cancelled distribution is an identical waveform 6 dB greater than the individual distributions. This is a result of both arrays contributing to the excitation of the $m = 2$ mode. The acoustic phases of the transducers are those given by equation 1.3-4 for $m = -2$ and $n = 8$, as expected.

Excellent agreement has been obtained between the wave equation theory and experimental results for the range of m, μ and frequency over which effective cancellation can be obtained.

FIGURE 80
SPL Versus Radial Distance for $m = 0$, $\mu = 1$
Mode at 2000 Hz

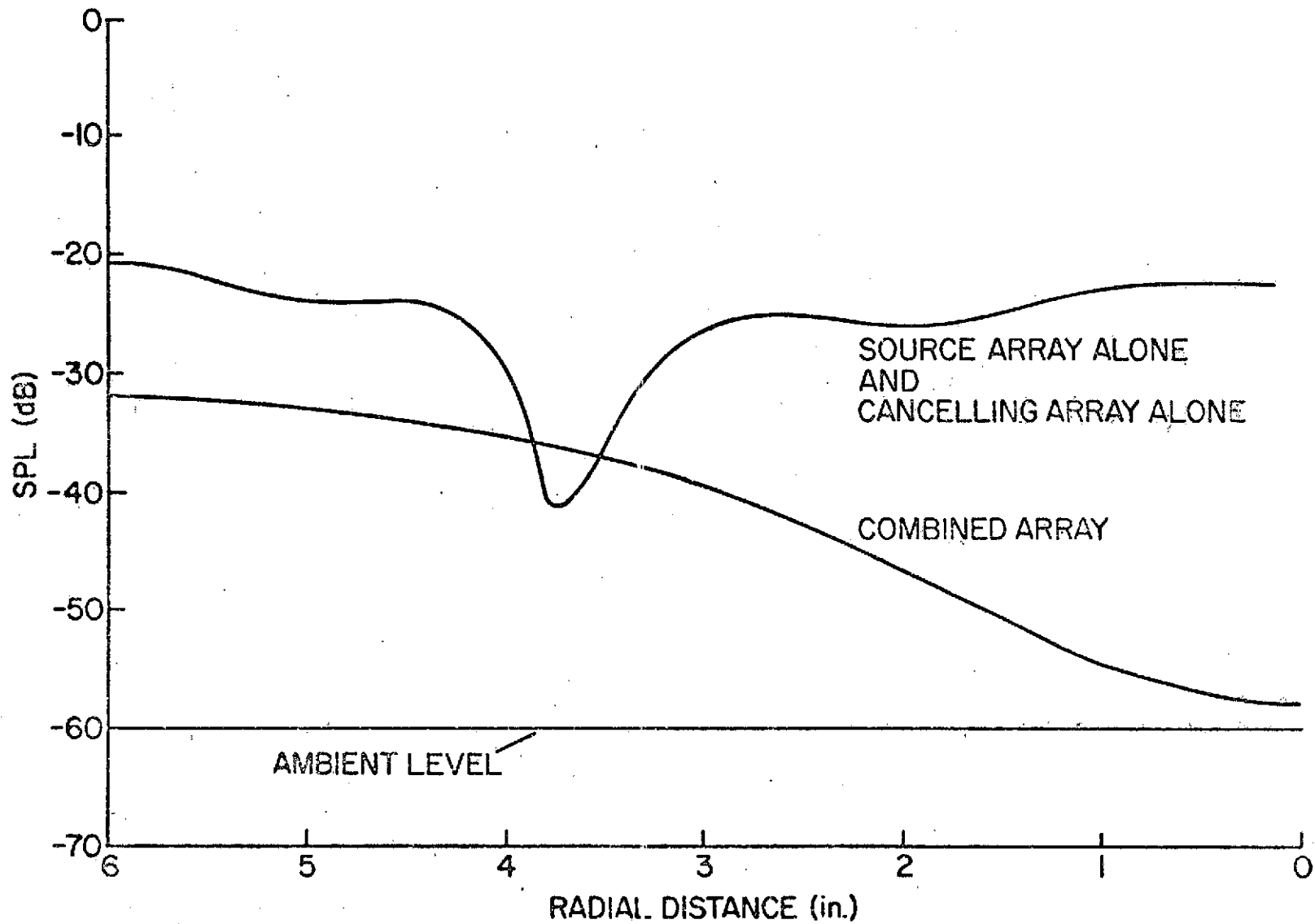
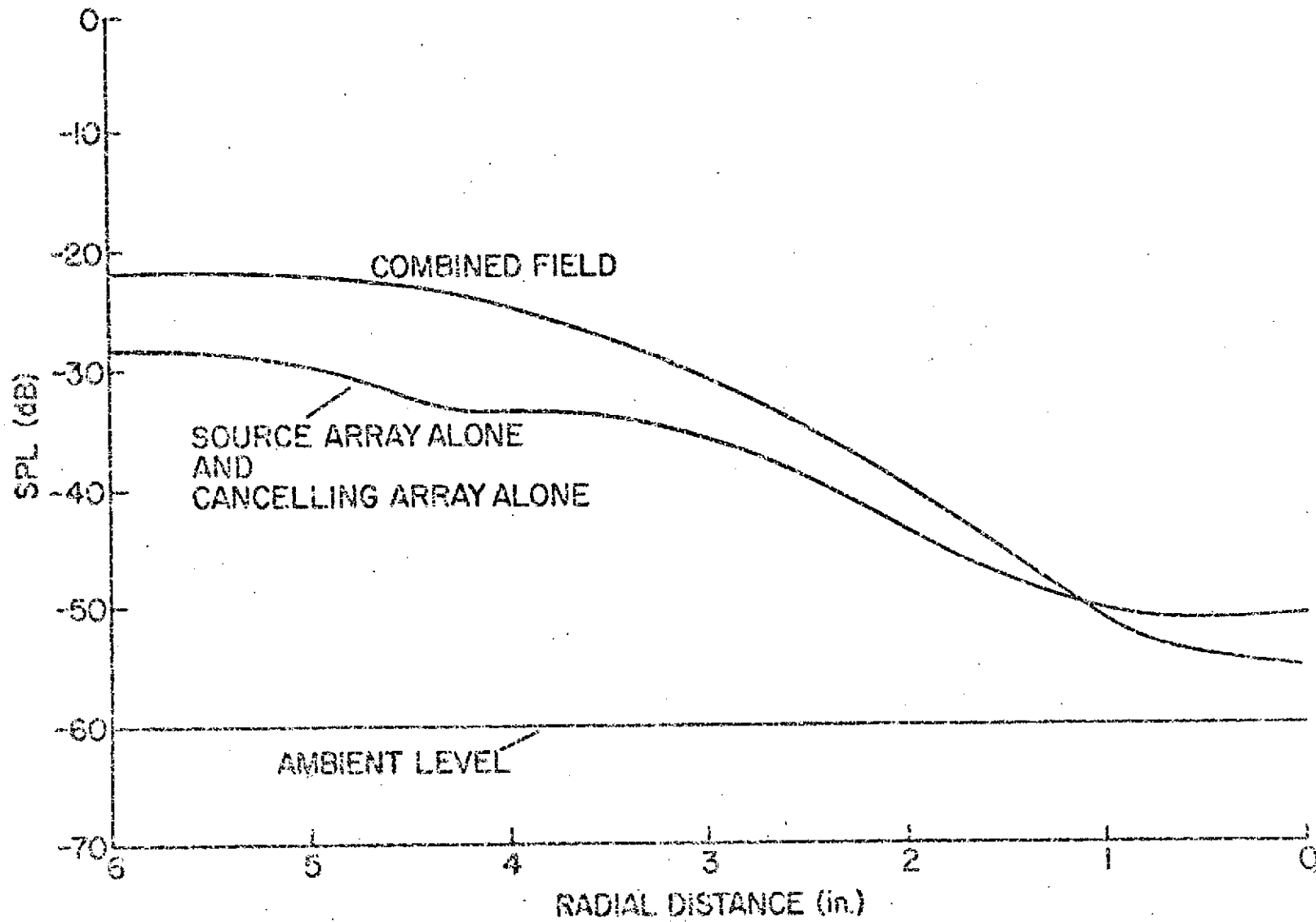


FIGURE 81

SPL Versus Radial Distance for

$m = 2, \mu = 0$ Mode at 1500 Hz



The explanation of the limited range of acceptable cancellation performance does not challenge the test results of Chapter II. Variation of transducer response, if uncompensated, can produce substantial performance degradation. Because transducers are relatively low impedance acoustic sources, circumferential variation of in-duct acoustic loading can also result in significant performance degradation.

This performance degradation may prove to be insignificant for many applications. The reduction of the discrete tone peaks observed in a sound pressure level versus frequency plot for a fan-duct system to the flow noise level is perfectly satisfactory performance. Further reduction will have negligible effect since it will be masked by the flow noise. Thus cancelling array performance requirements depend on the specific application.

If the performance degradation is at an acceptable level, the cancelling array can be governed strictly by the simple relations developed for a two dimensional cancellation system in Section 3.4. The reduction of the cancellation system dimensionality from $2n$, where n is the number of transducers, to 2 greatly simplifies system optimization and thus is very desirable. Transducer quality specification and symmetry specification in the duct design should be considered in the overall design concept so that the desired cancellation can be achieved.

Amplitude and phase compensation at each transducer can be employed to enable two dimensional control for cases of unsatisfactory

performance degradation. Fans are relatively high impedance acoustic sources and therefore would be effected little by small variations of the acoustic impedance of the duct in the circumferential direction at the plane of the source. Transducers, on the other hand, are relatively low acoustic impedance sources. Also, the variation of transducer performance can be expected to exceed the variation of source strength for the various generating mechanisms of a fan. Of significance are the individual rotor stator interactions and rotor blade pressure fields. So that the cancelling array generates a waveform of the proper symmetry, each transducer can be calibrated so that at its input would be correct for the desired acoustic output.

The development of a measurement system to provide an index of performance remains a difficult problem. The sound pressure level inside the duct is to be minimized so that the effective perceived noise level (EPNdB) of the sound radiating from the duct is minimized. The form presented in Section 3.3, given below, is most easily applied in the presence of a single mode.

IP = index of performance

$$= \frac{1}{w} \sum_{i=1}^w \beta_i \text{SPL}_i(t)$$

where w = number of probes

β_i = weighting factor related to position of probe

SPL_i = sound pressure level at i^{th} position

The probe positions and the corresponding weighting factors will

depend upon the radial distributions of the mode to be reduced, assuming m constant. A pattern recognition technique can be applied to determine w and β_i . Consideration must be given to the "point cancellation" effect so that the index of performance produces the desired minimum.

When more than one mode is present, pattern recognition should be utilized to isolate the modes which are to be reduced. For an actual fan, this can be difficult if there is significant energy in more than one mode for a given harmonic of the blade passage frequency.

Adaptive control techniques have been found to be appropriate for maximizing cancellation of spinning modes of sound by the Spinning Mode Synthesizer. Experiment and analysis have verified the predicted optimal solution (see Section 1.3) over the range of m , μ , and f for which effective cancellation can be achieved. Direct application of the optimal solution utilizing the input parameters to the source array would enable application of a simple, model based controller. But, such a design would not be consistent with the control system design objectives (see Section 3.1). Thus an unknown source strength and circumferential and axial phase angles have been assumed. The design process has been targeted toward final application by the use of adaptive control.

The reduction of the system dimensionality to two, an amplitude parameter and a phase parameter, by assuming the general form of the optimal solution (equations 3.4-1 and 3.4-2) has greatly simplified the control problem. Control system design was based on the following features:

- 1) 2-dimensional plant
- 2) unimodal cost function surface
- 3) time varying minimum
- 4) noisy cost function surface due to SPL measurement algorithm.

A perturbation signal, gradient technique is well suited for the design criteria. The plant is a high frequency electrical - acoustical system, enabling high perturbation frequencies and thus adequate time response.

Control system simplicity and reduced time response were obtained by the generation of a "perturbation circle". Plant output signal separation was obtained by multiplication by the two reference sinusoids and low pass filtering (see controller algorithms in Sections 5.2 and 5.3). The best overall system response was obtained with simple integral feedback (Section 5.4). Step change response on a normalized, centrally located, quadratic cost function surface satisfied feasibility requirements. Two thirds reduction for the convergence test case with $(X_1(0), X_2(0)) = (.8, .8)$ required .26 seconds. A step load change moving the minimum from $(0,0)$ to $(.8, .8)$ resulted in a two thirds reduction in .40 seconds. On line response of the same magnitude can be expected if the transducer voltage and phase are electronically controlled.

VII Summary, Conclusions and Recommendations

7.1 Summary

The reduction of the discrete tones generated by the fan, compressor, and turbine sections of jet engines is essential for jet aircraft to meet present and proposed noise rules. The EPNdB rating, where pure tones are penalized, would respond proportionately to reductions in the discrete tone levels. Present reduction methods, such as the installation of acoustical treatment, have high cost, as well as severe weight, efficiency, and maintenance penalties.

The reduction of the discrete tones, or spinning modes, by the cancellation effect due to the combination of two acoustic fields having equal amplitudes but opposite phase has been proposed by the Noise Control Laboratory at The Pennsylvania State University. Cancellation would be maximized by the optimization of an amplitude parameter and a phase parameter of another spinning mode source.

The Spinning Mode Synthesizer has provided the means for effective study of this noise reduction scheme. A modified SMS is the proposed source of the cancelling acoustic field in actual application. For the purposes of this feasibility study, the synthesizer consists of electrical-acoustical transducers located in an equally spaced circular array. Two arrays are obtained by assigning alternate transducers to each array. A specified spinning mode is generated by the "source" array. The identical mode with appropriate phase and amplitude for cancellation is then generated by the "cancelling" array.

Open loop control of the SMS has been found to be unsatisfactory for efficient parameter variation, rigorous evaluation of the synthesizer, and the introduction of complexities characteristic of jet engines. Adaptive control techniques have been found to be appropriate for automatic control to maximize cancellation. Design has been based on a 2-dimensional, unimodal, time varying, noisy cost function surface. A perturbation signal, gradient technique was found suited for the design criteria and developed. Analog simulation has shown favorable convergence and load change response.

7.2 Conclusions

The feasibility of the cancellation concept has been demonstrated. The functional dependence of the range of circumferential modes, radial distributions, and frequency on the number of transducers and the specified circumferential mode has been established for single arrays and two interacting arrays. The generation of single, specified modes to specified frequencies can therefore be accomplished by determining the minimum number of transducers.

A perturbation type, 2 dimensional controller for the closed loop control of the cancelling array of the Spinning Mode Synthesizer has been designed for eventual application to fan-duct systems. The good time response of the system obtained by analog simulation has shown the feasibility of application to time varying spinning mode sources. An example of such a source is the jet engine on takeoff and landing.

The development and analysis of the wave equation for the Spinning Mode Synthesizer has verified the predicted optimal solution for the minimization of the sound pressure level of a ducted spinning mode generated by a circular transducer array. The optimal solution has been shown to provide cancellation for a finite range of circumferential modes, radial distributions, and frequency. The frequency range of effective cancellation is limited by the set $\{M\}$ of circumferential modes whose elements are given by

$$m = m_0 + (2k+1)n$$

where m_0 = specified circumferential mode

$$k = \dots, -1, 0, 1, \dots$$

n = number of transducers in each array

The propagation of the modes $\{M\}$ due to excitation by the combined arrays masks the cancelled mode. Increasing n increases the range of effective cancellation.

Substantial sound pressure level reduction was obtained for modes within the limits imposed by the sets of $\{M\}$'s. Examination of the radial distributions of cancelled modes above the frequency limits verified the generation of higher order modes. Sound pressure level reduction within the allowed range of frequencies was slightly hampered by effects due to the lack of symmetry of the test system. The combined effects of different response characteristics from transducer to transducer, a non-circular duct, and plate radiation resulted in degradation of the cancellation performance.

7.3 Recommendations

It will be necessary to develop a measurement system to provide a cancellation index of performance to apply automatic control to a cancellation system. The weighted probe array discussed in Chapter VI is physically realizable and suitable for development. Pattern recognition techniques should be applied to determine probe positions and weighting factors.

The controller which has been developed should be employed if extensive experimental research is considered. The development of the measurement system to provide a cancellation index of performance should improve open loop efficiency to an extent that it would be appropriate for small scale testing. The measurement system is considered essential for productive testing at any scale.

The application of cancellation to a ducted, single stage fan by a modified Spinning Mode Synthesizer is the logical next step in the development of the cancellation system. The equations developed for a single transducer array can be used to specify the minimum number of transducers necessary to generate the appropriate modes to specified frequencies. Transducer quality and duct symmetry should be considered in the design of the system so that the desired cancellation can be achieved. It is recommended that a duct which is circular within 1/100 of an inch be used for such research. These considerations will also enable two dimensional control of the transducer array without amplitude and phase compensation at the individual transducers.

Bibliography

1. Federal Aviation Administration: Noise Abatement, February, 1970.
2. Neitzel, R.E., and Benzakein, M.J.: Noise Considerations in the Design of Advanced Subsonic Transport Turbofan Engines, SAE 700807, 1970.
3. Black, R.E., and Stern, J.A.: Expanding Horizons for Long-Haul Air Transportation, AIAA 9th Annual Meeting and Technical Display, Washington, D.C., January 8-10, 1973.
4. Tyler, J.M., and Sofrin, T.G.: Axial Flow Compressor Noise Studies, S.A.E. Trans., pp. 309-332, 1962.
5. Lawson, M.V.: Reduction of Compressor Noise Radiation, J. of Acoustical Soc. of Amer., 43:37-50, 1968.
6. Morfey, C.L. and Dawson, H.: Axial Compressor Noise, Some Results from Aero-Engine Research, ASME 11th Gas Turbine Conf., 1966.
7. Bragg, S.L., and Bridge, R.: Noise From Turbojet Compressors, J. of the Royal Aeronautical Society, 66:1-10, 1964.
8. Seiner, J.M.: The Design and Development of a Spinning Mode Synthesizer, Master of Science Thesis, The Pennsylvania State University, September 1969.
9. Eveleigh, V.W.: Adaptive Control and Optimization Techniques, McGraw-Hill, 1967.
10. Relton, F.E.: Applied Bessel Functions, Dover Publications, Inc., New York, 1965, p. 52.
11. Mendel and Fu: Adaptive, Learning, and Pattern Recognition Systems, Academic Press, Inc., New York, 1970.
12. Churchill, R.V.: Fourier Series and Boundary Value Problems, McGraw-Hill Book Company, Inc., New York, 1941.
13. Beranek, L.L.: Noise and Vibration Control, McGraw-Hill Book Company, Inc., New York, 1971.
14. Reethof, G.: The Propagation and Cancellation of Complex Acoustic Modes in Ducts, Research Proposal Submittal to the National Science Foundation by the Noise Control Laboratory, The Pennsylvania State University, 1972.
15. Skudrzyk, E.: Simple and Complex Vibratory Systems, The Pennsylvania State University Press, 1968.

APPENDIX 1

General Solution of the Wave Equation for a Semi-Infinite,
Constant Radius, Rigid-Walled, Cylindrical Duct

The system is shown in Figure 82

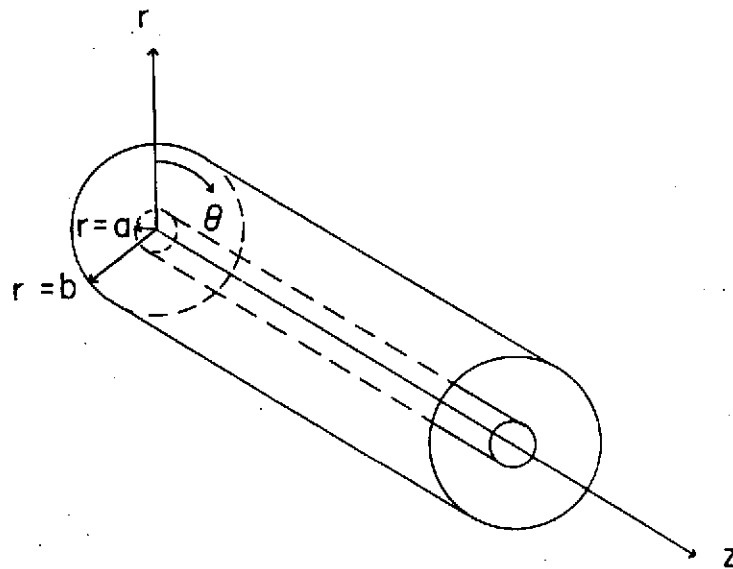


FIGURE 82

Cylindrical Coordinate System

Solution is based on the following premises:

- (1) Forcing occurs only at the plane defining the closed end of the duct.
- (2) Forcing will be steady sinusoidal, represented by the complex exponential $e^{-i\omega t}$ such that

$$A \cos \omega t = \text{Re} [A e^{-i\omega t}] \rightarrow A e^{-i\omega t}$$

Supplementary to premise 2, the following corollary is applied:

(1) All other system variables can be represented by the form

$$B(\omega) \cos(\omega t + \Psi) = \operatorname{Re} [\bar{B}(i\omega) e^{i\omega t}] \rightarrow \bar{B}(i\omega) e^{i\omega t}$$

where

$$\bar{B}(i\omega) = B(\omega) e^{i\Psi}$$

The general complex solution is obtained in this Appendix. The real component is evaluated in Chapter III for a specific forcing function.

The wave equation is:

$$\nabla^2 \Phi(r, \theta, z, t) = \frac{1}{c^2} \frac{\partial^2 \Phi(r, \theta, z, t)}{\partial t^2} \quad (1)$$

where Φ is the velocity potential and the ∇^2 operator for a cylindrical coordinate system is

$$\nabla^2 = \frac{1}{r} \left[\frac{\partial}{\partial r} \left(r \frac{\partial}{\partial r} \right) \right] + \frac{1}{r^2} \frac{\partial^2}{\partial \theta^2} + \frac{\partial^2}{\partial z^2}$$

assume (by the method of separation of variables) that a solution exists of the form

$$\begin{aligned} \Phi(r, \theta, z, t) &= R(r) \Theta(\theta) Z(z) T(t) \\ &= \bar{\Phi}(r, \theta, z) T(t) \end{aligned}$$

An exponential solution is desired for the time variable, so $T(t)$ will be of the form

$$T(t) = A e^{i(\omega t + \Psi)}$$

Then substitution of Φ into equation 1, yields

$$\nabla^2 (\bar{\Phi} T(t)) = \frac{1}{c^2} \frac{\partial^2 (\bar{\Phi} T(t))}{\partial t^2}$$

$$(\nabla^2 \bar{\Phi}) T(t) = - \frac{\omega^2}{c^2} \bar{\Phi} T(t)$$

$$\nabla^2 \bar{\Phi} = - \frac{\omega^2}{c^2} \bar{\Phi}$$

The Helmholtz equation follows:

$$\nabla^2 \bar{\Phi} + k^2 \bar{\Phi} = 0 \text{ where } k = \frac{\omega}{c}$$

The expanded form is

$$\frac{1}{r} \left[\frac{\partial}{\partial r} \left(r \frac{\partial \bar{\Phi}}{\partial r} \right) \right] + \frac{1}{r^2} \frac{\partial^2 \bar{\Phi}}{\partial \theta^2} + \frac{\partial^2 \bar{\Phi}}{\partial z^2} + k^2 \bar{\Phi} = 0$$

With the assumed solution

$$\Phi = R(r) \Theta(\theta) Z(z) T(t)$$

and the homogeneous boundary conditions

$$1) \Theta(\theta) = \Theta(\theta + 2\pi)$$

$$2) \frac{\partial \Theta(\theta)}{\partial \theta} = \frac{\partial \Theta(\theta + 2\pi)}{\partial \theta}$$

$$3) \left. \frac{\partial R}{\partial r} \right|_{r=a} = 0$$

$$4) \left. \frac{\partial R}{\partial r} \right|_{r=b} = 0$$

the solution components have been determined (for example, Morse (11)):

$$R(r) = L \left[J_m(k_{m\mu}^\sigma r) - \frac{J'_m(\sigma k_{m\mu}^\sigma b)}{Y'_m(\sigma k_{m\mu}^\sigma b)} Y_m(k_{m\mu}^\sigma r) \right]$$

$$\Theta(\theta) = A_1 e^{im\theta} + A_2 e^{-im\theta}$$

$$Z(z) = C_1 e^{i\gamma_{m\mu}^\sigma z} + C_2 e^{-i\gamma_{m\mu}^\sigma z}$$

$$T(t) = D_1 e^{i\omega t} + D_2 e^{-i\omega t}$$

such that

$$\Phi = \sum_{m=0}^{\infty} \sum_{\mu=0}^{\infty} \Theta(\theta) R(r) Z(z) T(t)$$

The boundedness condition is applied to $Z(z)$. For $\frac{\omega}{c} < k_{m\mu}^\sigma$, $\gamma_{m\mu}^\sigma$ is complex and positive. So that $Z(\infty)$ is finite, $C_2 = 0$. The complete solution for the homogeneous boundary conditions is, therefore,

$$\begin{aligned} \Phi = & \sum_{m=0}^{\infty} \sum_{\mu=0}^{\infty} L[L_{m\mu}^\sigma(k_{m\mu}^\sigma r)] [A_1 e^{im\theta} + A_2 e^{-im\theta}] \cdot \\ & \cdot [C_1 e^{i\gamma_{m\mu}^\sigma z}] [D_1 e^{i\omega t} + D_2 e^{-i\omega t}] \end{aligned}$$

where

$$L_{m\mu}^\sigma(k_{m\mu}^\sigma r) = [J_m(k_{m\mu}^\sigma r) - \frac{J'_m(\sigma k_{m\mu}^\sigma r)}{Y'_m(\sigma k_{m\mu}^\sigma r)} Y_m(k_{m\mu}^\sigma r)]$$

and m = circumferential mode number, a non-negative integer

μ = radial mode number, a non-negative integer

σ = hub-tip ratio = $\frac{a}{b}$

$k_{m\mu}^\sigma$ = eigenvalue of order μ for the m^{th} mode having a hub-tip ratio σ

$\gamma_{m\mu}^\sigma$ = wave number in axial direction

$$= \sqrt{\left(\frac{\omega}{c}\right)^2 - (k_{m\mu}^\sigma)^2}$$

J_m, Y_m = Bessel functions of order m

For the case under consideration, the inner radius a is zero,

so $\sigma = 0$ and $\frac{J'_m(0)}{Y'_m(0)} = 0$. Therefore,

$$L_{m\mu}(k_{m\mu}r) = J_m(k_{m\mu}r)$$

Propagation occurs only in the positive z direction, so the sign of ωt is negative. The solution is then:

$$\Phi = \sum_{m=0}^{\infty} \sum_{\mu=0}^{\infty} P_{m\mu} J_m(k_{m\mu}r) e^{i(\pm m\theta + \gamma_{m\mu}z - \omega t)}$$

This can be written as:

$$\Phi = \sum_{m=0}^{\infty} \sum_{\mu=0}^{\infty} [A_{m\mu} e^{im\theta} + B_{m\mu} e^{-im\theta}] J_m(k_{m\mu}r) e^{i(\gamma_{m\mu}z - \omega t)}$$

where $A_{m\mu}$ and $B_{m\mu}$ are amplitude coefficients to be determined.

The particle velocity at the source provides an inhomogeneous boundary condition. The particle velocity, \underline{v} , is given by

$$\underline{v} = -\nabla\Phi = -\left[\underline{a}_r \frac{\partial}{\partial r} + \underline{a}_\theta \frac{1}{r} \frac{\partial}{\partial \theta} + \underline{a}_z \frac{\partial}{\partial z}\right]$$

where \underline{a}_i are unit vectors. Also, the pressure is given by

$$P = \rho \frac{\partial \Phi}{\partial t} = i\omega\rho\Phi.$$

Thus

$$\underline{v}_r = -\underline{a}_r \frac{\partial \Phi}{\partial r}$$

$$\underline{v}_\theta = -\underline{a}_\theta \frac{1}{r} \frac{\partial \Phi}{\partial \theta}$$

$$\underline{v}_z = - \frac{a}{z} \frac{\partial \Phi}{\partial z}$$

$$P = i \omega \rho \Phi$$

The velocity at the source is given by:

$$\begin{aligned} v_s (r, \theta, z = 0) &= f (r, \theta) \cos \omega t \\ &= \underline{v}_z \Big|_{z=0} \end{aligned}$$

which is represented in complex form by:

$$v_s = f (r, \theta) e^{i\omega t}.$$

Since $v_s = \underline{v}_z \Big|_{z=0}$, we have

$$\underline{v}_z = - \frac{a}{z} \frac{\partial \Phi}{\partial z}$$

$$= - \sum_{m=0}^{\infty} \sum_{\mu=0}^{\infty} i \gamma_{m\mu} [A_{m\mu} e^{im\theta} + B_{m\mu} e^{-im\theta}] J_m(k_{m\mu} r) e^{i(\gamma_{m\mu} z - \omega t)}$$

$$\text{and } \underline{v}_z \Big|_{z=0} = - \sum_{m=0}^{\infty} \sum_{\mu=0}^{\infty} i \gamma_{m\mu} [A_{m\mu} e^{im\theta} + B_{m\mu} e^{-im\theta}] J_m(k_{m\mu} r) e^{i\omega t}$$

The amplitude of v_s is equal to

$$\begin{aligned} f(r, \theta) &= - \sum_{m=0}^{\infty} \sum_{\mu=0}^{\infty} i \gamma_{m\mu} [A_{m\mu} e^{im\theta} + B_{m\mu} e^{-im\theta}] J_m(k_{m\mu} r) \\ &= - \left\{ \sum_{m=0}^{\infty} e^{im\theta} \sum_{\mu=0}^{\infty} \gamma_{m\mu} A_{m\mu} J_m(k_{m\mu} r) + \right. \\ &\quad \left. \sum_{m=0}^{\infty} e^{-im\theta} \sum_{\mu=0}^{\infty} \gamma_{m\mu} B_{m\mu} J_m(k_{m\mu} r) \right\} \end{aligned}$$

For convenience, the amplitude coefficients $C_{m\mu}$ and $D_{m\mu}$ are defined to be:

$$C_{m\mu} (r) = \sum_{\mu=0}^{\infty} \gamma_{m\mu} A_{m\mu} J_m(k_{m\mu} r)$$

$$D_{m\mu} (r) = \sum_{\mu=0}^{\infty} \gamma_{m\mu} B_{m\mu} J_m(k_{m\mu} r).$$

Then,

$$f(r, \theta) = -i \left\{ \sum_{m=0}^{\infty} C_{m\mu} (r) e^{im\theta} + \sum_{m=0}^{\infty} D_{m\mu} (r) e^{-im\theta} \right\}$$

Applying orthogonality to the angular variable,

$$\int_0^{2\pi} f(r, \theta, 0) e^{in\theta} d\theta = -i \left\{ \int_0^{2\pi} \sum_{m=0}^{\infty} C_{m\mu}(r) e^{-im\theta} e^{-in\theta} d\theta \right. \\ \left. + \int_0^{2\pi} \sum_{m=0}^{\infty} D_{m\mu}(r) e^{im\theta} e^{-in\theta} d\theta \right\}$$

$$\int_0^{2\pi} \sum_{m=0}^{\infty} C_{m\mu}(r) e^{im\theta} e^{-in\theta} d\theta = \begin{cases} 0 & \text{for } m \neq n \\ 2\pi C_{m\mu}(r) & \text{for } m = n = 0 \\ 2\pi C_{m\mu}(r) & \text{for } m = n \neq 0 \end{cases}$$

$$\int_0^{2\pi} \sum_{m=0}^{\infty} D_{m\mu}(r) e^{-im\theta} e^{-in\theta} d\theta = \begin{cases} 0 & \text{for } n \neq m \\ 2\pi D_{m\mu}(r) & \text{for } n = m = 0 \\ 0 & \text{for } n = m \neq 0 \end{cases}$$

Therefore,

$$\int_0^{2\pi} f(r, \theta, 0) e^{-im\theta} d\theta = -i 2\pi \{C_{m\mu}(r) + \epsilon_0 D_{m\mu}(r)\}$$

$$\text{where } \epsilon_0 \begin{cases} = 1 & \text{for } m = 0 \\ = 0 & \text{for } m \neq 0 \end{cases}$$

Applying orthogonality again,

$$\int_0^{2\pi} f(r, \theta, 0) e^{im\theta} d\theta = -i \left\{ \int_0^{2\pi} \sum_{m=0}^{\infty} C_{m\mu}(r) e^{im\theta} e^{+in\theta} d\theta + \right. \\ \left. + \int_0^{2\pi} \sum_{m=0}^{\infty} D_{m\mu}(r) e^{-im\theta} e^{in\theta} d\theta \right\}$$

which results in:

$$\int_0^{2\pi} f(r, \theta, 0) e^{im\theta} d\theta = -i 2\pi \{\epsilon_0 C_{m\mu}(r) + D_{m\mu}(r)\}$$

For $m = 0$,

$$C_{0\mu}(r) + D_{0\mu}(r) = \frac{i}{2\pi} \int_0^{2\pi} f(r, \theta, 0) d\theta.$$

for $m \neq 0$,

$$C_{m\mu}(r) = \frac{i}{2\pi} \int_0^{2\pi} f(r, \theta, 0) e^{-im\theta} d\theta$$

$$D_{m\mu}(r) = \frac{i}{2\pi} \int_0^{2\pi} f(r, \theta, 0) e^{im\theta} d\theta.$$

Now, for $m = 0$,

$$\begin{aligned} C_{0\mu}(r) + D_{0\mu}(r) &= \sum_{\mu=0}^{\infty} \gamma_{0\mu} [A_{0\mu} + B_{0\mu}] J_0(k_{0\mu}r) \\ &= \frac{i}{2\pi} \int_0^{2\pi} f(r, \theta, 0) d\theta \end{aligned}$$

Applying orthogonality to the radial variable yields

$$\begin{aligned} \int_0^b \sum_{\mu=0}^{\infty} r \gamma_{0\mu} [A_{0\mu} + B_{0\mu}] J_0(k_{0\mu}r) J_0(k_{0q}r) dr \\ = \frac{i}{2\pi} \int_0^{2\pi} \int_0^b r f(r, \theta, 0) J_0(k_{0q}r) dr d\theta \end{aligned}$$

and

$$\int_0^b r J_0(k_{0\mu}r) J_0(k_{0q}r) dr$$

$$= \begin{cases} 0 & \text{for } \mu \neq q \\ \frac{1}{2k_{0\mu}^2} [k_{0\mu}^2 b^2 - 0] J_0^2(k_{0\mu}b) & \text{for } \mu = q \\ = \frac{1}{2} b^2 J_0^2(k_{0\mu}b) & \end{cases} \quad (\text{Ref. 12})$$

Thus,

$$A_{0\mu} + B_{0\mu} = \frac{i}{\pi b^2 J_0^2(k_{0\mu} b) \gamma_{0\mu}} \int_0^{2\pi} \int_0^b r f(r, \theta, 0) J_0(k_{0\mu} r) dr d\theta$$

For $m \neq 0$,

$$\begin{aligned} C_{m\mu}(r) &= \sum_{\mu=0}^{\infty} \gamma_{m\mu} A_{m\mu} J_m(k_{m\mu} r) \\ &= \frac{i}{2\pi} \int_0^{2\pi} \int_0^b r f(r, \theta, 0) e^{-im\theta} d\theta \end{aligned}$$

Applying orthogonality again,

$$\begin{aligned} \int_0^b \sum_{\mu=0}^{\infty} r \gamma_{m\mu} A_{m\mu} J_m(k_{m\mu} r) J_m(k_{mq} r) dr \\ = \frac{i}{2\pi} \int_0^{2\pi} \int_0^b r f(r, \theta, 0) e^{-im\theta} J_m(k_{mq} r) dr d\theta \end{aligned}$$

$$\begin{cases} \int_0^b r J_m(k_{m\mu} r) J_m(k_{mq} r) dr \\ = 0 & \text{for } \mu \neq q \\ = \frac{1}{2k_{m\mu}^2} [k_{m\mu}^2 b^2 - m^2] J_m^2(k_{m\mu} b) & \text{for } \mu = q \end{cases} \quad (\text{Ref. 12})$$

Thus,

$$\begin{aligned} A_{m\mu} &= \frac{i k_{m\mu}^2}{\pi \gamma_{m\mu} [k_{m\mu}^2 b^2 - m^2] J_m^2(k_{m\mu} b)} \int_0^{2\pi} \int_0^b r f(r, \theta, 0) e^{-im\theta} \\ &\quad \cdot J_m(k_{m\mu} r) dr d\theta \end{aligned}$$

By the same procedure

$$\begin{aligned} B_{m\mu} &= \frac{i k_{m\mu}^2}{\pi \gamma_{m\mu} [k_{m\mu}^2 b^2 - m^2] J_m^2(k_{m\mu} b)} \int_0^{2\pi} \int_0^b r f(r, \theta, 0) e^{im\theta} \\ &\quad \cdot J_m(k_{m\mu} r) dr d\theta \end{aligned}$$

which completes the solution for a general harmonic source at $z = 0$.

The pressure distribution is given by:

$$P(r, \theta, z, t) = i \rho \omega \Phi$$

$$= i \rho \omega \sum_{m=0}^{\infty} \sum_{\mu=0}^{\infty} [A_{m\mu} e^{im\theta} + B_{m\mu} e^{-im\theta}] J_m(k_{m\mu} r) e^{i(\gamma_{m\mu} z - \omega t)}$$

where $A_{m\mu}$, $B_{m\mu}$, and $[A_{0\mu} + B_{0\mu}]$ are given above. This can be rewritten as:

$$P(r, \theta, z, t) = + \sum_{m=0}^{\infty} \sum_{\mu=0}^{\infty} E_{m\mu} [G_{m\mu} e^{im\theta} + H_{m\mu} e^{-im\theta}] \cdot$$

$$\cdot J_m(k_{m\mu} r) e^{i(\gamma_{m\mu} z - \omega t)}$$

where

$$= \bar{P}(r, \theta, z, i\omega) e^{i\omega t}$$

$$E_{m\mu} = \frac{\rho \omega k_{m\mu}^2}{\pi \gamma_{m\mu} [k_{m\mu}^2 b^2 - m^2] J_m^2(k_{m\mu} b)}$$

$$G_{m\mu} = \int_0^{2\pi} \int_0^b r f(r, \theta, 0) J_m(k_{m\mu} r) e^{-im\theta} dr d\theta, \quad m \neq 0$$

$$H_{m\mu} = \int_0^{2\pi} \int_0^b r f(r, \theta, 0) J_m(k_{m\mu} r) e^{im\theta} dr d\theta, \quad m \neq 0$$

$$G_{0\mu} + H_{0\mu} = \int_0^{2\pi} \int_0^b r f(r, \theta, 0) J_0(k_{0\mu} r) dr d\theta, \quad m = 0$$

The above development was derived from analysis in unpublished notes by M. J. Oslac, Research Assistant at The Pennsylvania State University's Noise Control Laboratory.

For convenience in early treatment in Chapter I, the symbols g_+ and g_- are employed where g_+ and g_- are as follows:

$$g_+ = E_{m\mu} G_{m\mu} J_m(k_{m\mu} r) e^{i(\gamma_{m\mu} z - \omega t)}$$

$$g_- = E_{m\mu} H_{m\mu} J_m(k_{m\mu} r) e^{i(\gamma_{m\mu} z - \omega t)}$$